MODELLING DEFORMATION, POROSITY AND ELASTIC CONSTANTS IN POROUS ROCKS

A DISSERTATION
SUBMITTED TO THE DEPARTMENT OF GEOPHYSICS
AND THE COMMITTEE ON GRADUATE STUDIES
OF STANFORD UNIVERSITY
IN PARTIAL FULFILLMENT OF THE REQUIREMENTS
FOR THE DEGREE OF
DOCTOR OF PHILOSOPHY

By
Jorge Segundo Mendoza
January 1987

ABSTRACT

Pore spaces are responsible for most of the physical properties of rocks. In particular, they can drastically reduce the effective elastic moduli of porous materials. Several analytical methods have been constructed in the past to explain the behavior of porous materials. However, they have been limited to a few rectilinear pore geometries in homogeneous and inhomogeneous media. These simple solutions are clearly inadequate to describe the elastic behavior of complex rocks containing a broad distribution of pore sizes with irregular shapes.

An efficient numerical technique has been used to compute the deformation of arbitrary shaped pores embedded in a two-dimensional homogeneous elastic solid under the influence of applied stresses. The scheme is based in the boundary elements method where single linear elements are used to generate solutions which satisfy the prescribed boundary conditions. These solutions can be employed to describe the behavior of the elastic moduli and seismic velocities in porous rocks. Also, the numerical algorithm allows to compute the stress field induced by the pores in the solid. In this way the effect of the interactions between pores caused by stress concentrations can be studied from a quantitative point of view.

Based on the results obtained with the boundary elements technique, we construct a discrete theoretical model which explains the observed changes in porosity and the static bulk modulus with pressure for selected samples of sandstones.

CHAPTER I

THE ELASTIC MODULI OF POROUS ROCKS: A REVIEW

1. INTRODUCTION

Pore spaces are in many cases responsible for most of the physical properties of rocks such as permeability, electrical resistivity, and porosity. In particular, they can drastically reduce the effective elastic moduli of rocks. Several methods have been constructed in the past to explain the behavior of porous materials. Some of them are applicable to particular materials while others claim to produce the correct response for a wide variety of solids. Due to the great amount of scientific papers published on this subject and the diversity of methods and techniques, it becomes cumbersome for the newcomer as well as the experienced scientist to search for the most convenient and effective approach, if any, which can solve his particular problem. To remedy this problem, several authors have written reviews that summarize most of the approaches developed in this field. Among others, we can cite the excellent work by *Watt et al. (1976)* about the elastic properties of composite materials.

In this study we intend to summarize some of the recent scientific trends in the determination of the static elastic constants in sedimentary rocks with emphasis on sandstones. We must point out that this work does not pretend to substitute past reviews but extends or updates some of the techniques currently used in order to determine the mechanical and elastostatic behavior of sedimentary rocks.

We start by dividing the different methods in five major trends:

CLASSICAL METHODS

DISLOCATION METHODS

SELF-CONSISTENT METHODS

GRANULAR METHODS

NUMERICAL METHODS

As it was indicated before, we limit the scope of this paper to the description of the static elastic moduli. It is important to make such a distinction because the dynamic moduli (moduli measured or calculated at frequencies greater than zero) can be in many cases up to one order of magnitude larger than the corresponding static case. Treatments for the dynamic moduli can be found in *Biot (1956)*, *Simmons et al. (1965)*, *Toksöz et al. (1976)* and *Winkler (1983)*.

Although much of the following review is general, some of the approaches will be discussed in more detail when they lead to an interesting (but not necessary correct) result for sedimentary rocks.

2. GENERAL CONSIDERATIONS

Most authors use a particular notation to define similar concepts. This leads to a tremendous misunderstanding in the scientific work and also requires a great effort by the reader to link ideas expressed in several studies. To alleviate in part that problem, we will introduce or clarify elementary concepts that will be used in the rest of this paper.

Porosity of a solid is the ratio between the total volume of the pore space inside the solid and the total volume of the solid.

The aspect ratio is the ratio between the minor and major semi-axes in an ellipse. This concept is applicable only to ellipsoidal or rectangular pores.

Interactive pores are those which interchange a non-negligible induced stress field.

We must also state that all the approaches considered assume that the solid is linear elastic, i.e. the components of the stress tensor are linearly related to the components of the strain tensor. Then, the stress-strain relation can be written as:

$$\sigma_{ij} = c_{ijkl}\epsilon_{kl} \qquad (2-1)$$

where c_{ijkl} denotes the stiffness tensor. We have also used the Einstein summation convention.

Now, the stiffness tensor of an isotropic body holds only two independent components which are written as:

$$c_{ijkl} = \lambda\delta_{ij}\delta_{kl} + \mu(\delta_{ik}\delta_{jl} + \delta_{il}\delta_{jk}) \qquad (2-2)$$

These two components are part of the elastic moduli of the solid. The rest of the moduli can be calculated from these two. For instance, the bulk modulus is related to λ and μ by:

$$K = \lambda + \frac{2}{3}\mu \qquad (2-3)$$

Other important relations are given in table 8-1 in chapter II.

Equation (2-1) together with equation (2-2) give us the clue to compute the elastic moduli of a solid. First, the stresses and strains in the solid are calculated. Then the elastic moduli are inferred by inverting (2-1) and using the definition of the elastic moduli in (2-2) as the components of the stiffness tensor. Although this procedure seems to be straightforward, in practice it becomes cumbersome because calculations of the stress and strain fields within the porous solid are very complex. Besides, a porous solid is no longer isotropic, so instead of computing the intrinsic moduli, we must be content to calculate the average strain and stress fields which give us the effective elastic moduli of the composite material. To clarify this concept, let us write the average stress field in a solid with a volume V *(Hill, 1963)*:

$$\begin{aligned} < \sigma_{ij} > &= \frac{1}{V} \int_V \sigma_{ij} dV \\ < \epsilon_{ij} > &= \frac{1}{V} \int_V \epsilon_{ij} dV \end{aligned} \qquad (2-4)$$

These volume integrals can be converted to surface integrals by using the Gauss' theorem. Then, (2-4) becomes:

$$\begin{aligned} < \sigma_{ij} > &= \frac{1}{2V} \int_S (T_i x_j + T_j x_i) dS \\ < \epsilon_{ij} > &= \frac{1}{2V} \int_S (n_i u_j + n_j u_i) dS \end{aligned} \qquad (2-5)$$

which give the average stress and strain in terms of the components of the traction T_i and the displacement u_i on the surface of the region occupied by the volume V. The x_i denotes the spatial coordinate, and n_i is the component of the unit normal vector to the surface. Equation (2-5) tells us that to calculate the effective elastic moduli; it is only necessary to know the tractions and displacements at the surface of the solid. The average stress and strain are linked now by:

$$< \sigma_{ij} >= c^*_{ijkl} < \epsilon_{kl} > \qquad (2-6)$$

where c^* represents the effective stiffness tensor.

In the next sections, we will see that the c^* as well as the average elastic field can also be evaluated using other methodologies.

Another important point to consider is the type of porous material we want to model. Basically, most of the analytical approaches give solutions for solid bodies composed of simple and symmetrical pore spaces like the circular and elliptical cavities. This is due to the fact that the equations that govern the elastic behavior of more complex geometries cannot be expressed in closed form, i.e. analytical solutions are difficult and in many cases impossible to obtain. Then, a previous knowledge of the structure of the solid as well as its petrophysical characteristics is of capital importance to choose the analytical or numerical method that best represents the particular sample analyzed.

3. CLASSICAL METHODS

We will not spend much time on these methods because most of them are old —but not obsolete— so they have been described elsewhere. We have included them for the sake of completeness.

In principle, these methods try to solve the differential equations derived of the basic relations of elastostatic:

The equilibrium equation:

$$\sigma_{ij,j} + F_i = 0 \qquad (3-1)$$

stress-strain relation:

$$\sigma_{ij} = c_{ijkl}\epsilon_{kl} \qquad (3-2)$$

and the strain definition:

$$\epsilon_{ij} = \frac{1}{2}(u_{i,j} + u_{j,i}) \qquad (3-3)$$

subjected to specific phase boundaries and external boundary conditions. Several types of boundary value problems can be defined for a solid according to the kind of data prescribed at the boundaries. Then, a stress boundary value problem is one for which the components of traction T_i are specified at all points of the boundaries while a displacement boundary value problem is one for which the components of displacement u_i are specified at these points. We can also have a problem which combines the two boundary problems. In that case we must solve a mixed boundary value problem.

Methods like those described above have been solved by many authors for the case of simple circular and elliptical cavities embedded in an infinitely elastic isotropic and homogeneous solid. Among other we can cite *Muskelishvili (1953), Sokolnikoff (1956), Landau and Lifshitz (1959), Hill (1963), Timoshenko and Goodier (1970) and Pollard (1973).*

Some of the methods which fall into this category make use of mathematical artefacts to solve the basic elastostatic equations. For instance, a convenient choice of a particular system of coordinates like the curvilinear coordinates *(Timoshenko and Goodier, 1970)* reduces the differential equations for boundary problems of ellipses, hyperbolas and less simple curves. In other cases, one can make use of complex variables to transform the region outside the cavity to the region inside a unit circle and find the appropriate stress function for this simpler geometry. Such a technique is known as conformal mapping *(Muskhelishvili, 1953; Savin, 1961; Timoshenko and Goodier, 1970).*

As it was stated before, most of the solutions obtained by the classical methods are valid only for simple geometries with the exception of the conformal mapping *(Muskhelishvili, 1953)*, where solutions for quasi-triangle shapes can be found. Also, such solutions are only valid for the static case and because they are derived for

isolated pores, they do not take into account the effect of the interactions of the cavities embedded in the solid.

4. DISLOCATION METHODS

The techniques under this category are based in the well known theory of dislocations which has been described by several authors such as *Volterra (1907)*, *Somigliana (1914)*, *Bilby (1950, 1967)*, *Landau and Lifshitz (1959)*, *Bilby and Eshelby (1968)*, and *Weertman (1971)* among others.

We can define a dislocation as the type of defect produced when cuts are made in a medium which is not completely rigid. Then, the two sides of the cut are displaced relative to each other and material is added or removed as necessary. Finally, the cuts are rewelded. The displacement of the cut is called the Burgers vector of the dislocation. We can represent a big straight cut along the y axis as a continuous distribution of small dislocations, each of them represented by an infinitesimal Burgers vector. Now, let's define $U(x)$ as a function that represents the relative displacement of the two sizes of the dislocation and $B(x)dx$ as the number of dilocations with Burgers vectors along dx. $B(x)$ is called the dislocation density function which is then given by $B(x) = (d/dx)U(x)$. This is the simplest case of dislocation, since all the Burgers vectors are parallel to one axis. Because Burgers vectors are all parallel, they do not interact with each other *(Bilby and Eshelby, 1968)*.

The above description is very useful to describe ellipsoidal flat cracks with nonblunted walls where the displacement is concentrated along one axis and most of the Burgers vectors (except in the small edges) are parallel. In the case of real two-dimensional displacements (along two axes), we must introduce density functions for each component of the Burgers vectors and we also must include interaction

terms between non-parallel vectors. Then, the equations we need to solve become very complex and in many cases it is necessary to use a numerical technique as will be shown in a later section. In this section, we will revise a noninteractive dislocation method used by *Mavko and Nur (1978)* to calculate the deformation of nonelliptical thin cracks with aspect ratios much less than one. The main difference with respect to elliptical pores is that the edges of the crack have been tapered. We refer to this particular geometry as the tapered pore.

Tapered pores are more suitables to represent cracks in rocks than elliptical pores because of their more irregular shapes. This is specially true for sedimentary rocks like sandstones where visual inspection and common sense suggest that almost no cracks are ellipsoidal cavities.

We start by representing the shape of the pore by a function $U(x)$ which is given by a polynomial such as $dU(\pm c_0)/dx = 0$, where c_0 represents the half-length of the pore. Also, $U(x)$ must be smooth and nonblunted in the interval $(-c_0 \leq x \leq c_0)$ so most of the Burgers vectors are parallel to the y axis. Then, the dislocation density function is related to the shape of the pore by:

$$B(x) = \frac{dU(x)}{dx} \qquad (4-1)$$

The next derivation assumes that the crack is closed completely by a hydrostatic pressure P, then pressure is reduced and the crack starts to relax. In this case, the normal stress on the plane $y = 0$ due to the closed crack is:

$$\sigma^c(x) = \frac{\mu}{2\pi(1-\nu)} \int_{-c_0}^{c_0} \frac{B(z)}{x-z} dz \qquad (4-2)$$

It also can be shown that the external pressure P and the normal stress $\sigma^c(x)$ are related by the following integral equation:

$$\int_{-c}^{c} \frac{\sigma^c(x) - P}{(c^2 - x^2)^{1/2}} dx = 0 \qquad (4-3)$$

where c is the half length of the pore for a pressure P.

For a given pore shape $U(x)$ with length $2c_0$, equation (4-3) gives the relation between the applied pressure P and the reduced length c.

To derive the deformation of a tapered pore, we represent the shape by:

$$U(x) = 2b[1 - (x/c_0)^2]^{3/2} \qquad (4-4)$$

By solving the integral equation (4-3) we obtain the relation between applied pressure P and pore half length c:

$$c = c_0[1 - \frac{4(1-\nu^2)P}{3\alpha E}]^{1/2} \qquad (4-5)$$

and the deformed shape:

$$U(x,P) = 2b(c/c_0)^3[1 - (x/c)^2]^{3/2} \qquad (4-6)$$

$$\text{for } |x| \leq c$$

Once the deformed shape $U(x,P)$ is obtained, the bulk modulus of the solid can be computed using the reciprocal theorem *(Timoshenko and Goodier, 1970)*. The application of this theorem to a solid that contains N non-interactive pores produces the following relationship:

$$\frac{1}{K_F} = \frac{1}{K_0} - \sum_{i=1}^{N} \frac{d}{dP} \int_{-c_i}^{c_i} U(x,P)dx \qquad (4-7)$$

Let's compare the above results to those obtained by using elliptical geometries. When pressure is applied to an elliptical pore, the length of the crack c remains constant until the external pressure is big enough that the walls of the cavity collapse and the pore virtually disappears. In the interval in which the pore remains opened, the stress-strain relation remains linear. Once the pore closes, it stops contributing to the elastic constant of the solid. The critical pressure at which the pore walls

collapse is proportional to its aspect ratio. In a solid with several populations of elliptical pores —each of them characterized by an aspect ratio— the stress-strain curve looks like that presented in figure 4-1. This curve behaves like a continuous straight line until a whole population disappears. Then there is a jump in the stress-strain curve. The only way to achieve a smoothly varying curve is to have a smooth distribution of aspect ratios. On the other hand, the stress-strain curve for tapered pores is neither linear nor shows jumps because of the shortening of the pore length c as shown in figure 4-1. The inherent nonlinearity in the stress-strain curve resulting from tapered pores offers a more reasonable explanation for the observed nonlinearity at very low pressure. For elliptical pores, the behavior of the elastic moduli at low pressure (from 1 to 100 bars) can be explained only by using unreasonably small aspect ratios (10^{-4} to 10^{-6}). However, because of the shortening of the pore length c, the tapered pores with higher aspect ratios can account for the same elastic behavior. However, since the tapered pores are basically flat thin pores, the internal area does not contribute much to the overall porosity of the solid. Because of the low internal area, tapered pores cannot be used alone to construct a model for rocks with high porosity as in the case of sandstones.

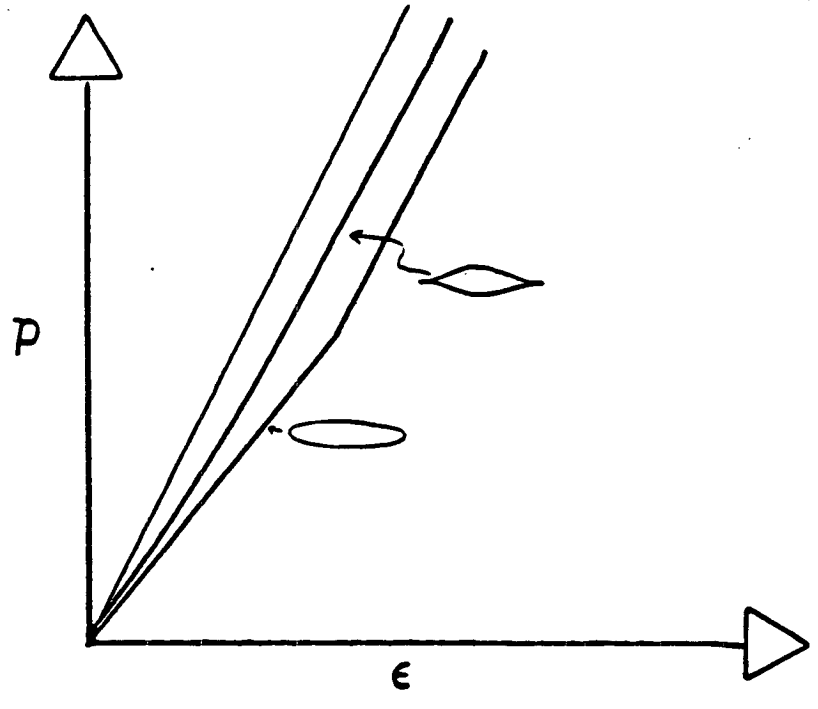

Figure 4-1: Applied pressure versus volumetric strain for a rock with a distribution of pores. The upper curve is for the elastic solid with no pores. The middle curve is for a solid with a uniform distribution (same aspect ratio) of tapered pores. The lower curve is for a solid with uniform distribution of elliptical pores with unstressed dimensions equal to those of the unstressed tapered pores. After *Mavko and Nur (1978)*.

5. SELF CONSISTENT METHODS

The analytical solutions derived in the previous methods can only be applied to dilute concentrations of pores. The pores are sufficiently far apart so the interaction among the inclusions could be neglected. To overcome this limitation, *Hill (1965) and Budiansky (1965)* independently introduced a technique called the self-consistent method in which the effective elastic properties of the solid are calculated iteratively as each pore is embedded. In this way, possible interactions between close pores are simulated.

To apply the method to a porous material, one must calculate the effective elastic properties of an infinity matrix with one inclusion. This is known as the auxiliary problem. Then the self-consistent method presumes that certain averages for the many-inclusion solid, such as the average stress or strain within an inclusion, can be found by replacing the matrix of the auxiliary problem by a medium whose elastic moduli are those of the composite material. Thus the method uses the same elastic solution of the auxiliary problem but accounts for interactions among inclusions.

For a dry elliptical pore the above formulation leads to equations which relate the effective elastic constants to the crack density parameter ε defined by:

$$\varepsilon = (2N/\pi) < A^2/P > \qquad (5-1)$$

where A is the area of the pore and P is the perimeter. N is the total number of pores in the solid. The notation $< \cdots >$ denotes an average value. The crack density parameter is related to the Poisson's ratio by:

$$\varepsilon = \frac{45}{8} \frac{(\nu - \nu_f)}{(1-\nu_f^2)[2 - T(\alpha,\nu_f) + 2\nu(3 + T(\alpha,\nu_f))]} \qquad (5-2)$$

$T(\alpha, \nu_f)$ is an expression including elliptical integrals given in *O'Connel and Budiansky (1974)*. Once the effective Poisson's ratio is calculated using (5-1) and (5-2), the bulk modulus can be found by:

$$\frac{K_f}{K_0} = 1 - \frac{16}{9}\left(\frac{1-\nu_f^2}{1-2\nu_f}\right)\epsilon \qquad (5-3)$$

A strange property derived from this formulation is evident when the cracks are totally filled with water. In this case, the relation between the effective bulk modulus and the bulk modulus of the matrix is given by $K_f/K_0 = 1$. However, shear motion is possible. This is equivalent to saying that once the rock is fully saturated, the effect of the pore spaces on the compressibility of the rock disappears. This result is contrary to what we observe in rocks *(Nur and Simmons, 1969; Han and Nur, 1986)*. *Bruner (1976)* has suggested that the self-consistent method overestimates the effect that pores have in lowering the elastic moduli because it takes interactions between pairs of pores into account twice. Also, the results are physically unreasonable, predicting negative Young's shear and bulk moduli, and a Poisson's ratio greater than 1/2 for very high ϵ. A modification of the self-consistent method that avoids counting these interactions twice has been outlined by *Henyey and Pomphrey (1982)*. They apply the method to solids with randomly distributed penny-shaped cracks. In general, the equations derived by this approach must be solved numerically. A general review of several forms of self-consistent methods is given by *Cleary, Chen and Lee (1980)*.

6. GRANULAR METHODS

So far we have described different approaches to the problem of computing the elastic constants of rocks. The solid has been characterized by an elastic matrix with inclusions or cavities embedded in it. However, several types of rocks, especially sandstones, were formed by the cumulation of grains of many different sizes. Due to petrophysical processes acting on these rocks, the grains posses a very rigid structure (grains are not longer loose as in beach sands). In many cases that structure is so stiff and the contact among grains is so strong that its elastic behavior resembles that found in solids made of elastic matrices. Therefore, we may use the elastic approaches describe above to study this kind of granular material.

Many authors have attacked the problem by using more natural approaches in which the properties of the rocks are determined by studying the interactions of spherical packs of particles in contact. Most of these methods are based on the Hertz contact theory *(Hertz, 1881; Timoshenko and Goodier, 1970)*. Many earlier papers treating this problem *(Duffy and Mindlin, 1957; Deresiewicz, 1958)* considered regular packing of identical solid spherical grains. The main prediction of this type of configuration is that the effective elastic moduli are directly proportional to the cube root of the confining pressure. Also, the porosity of the pack depends only on the way the spheres are distributed. Because of the limited ways that a pack of spheres can be symmetrically organized, the effective elastic constants for this model have been only predicted for a few values of porosity.

A more general and realistic approach has been considered by *Brandt (1955)*. In his approach, the granular rock has been modeled by a random packing of spherical particles of different radii. From this model, *Brandt* was able to calculate the effective bulk modulus of a porous rock as a function of the confining pressure, porosity

and fluid saturation. Also, the effective shear stress as well as the sonic velocities are computed assuming that the Poisson's ratio for the rock is known. In all of the papers described above, the grains composing the rock were not bonded together initially. The contact over small areas of the grains was achieved by subjecting the rock to large confining pressure.

Grains in well-cemented and well-consolidated sandstones are already bonded and in many cases the contact area is deformed due to the conditions (pressure and temperature among others) in which the rock was formed. Then the above methods cannot describe accurately the initial conditions of the grains in the rock. *Digby (1981)* calculated the effective bulk and the effective shear modulus of a random packing of identical solid spherical grains. The method also considered the effect of the initial bonding of the particles as indicated in figure 6-1. The deformation of the contact region is small compared with the radius of the grain. Because all the grain are identical, the magnitude of the initial porosity of the aggregate is fixed and independent of the grain size. For randomly stacked spherical particles, the porosity is about 39.2% *(Westman and Hugill, 1930)*. Also the average number of contacts per particle is fixed and equal to 8.84 *(Smith, Foote and Busang, 1929)*. This imposes a limitation on the type of rocks that can be modeled by this approach. Well-consolidated sandstones hold porosity values much lower than those presented by this model. Figure 6-2 shows the effective bulk modulus calculated from this model and the data for a sample of Fontainebleau A sandstone (see chapter III) as a function of confining pressure. The adhesion radius B which is the ratio between the adhesion region b (figure 6-1) and the particle radius R was 0.02. The first thing to note is that the magnitude of the bulk modulus in the model is much lower than the sample bulk modulus. However, the relative change in bulk modulus from 0 to 225 bars is smaller than the change observed in the Fontainebleau A sample.

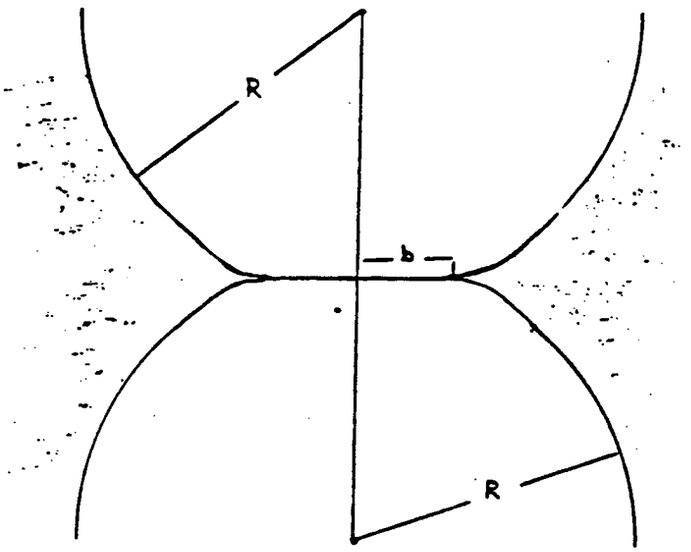

Figure 6-1: Cross-section of the surface profile of two spherical particles in contact. b indicates the radius of contact while R indicates the radius of curvature of the spheres.

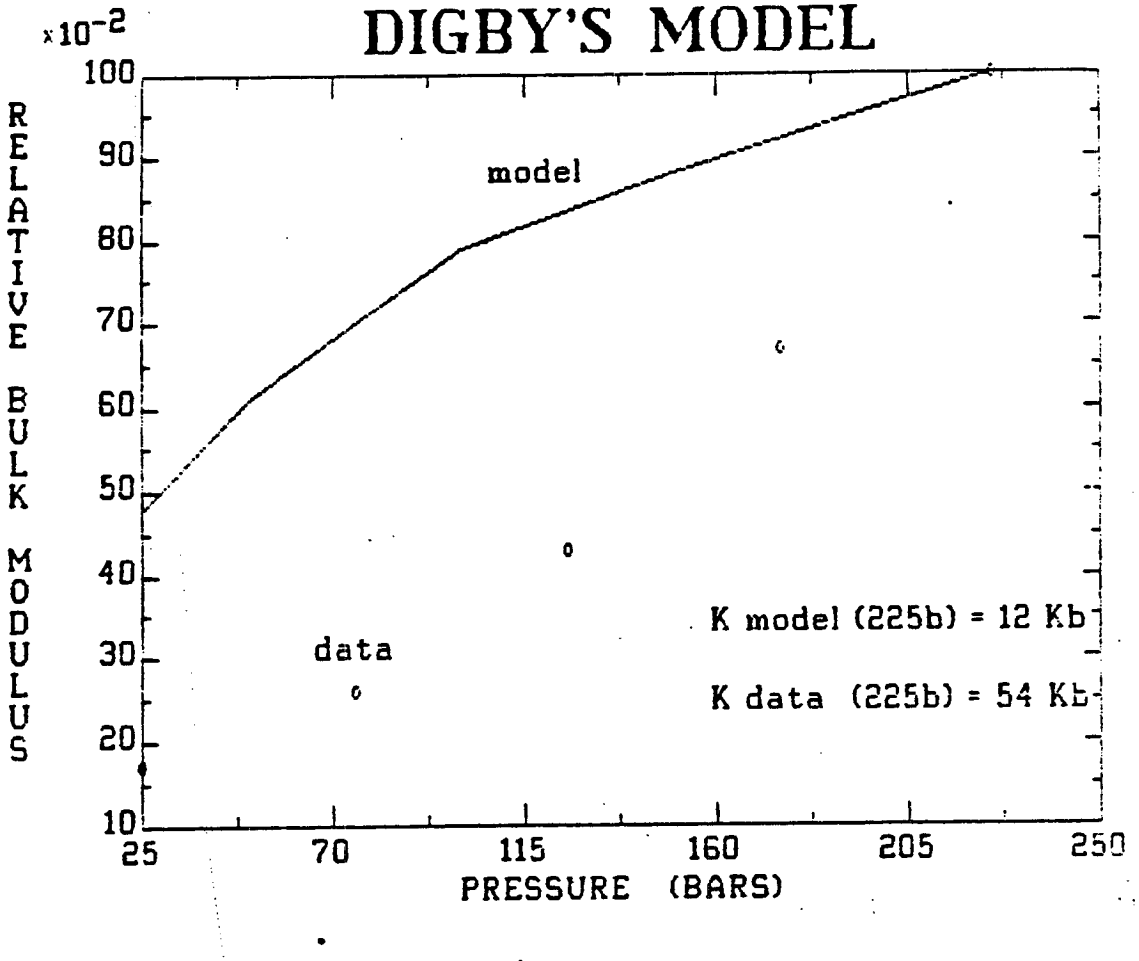

Figure 6-2: Relative bulk modulus for the Fontainebleau A sandstone (open circles) and the *Digby* model (solid line). The magnitudes of the absolute bulk modulus (in kilobars) for the sample and model at 225 bars are given at the right lower corner of the plot.

We conclude that although the overall bulk modulus of the model is low, due in part to its high porosity, the structure formed by the random packing of spheres is stiff enough to resist further changes caused by external forces. The data obtained by the Fontainebleau A (porosity of 15.8%) show it to be much less stiff, probably because it possesses very complain pores (among others) embedded in its elastic matrix.

7. NUMERICAL METHODS

In previous sections, the behavior of the elastic moduli in rocks has been analyzed from the analytical point of view, i.e. we have looked for explicit equations that describe such behavior. With the exception of the granular methods, all the approaches have been limited to very simple and regular pore geometries. This is mainly due to the fact that solutions for more complex pores are not available in closed form. This limited set of shapes, however, renders the analytical methods virtually useless for the study of real rocks where we can expect any kind of irregular pore geometries. Nevertheless, we must state that many types of synthetic materials can be accurately modeled by those simple and regular shapes.

To study the elastic behavior of solids with complex pore spaces, we turn to numerical techniques in order to provide the link between microstructure and effective elastic properties. The three best known methods are: *the finite differences method, the finite elements method and the boundary elements or integral method.* In the last few years, the last two methods have been objects of extensive study for which a great number of computer packages are currently available.

In the finite differences method, the differential equations are approximated by difference equations. For instance, let's suppose that a smooth function $f(x)$ is given by a series of equidistant values $f_1, f_2, ..., f_n$ for $x = 0, x = h, x = 2h, ..., x = (n-1)h$.

Then we approximate the derivative df/dx by:

$$(\frac{df}{dx})_{x=0} \approx \frac{f_1 - f_0}{h} \qquad (7-1)$$

The resulting difference equations subjected to specific boundary conditions lead to a system of algebraic linear equations. The solution of the system of equations for the case of elastostatic problems gives us a discrete distribution of the values for the stresses and strains *(Timoshenko and Goodier, 1970)*.

The finite elements method is a technique for solving partial differential equations by first discretizing these equations in their space dimensions. The discretization is carried out locally over small regions of simple but arbitrary shape which are called the finite elements. As in the case of the finite differences method, the discretization of the equations leads to a system of algebraic equations which must be solved to calculate the stresses and strains in a finite number of points. The finite elements technique is described in many texts, for example *Zienkiewicz (1971)*, *Cook (1974)*, *Connor and Brebbia (1976)* and *Smith (1982)*.

To better understand how the finite elements technique differentiates from the finite differences method, let us review a simple elastostatic problem. Figure 7-1 shows an elastic and homogeneous rod with end nodes 1 and 2. The length of the rod is L and u denotes the longitudinal displacement of points on the rod. The rod is subjected to a uniform longitudinal force F. The equilibrium differential equation that describes the system is *(Smith, 1982)*:

$$\kappa A \frac{\partial^2 u}{\partial x^2} + F = 0 \qquad (7-1)$$

where κ is the one-dimension equivalent of the stiffness tensor, and A is the cross-sectional area of the rod.

In the finite elements technique, the variable u is approximated in terms of its nodal values, u_1 and u_2, through elementary functions of the space variable called

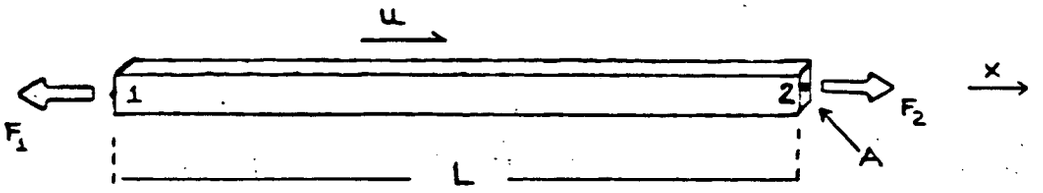

Figure 7-1: Sketch of a rod element. The nodes 1 and 2 are at the opposite edges of the rod. Two body forces F_1 and F_2 are acting on the nodes along the x axis. L is the length of the rod, A is the cross section and u is the longitudinal displacement.

'shape functions' which are given by:

$$u \simeq N_1 u_1 + N_2 u_2$$

or using matrix notation:

$$u = (N_1 \;\; N_2) \begin{pmatrix} u_1 \\ u_2 \end{pmatrix} \qquad (7-2)$$

$$\text{for } N_1 = (1 - \tfrac{x}{L}), \text{ and } N_2 = \tfrac{x}{L}.$$

Using (7-2) in (7-1) we have:

$$\kappa A \frac{\partial^2}{\partial x^2} (N_1 \;\; N_2) \begin{pmatrix} u_1 \\ u_2 \end{pmatrix} + F = 0 \qquad (7-3)$$

Then, the partial differential equation has been replaced by a pair of ordinary differential equations in the discretized space variables u_1 and u_2. Now, if we multiply (7-3) by the shape functions and integrate over the element (in this case the rod), we find *(Smith, 1982)*:

$$\kappa A \begin{pmatrix} \frac{1}{L} & -\frac{1}{L} \\ -\frac{1}{L} & \frac{1}{L} \end{pmatrix} \begin{pmatrix} u_1 \\ u_2 \end{pmatrix} = \begin{pmatrix} F_1 \\ -F_2 \end{pmatrix} \qquad (7-4)$$

Solving the system of equations (7-4), the nodal values u_1 and u_2 can be calculated as a function of the rod length and the forces F_1 and F_2 acting on the nodes.

To apply the finite differences and finite elements techniques to a porous solid, the whole body must be covered by a mesh as shown in figure 7-2a. The number of algebraic equations to solve is equal to the number of nodes in the mesh. As a rule of thumb, the finer the mesh, the more accurate the solution. In practical applications, the system of equations turns out to be very large and in many cases sparse *(Portney, 1982)*.

The boundary elements method —which will be described in detail in the next chapter— represents a more attractive approach because the discretization process

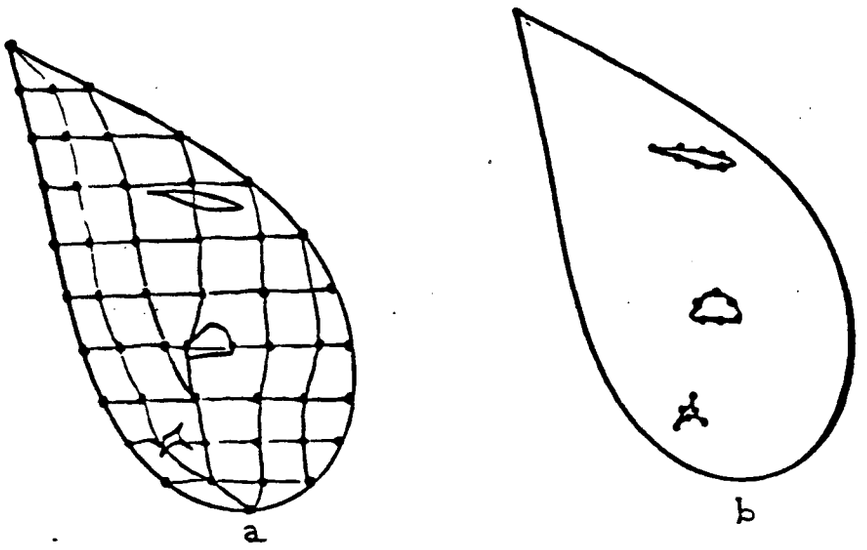

Figure 7-2: (a) Elastic solid covered by a mesh. This mesh is used by the finite elements technique to discretize the corresponding differential equations. (b) In the boundary elements technique, only the boundaries of the region to analyze (the pores in this case) are discretised.

is applied only on the points of interest within the solid, i.e. the surface of the pores (figure 7-2b). Then the system of linear equations is much smaller than the system needed to solve the same boundary value problem by the finite elements technique. Also the system of equations is no longer sparse and the numerical technique becomes much more efficient.

Among the few authors who have used the boundary elements method to solve elastostatic problems, we can cite *Narendran and Cleary (1984)*. They employ a technique based on the highly efficient and physically realistic insertion of mathematically equivalent dislocation distributions to represent crack openings. This method allows us to compute the stress and strain fields in arbitrarily shaped two-dimensional cracks inside inhomogeneous regions as well as their associated stress intensity factors.

8. CONCLUSIONS

Throughout this chapter, we have described some of the current techniques used to calculate the elastic constants in rocks. The present state of the art —based mainly on the analytical methods— attacks this problem by modeling the rock with only one type of pores (elliptical, spherical or tapered). These models are inadequate to represent complex rocks like sandstones where the behavior of the elastic constants is probably controlled by more than one kind of pore.

To obtain a more realistic representation of the pore spaces, we need to consider more complex shapes that resemble what we observe in real rocks. Numerical techniques are the best alternative to investigate the elastic behavior of complex shapes.

In the next chapter, we will describe in detail the principles involved in the boundary elements method and its application to the determination of the elastic

constants in porous rocks. Chapter III will outline the construction of a porous model in which more than a pore geometry is considered.

REFERENCES

Bilby, B. A., 1950, *J. Inst Metals, vol 76.*

Bilby, B. A., 1967, In 'Modern theory in the design of Alloys'. *Iliffle, London.*

Bilby, B. A., and J. D. Eshelby, 1968, Dislocations and the theory of fracture. *Fracture: An Advanced Treatise, vol 1, edited by H. Liebowitz, Academic, New York.*

Biot, M. A., 1956, Theory of propagation of elastic Waves in a fluid-saturated porous solid. I. Low-frequency range, II. Higher frequency range. *J.A.S.A. vol 28 No. 2.*

Brandt, H., 1955, A study of the speed of sound in porous granular media. *J. Appl. Mech., vol 22.*

Bruner, W. M., 1976, Comment on 'Seismic velocities in dry and saturated cracked solids' by Richard J. O'Connel and Bernand Budiansky, and Reply. *J. Geophys. Res., vol 81.*

Budiansky, B., 1965, On the elastic moduli of some heterogeneous materials. *J. Mech. Phys. Solids, vol. 13.*

Clearly, M. P., I. W. Chen, and S. M. Lee, 1980, Self-consistent technique of heterogeneous media. *ASCE Eng. Mech. Div. J., vol 106.*

Connor, J. J. and Brebbia, C. A., 1976, Finite element techniques for fluid flow. *Newnes-Butterworth, London.*

Cook, R. D., 1974, Concepts and applications of finite element analysis. *Wiley, New York.*

Deresiewicz, H., 1958, Stress-strain relation for a simple model of a granular medium. *J. Appl. Mech., vol 25.*

Digby, P. J., 1981, The effective elastic moduli of porous granular rocks. *J. Appl. Mech., vol 48.*

Duffy, J. and R. D. Mindlin, 1957, Stress-strain relations and vibrations of a granular medium. *J. Appl. Mech., vol 24.*

Han, D., and A. Nur, 1986, Effects of porosity and clay content on velocities of sandstones. *Geophysics, in print.*

Henyey, F. S. and N. Pomphrey, 1982, Self-consistent elastic moduli of a cracked solid. *Geophys. Res. Letters, vol. 9.*

Hertz, H., 1881, *J. Math (Crelle's J.), vol. 92.*

Hill, R., 1963, Elastic properties of reinforced solids: some theoretical principles. *J. Mech. Phys. Solids, vol. 11.*

Hill, R., 1965, A self-consistent mechanics of composite materials. *J. Mech. Phys. Solids, vol. 13.*

Landau, L. D., and E. M. Lifshitz, 1959, Theory of Elasticity. *Addison-Wesley, Reading, Mass.*

Mavko, G., and A. Nur, 1978, The effect of nonelliptical cracks on the compressibility of rocks. *J. Geophys. Res., vol 83.*

Muskelishvili, N. I., 1953, Some basic problems of the mathematical theory of elasticity. *4th ed., Trans. JRM Rodok Groningen, Noordhoff*

Narendran, V. M. and M. P. Cleary, 1984, Elastostatic interaction of multiple arbitrarily shaped cracks in plane inhomogeneous regions. *Eng. Frac. Mech., vol 19, no. 3.*

Nur, A. and G. Simmons, 1969, The effect of saturationon velocity in low porosity rocks. *Earth Planet. Sci. Lett., vol. 7.*

O'Connel, R. J. and B. Budiansky, 1974, Seismic velocities in dry and saturated cracked solids. *J. Geophys. Res., vol 79.*

Pollard, D. D., 1973, Equations for stress and displacement fields around pressurized elliptical holes in elastic solids. *Math. Geolog., vol. 5, no. 1.*

Portney, M. N., 1982, Elastic moduli of long aligned inclusions in a matrix: analytic theory vs. numerical results. *Report T82-E-30, Amoco Production Company, Research Department, Tulsa.*

Savin, G. N., 1961, Stress concentration around holes. *Pergamon Press, New York.*

Simmons, G., and W. F. Brace, 1965, Comparison of static and dynamic measurements of compressibility of rocks. *J. Geophys. Res., vol 70, No. 22.*

Smith, I. M., 1982, Programming the finite element method with application to geomechanics. *John Wiley & Sons Ltd..*

Smith, W. O., P. D. Foote and P. F. Busang, 1929, Packing of homogeneous spheres. *Physical Review, series 2, vol 34.*

Sokolnikoff, I. S., 1956, Mathematical theory of elasticity. *2nd edn. McGraw-Hill, New York.*

Somigliana, C., 1914, *Rend. Circ. Accad. Lincei, vol 24.*

Timoshenko, S. P., and J. N. Goodier, 1970, Theory of elasticity. *3rd edn. McGraw-Hill, New York.*

Toksöz, M. N., and C. A. Cheng, and A. Timur, 1976, Velocities of seismic waves in porous rocks. *Geophysics, vol 41, No. 4.*

Volterra, V., 1907, *Am. Ecole Norm. Super. vol 24.*

Watt, J. P., G. F. Davies, and R. J. O'Connel, 1976, The elastic properties of composite materials. *Rev. Geophys. Sp. Phys., vol. 14.*

Weertman, J., 1971, Theory of water-filled crevasses in glaciers applied to verti magma transport beneath oceanic ridges. *J. Geophy. Res., vol. 76, no. 5.*

Westman, A. E. R. and H. R. Hugill, 1930, The packing of particles. *J. Am. Ceram. Soc., vol 13, no. 10.*

Winkler, K. W., 1983, Frequency dependent ultrasonic properties of high-porosity sandstones. *J. Geophys. Res., vol 88, No. B11.*

Zienkiewicz, O. C., 1971, The finite element method in engineering science. *McGraw-Hill, London.*

CHAPTER II

COMPUTING DEFORMATION AND ELASTIC CONSTANTS IN ROCKS USING A BOUNDARY ELEMENTS TECHNIQUE: THE DISPLACEMENT DISCONTINUITY METHOD

1. INTRODUCTION

Although two-dimensional elastic problems have been studied for many years, they have been limited to a few rectilinear pore geometries in homogeneous and inhomogeneous media (*Sokolnikoff, 1956; Billby and Eshelby, 1968; Timoshenko and Goodier, 1970; Mavko and Nur, 1978*). This is due to the fact that solutions for more complex shapes are generally not available in closed form. These simple solutions are clearly inadequate to describe the elastic behavior of porous rocks where we can expect a broad distribution of pore sizes with irregular shapes. An accurate approximate solution then must be found, using a numerical technique. Finite elements is perhaps the most used technique to solve such problems. However, that method is time and memory consuming since it requires that the solution must be found throughout the whole region where the pores are embedded. In this study we use a numerical technique called the boundary elements method. This method has the main advantage of computing the solutions only on the boundaries of the pores and consequently, it leads to a more compact and efficient algorithm.

This study will be concentrated in the application of a boundary elements method (sometimes known as the displacement discontinuity method), to the problem of the deformation of arbitrarily shaped pores embedded in an elastic solid, and under the influence of external stresses. To test the numerical algorithm, some interesting results are compared with existing results, for the special cases where those are available in the literature.

The study of the deformation of irregular pores can be very useful in obtaining a clearer vision of the behavior of pores and cracks in real rocks, as individual entities, instead of getting some average values over the whole material. Then, we use these results to calculate some of the effective elastic properties of porous rocks, for example: the elastic moduli, seismic velocities and elastic stress concentrations.

2. METHOD OVERVIEW

The boundary elements method is a numerical technique used to solve boundary value problems in a very efficient way. Although the method is not new, it is not very well known. This perhaps is due to the fact that many people have dedicated so much time to improving other numerical methods, for example, the finite differences and the finite elements for which a great amount of software packages are currently available. Also, most of the boundary elements programs which have been written in the past are only useful to solve very specific problems and then it is not clear how can they be extended to solve other types of problems. However, once the basis of the method is understood, it is clear that it can be applied to solve a wide range of problems in the physical sciences in a more efficient way than traditional numerical methods. We can cite many areas where the boundary elements method has been successfully applied such as heat flow *(Chang et al., 1973)*, viscoelasticity *(Rizzo and Shippy, 1971)* and elastodynamics *(Cole et al. ,1978)*.

Although our intention is to employ the boundary elements technique to solve specific problems, we will try to keep the method as general as possible. In sections 3 and 4, we will follow very closely the general outline presented by *Crouch and Starfield (1983)* in their excellent book, with emphasis on the physical meaning of the method, skipping most of the algebraic manipulations.

In the rest of this section, we will present an overview of the technique. Suppose

that we are interested in comp e (i.e. internal str
strain fields) of a cavity C em c solid, which is su
to specific boundary condition e an auxiliary curve
2-1b) which is the image of C e of N ed linear
elements. Let us assume that the elastic response of a lin ubjected
to an external field is known (i.e. the analytical equatio cribe the
stress and strain fields at any point outside of the element). s solution
in hand, we add the response of the N elements acting over the midpoint of a particular element. This addition is warranted by the fact that the governing partial differential equations are linear. At this point, a question arises: what should be the strength of each element? Although we do not know these strengths, we know, via the boundary conditions on C, what their combined effect should be. Now applying the same procedure to the rest of the elements, we can write a system of N linear algebraic equations in which the unknowns are the strengths of each element. From the computational point of view, a boundary elements method leads to a much smaller system of algebraic equations than a finite elements scheme applied to the same problem. Once the elastic response on the boundary is known, we can use that solution to compute the stress and displacement fields at any location of the solid.

The above description suggests that the method can be used to solve other physical problems for which the principle of superposition is applicable. For instance, the wall of the cavity considered in figure 2-1 can be thought of as a line of charges embedded in an external electric field. Then, the interaction between the external electric field and the induced field which is generated by the charged surface, can be studied by mean of a boundary elements method.

In the next section, we will settle the fundamentals of the numerical technique

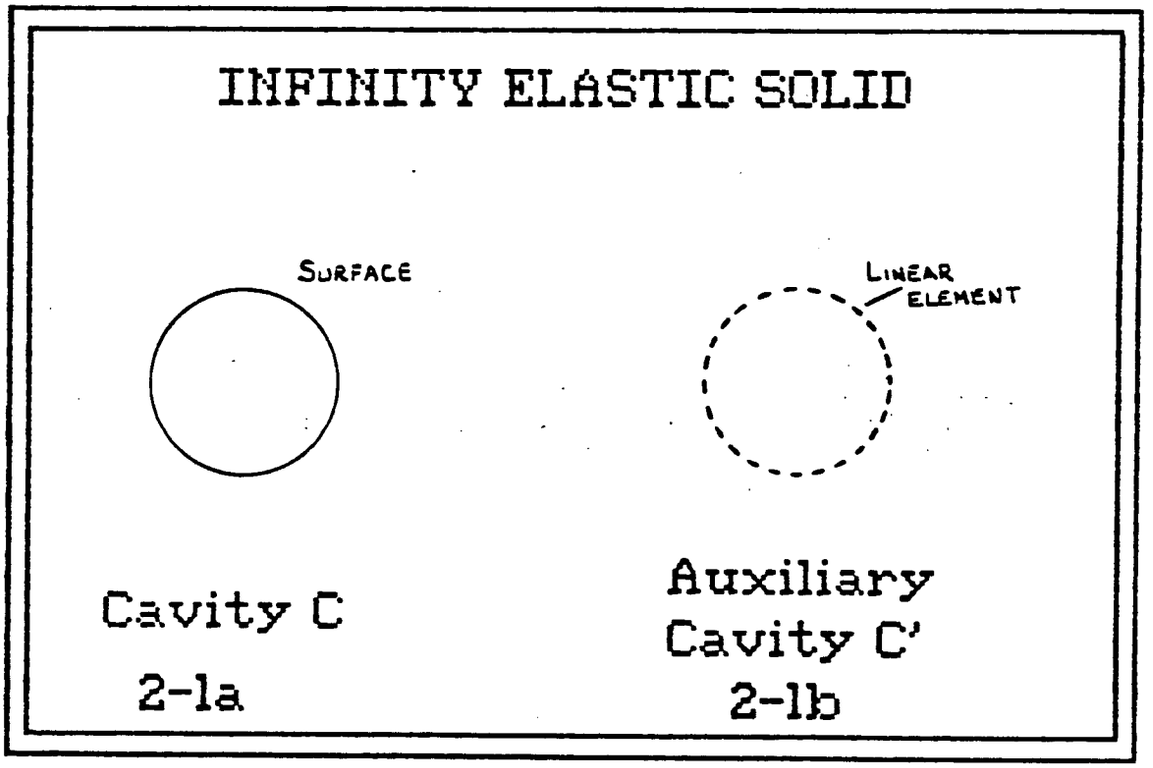

Figure 2-1. a) Cavity C embedded in an infinity elastic solid. b) Auxiliary cavity C' made of N linear elements which is used to represent the cavity C.

from the point of view of the theory of linear elasticity.

3. GENERAL THEORY

Based on the above description we will write a numerical procedure to solve a boundary value problem. Although we will emphasize in elastostatic problems, we will keep the procedure as general as possible so it can be easily adapted to solve a wide range of physical and petrophysical problems.

The first step is to find the solution for a very simple problem which will be used to build a more complex one. Suppose that there is a rectilinear element embedded in an elastic body, which lies on the plane $x - y$. The normal stresses and displacements induced by that element at any location within the solid, can be written in general as:

$$\begin{aligned} \sigma_n(i,j) &= I_{\sigma 1}(i,j)S_1 + I_{\sigma 2}(i,j)S_2 \\ u_n(i,j) &= I_{d1}(i,j)S_1 + I_{d2}S_2 \end{aligned} \qquad (3-1)$$

$$\text{for } i,j = 1,2$$

The subindexes i and j represent the coordinates of the reference system chosen to define the solutions in (3-1). Since we are solving a plane problem, only two coordinates are needed. It is important to note that we should choose the coordinate system that best describes the symmetry of the particular problem (i.e., cartesian, cylindrical, etc.). S_1 and S_2 represent external perturbation factors from which the local stresses and displacements in (3-1) will derive their strengths or magnitudes. These factors can be visualized as applied forces, external stresses or prescribed displacements. Then the solution in (3-1) is the response of the system to that perturbation. In our case, the response will always be linear. The I terms in (3-1) are coefficients which depend only on the location and type of the system of coordinates

used to pose the problem and they are independent of the external perturbation. These coefficients are called **influence coefficients or influence functions**. Although we have written (3-1) to represent the response of a rectilinear element due to the perturbation produced by external sources, that type of expression can be generalized in such a way that the elastic response for most problems in linear elasticity can be written as a linear combination of influence coefficients and external perturbations. For a two-dimensional problem that expression takes the form of:

$$r(i,j) = I_{r1}(i,j)S_1 + I_{r2}(i,j)S_2 \qquad (3-2)$$

The r represents the response of the system caused by the perturbations S_1 and S_2. Notice that in case the response has more than one component (for example normal and shear stresses), equation (3-2) must be written in matrix form.

As an example, let us consider a very simple but illustrative physical situation known as the Kelvin's problem *(Sokolnikoff, 1956)*. In this problem a line of concentrated force is applied along the z axis in an infinite elastic solid as shown in figure 3-1. The components of the force are F_x and F_y. The solution for the displacement in the y direction is given by:

$$u_y = \frac{F_y}{2\mu}[(3-4\nu)g - y\frac{\partial g}{\partial y}] + \frac{F_x}{2\mu}[-x\frac{\partial g}{\partial y}] \qquad (3-3)$$

where:

$$g(x,y) = \frac{-1}{4\pi(1-\nu)} \ln\sqrt{(x^2+y^2)}$$

μ and ν are respectively the shear modulus and Poisson's ratio of the solid. Com-

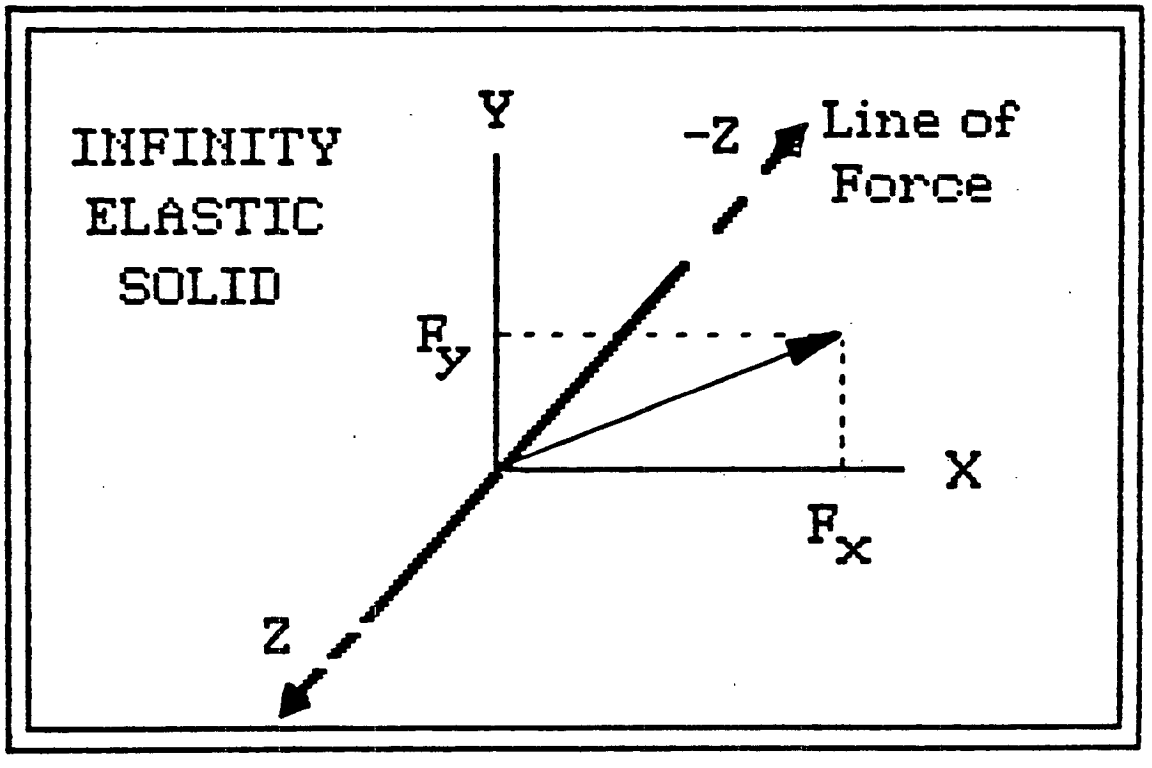

Figure 3-1. Line of concentrated force along the z axis and embedded in an infinity elastic solid. The components of the force (F_x and F_y) are acting on the plane $x - y$.

paring (3-2) and (3-3) we have that:

$$S_1 = F_x$$

$$S_2 = F_y$$

$$I_{r1} = \frac{1}{2\mu}[-x\frac{\partial g}{\partial y}]$$

$$I_{r2} = \frac{1}{2\mu}[(3-4\nu)g - y\frac{\partial g}{\partial y}]$$

As we can see, the influence coefficients can be thought of as the Green functions of the system, and the S terms are the perturbations which control the strength of the displacements.

As was pointed out before, the influence coefficients depend on the spatial location of the elements with respect to the system of coordinates used to define the problem. If we change the orientation of the elements with respect to the fixed system of reference using a translation, rotation or a combination of both, the functional form of the influence coefficients will also change. However, since the influence coefficients are basically geometric entities, we can compute the new coefficients in terms of the old ones by means of simple coordinate transformations *(Crouch and Starfield, 1983)*. We can better understand that property by saying that the influence coefficients are also the elements of a tensor. A tensor can be defined in a new coordinates system, using rotation and translation transformations *(Sokolnikoff, 1956)*.

With these concepts in mind, we can continue to develop the numerical method. Suppose that we have a cavity embedded in an infinitely elastic solid as shown in figure 3-2a. Now we draw an auxiliary cavity as shown in figure 3-2b and we divide its surface in N linear elements. These elements are small enough so they follow the contour very closely. The walls of the cavity are subjected everywhere to particular boundary conditions. These boundary conditions can be expressed

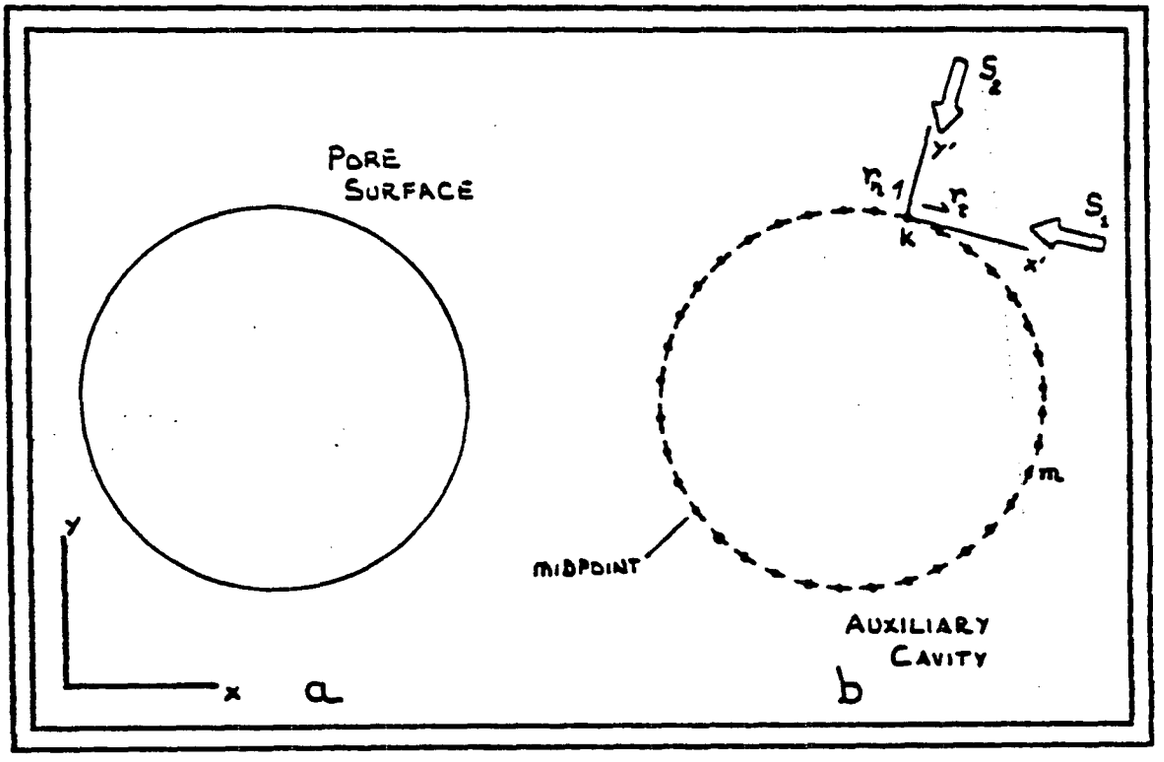

Figure 3-2. a) Cavity embedded in an infinity elastic solid. Attached to the solid, there is a system of coordinates (lower left corner). b) Auxiliary cavity made of N linear elements. Attached to the element k, there is a local system of coordinates. The x' axis is normal to the element while the y' axis is perpendicular to it. r_n and r_s are respectively the normal and shear responses of the system at k. S_1 and S_2 indicate the perturbation terms. Boundary conditions are also defined along the pore surface. Midpoints are indicated by dots within each element.

in term of external stresses, prescribed displacements of the external surface of the cavity or both. Now, we will focus our attention on the particular element k in figure 3-2b. We will place a local coordinate system to that element so we can measure the amount of rotation and translation suffered by the element with respect to a fixed coordinate system attached to the solid. The next step is to superimpose the response produced by every single element at the midpoint of the element k. This procedure is repeated for every element on the contour and for every component of the response. Then, the actual response (two components) of the system can be written as:

$$\begin{aligned} r^1\rfloor_k &= \sum_{m=1}^{N} I_{km}^{11} S_m^1 + \sum_{m=1}^{N} I_{km}^{12} S_m^2 \\ r^2\rfloor_k &= \sum_{m=1}^{N} I_{km}^{21} S_m^1 + \sum_{m=1}^{N} I_{km}^{22} S_m^2 \end{aligned} \qquad (3-4)$$

$$\text{for } k = 1 \text{ to } N$$

The subindexes k and m indicate that the element m is acting on the midpoint of element k. The first superindex of the influence coefficients refers to the component of the response on element k (row), while the second superindex refers to the component of the perturbation acting on element m (column).

Now, the total response of the system at the midpoint of a particular element must be equal to the value of the boundary condition at that specific point. In this way, we construct a system of $2N$ linear simultaneous algebraic equations with $2N$ unknowns, where the unknown values are the perturbation terms S. Once the system of equations has been solved, the values of the perturbation terms S can be used to compute the elastic responses in other points of the solid. In the next section, we will use this methodology to solve a specific elastic problem.

So far, we have applied the foregoing method to solve boundary value problems

in plane bodies. Although many interesting problems in elasticity are essentially two dimensional in nature, there are cases where the approximation of plane strain or plane stress is no longer valid, mainly because stresses and strains acting on the z axis are unconstrained. In that case, we have to deal with three-dimensional tensors to correctly describe the elastic properties of the solid under study. For such problems, it is not clear how can we apply the boundary elements method. This is mainly due to the fact that instead of discretizing the contour using linear unidimensional elements, we have to consider thin surfaces. Then the process of dividing a solid surface in small plane slices becomes cumbersome even for very simple three-dimensional bodies. Also, equations for the system response are no longer easy to write in the form given by (3-2). This does not mean that the boundary elements method cannot be applied to three-dimensional bodies but a more careful methodology is required in order to establish an unambiguous way to discretize the surface of a solid of revolution *(See for example, Brebbia, 1980 and Malbéqui et al., 1986)*. Nevertheless, there are abundant examples in nature, especially in the case of pores in rocks, where the plane strain and plane stress approximation can be used to produce excellent results. For the time being, we will concentrate on solving two-dimensional linear elastic problems under the plane strain approximation.

4. THE DISPLACEMENT DISCONTINUITY METHOD.

In the last section we reviewed the general methodology used to implement a boundary elements program. In this section, we will use that procedure to calculate the stresses and displacements of a two-dimensional pore embedded in an elastic solid, under the influence of external stresses.

In order to find an adequate solution, we must make some fundamental assumptions about the properties of the pores and the solid we want to analyze. First of all, the behavior of the porous solid is totally linear elastic. The solid is isotropic in the sense that the properties of its matrix are essentially the same for any point within the body. Pores are not restricted to specific sizes and their tips can be rounded or very sharp. The reason to request this class of pores is that we are interested in modelling the behavior of real rocks, specifically *sedimentary rocks*. But rocks like sandstones present a broad distribution of pore sizes and shapes. This means that if we want to model complex rocks we have to allow our model to be general but flexible. Last, we will restrict the differential equations which govern the elastic behavior of the solid to obey the plane strain approximation. In this case, the pore will be visualized as a tube as shown in figure 4-1, where the stresses and displacements are unconstrained in the $x - y$ plane but the length of the pore tube along the z axis is fixed.

Because we will be dealing with pores with sharp and narrow tips, we should choose a solution for our linear element so that will not break down when the two surfaces of the pore are close. Fortunately, there is an available solution that takes into account that fact. This solution is based on the displacement discontinuity of a line whose opposing surfaces have been displaced relatively by a constant amount along the line. To better visualize the problem, let's consider a thin linear element

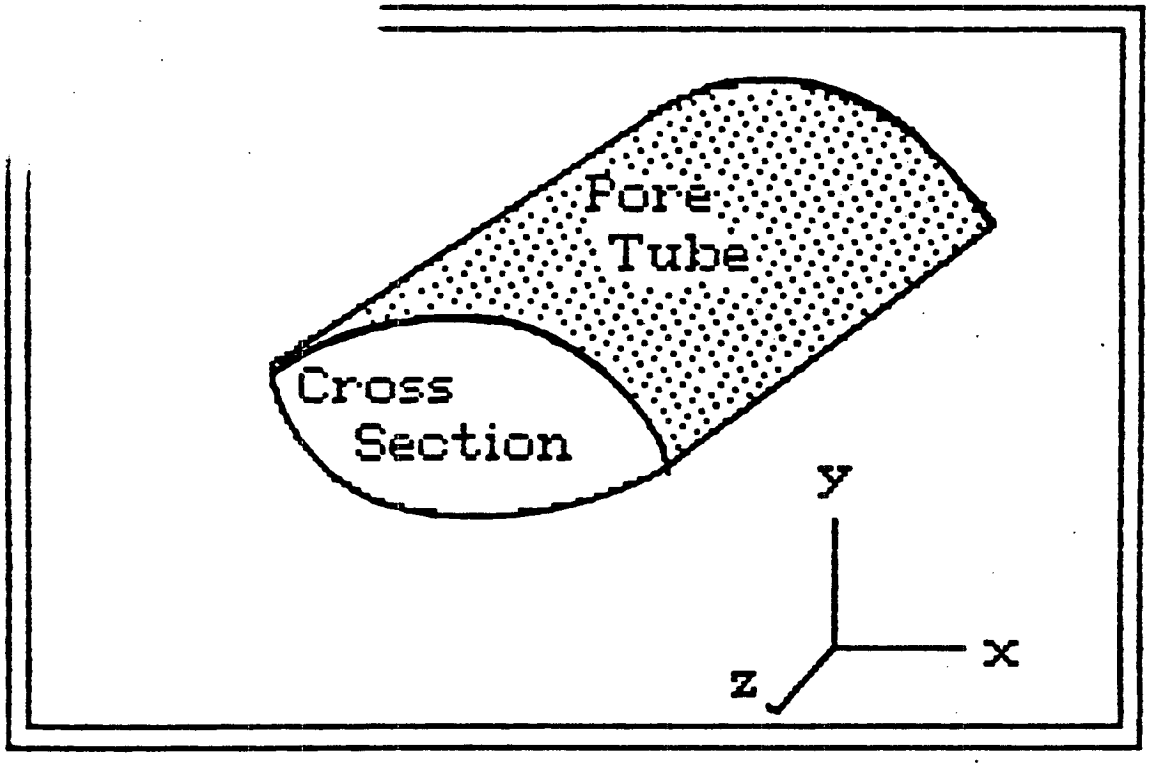

Figure 4-1. Three dimensional representation of a pore. The cross section lays in the $x-y$ plane while the pore tube is defined along the z axis. The cross section can possess different geometrical forms.

of length $2a$ as shown in figure 4-2. We can say that the upper surface is on the positive side of $y = 0$ and is denoted by $y = 0_+$ while the lower surface is on the negative side of $y = 0$ and is denoted by $y = 0_-$. Then the displacement discontinuity is defined as the difference in displacement between the two sides of the linear element and is given by:

$$D_i = u_i(x, y = 0_-) - u_i(x, y = 0_+) \qquad (4-1)$$

where i can be the x or y coordinates.

D_x and D_y are positives in the directions indicated in figure 4-2. To avoid an overlap in the y axis, since the two components of D_y ($+D_y$ and $-D_y$) are pointing in opposite directions, we will consider that the thickness of the element is larger than the magnitude of the displacement D_y.

Solutions for this problem have been found by *Crouch (1976)* and they are given by:

$$\begin{aligned}
u_x &= D_x[2(1-\nu)\frac{\partial f}{\partial y} - y\frac{\partial^2 f}{\partial y^2}] + D_y[-(1-2\nu)\frac{\partial f}{\partial x} - y\frac{\partial^2 f}{\partial x \partial y}] \\
u_y &= D_x[(1-2\nu)\frac{\partial f}{\partial x} - y\frac{\partial^2 f}{\partial x \partial y}] + D_y[2(1-\nu)\frac{\partial f}{\partial y} - y\frac{\partial^2 f}{\partial y^2}] \\
\sigma_{xx} &= 2\mu D_x[2\frac{\partial^2 f}{\partial x \partial y} + y\frac{\partial^3 f}{\partial x \partial y^2}] + 2\mu D_y[\frac{\partial^2 f}{\partial y^2} + y\frac{\partial^3 f}{\partial y^3}] \\
\sigma_{yy} &= 2\mu D_x[-y\frac{\partial^3 f}{\partial x \partial y^2}] + 2\mu D_y[\frac{\partial^2 f}{\partial y^2} - y\frac{\partial^3 f}{\partial y^3}] \\
\sigma_{xy} &= 2\mu D_x[\frac{\partial^2 f}{\partial y^2} + y\frac{\partial^3 f}{\partial y^3}] + 2\mu D_y[-y\frac{\partial^3 f}{\partial x \partial y^2}]
\end{aligned} \qquad (4-2)$$

where:

$$\begin{aligned}
f(x,y) = \frac{-1}{4\pi(1-\nu)}[&y(\tan^{-1}\frac{y}{x-a} - \tan^{-1}\frac{y}{x+a}) \\
&- (x-a)\ln\sqrt{[(x-a)^2+y^2]} + (x+a)\ln\sqrt{[x+a)^2+y^2]}]
\end{aligned} \qquad (4-3)$$

Because the group of equations in (4-2) have the same functional structure as equation (3-2), they can be used to develop a numerical procedure for the boundary

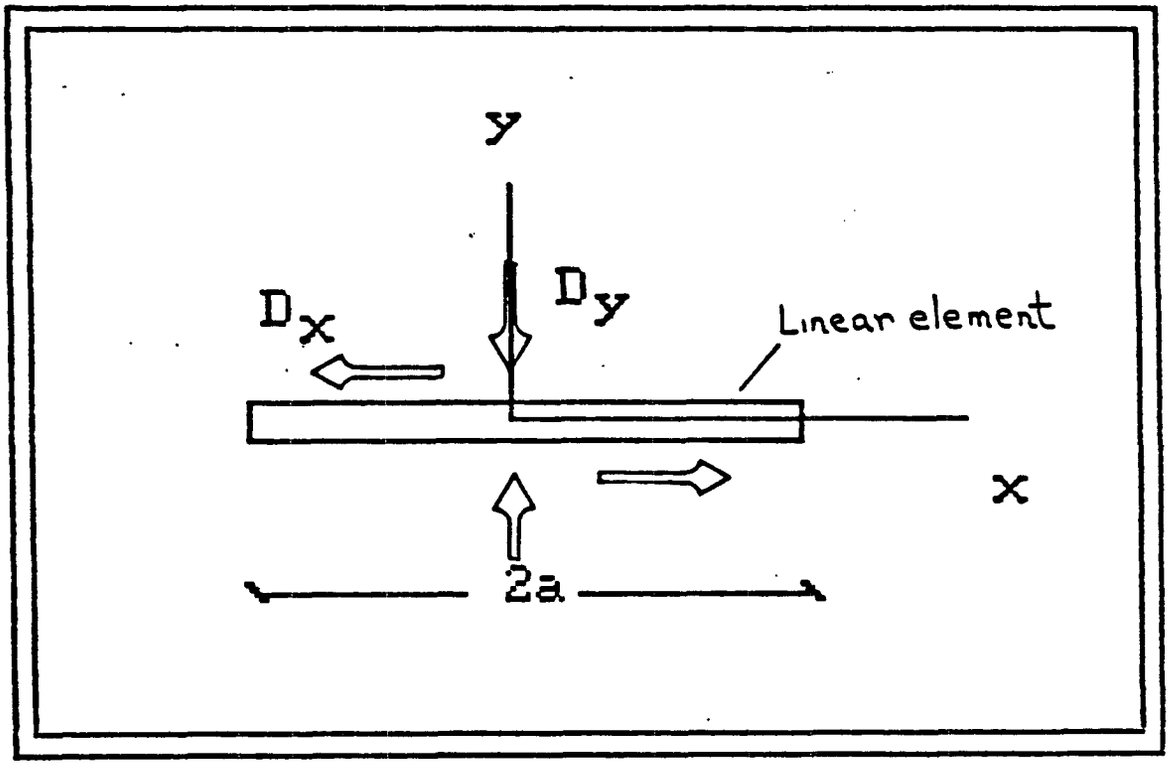

Figure 4-2. Representation of a displacement discontinuity across a linear element. The displacements D_x and D_y are positives in the directions indicated by the arrows. The length of the linear element is $2a$.

elements method. In this case, the perturbation terms are given by the displacement discontinuities D_i along the surface of the cavity while the displacements u_i and stresses σ_{ij} represent the responses of the system. The solutions given by (4-2) are valid only for the system of coordinates defined in figure 4-2. If the element needs to be moved to a new position with respect to the original system of reference, we must use coordinate transformations to obtain the valid influence coefficients for the new position of the element. Because the boundaries of the cavity will be discretized by N linear elements, the position and orientation of each element can be calculated easily with respect to the system of reference used to define the shape.

To compute the displacements or stresses along the boundary of the cavity, we will proceed in the same way as we did in the last section. We will divide the boundary of the cavity into N small linear elements. Again, these elements are small enough so that they match the contour very accurately. Each element represents an elemental displacement discontinuity. The next step is to form a system of linear equations analogous to that given by (3-4). Depending on the type of boundary conditions specified for the particular problem, we can write a system of equations in which the response terms are: *a)* the stresses at the boundary, *b)* the displacements at the boundary, or *c)* a mixed formulation in which either stresses and displacements are prescribed. In the last case, we select the appropriate stress and displacement equations to form a system of $2N$ linear equations with $2N$ unknowns. Applying convenient coordinates transformation on (4-1) *(Crouch and Starfield, 1983)*, we can derive expressions for the normal and shear stresses at the midpoints of every element. Let's denote the normal stress by σ_n and the shear stress by σ_s. Then, the resulting stresses at the midpoint of the k element can be expressed in terms of the superposition of the displacement discontinuity components of the N elements (including the element k) as:

$$\sigma_s\rfloor_k = \sum_{m=1}^{N} A_{km}^{11} D_m^1 + \sum_{m=1}^{N} A_{km}^{12} D_m^2$$
$$\sigma_n\rfloor_k = \sum_{m=1}^{N} A_{km}^{21} D_m^1 + \sum_{m=1}^{N} A_{km}^{22} D_m^2 \qquad (4-4)$$
$$\text{for } k = 1 \text{ to } N$$

where the A factors represent the influence coefficients for the stress equations and are given by:

$$A_{km}^{11} = 2\mu[-\sin 2(\beta_k - \beta_m)\Gamma_1 - \cos 2(\beta_k - \beta_m)\Gamma_2 - \overline{y}(\sin 2(\beta_k - \beta_m)\Gamma_3 + \cos 2(\beta_k - \beta_m)\Gamma_4)]$$

$$A_{km}^{12} = 2\mu[-\overline{y}(\cos 2(\beta_k - \beta_m)\Gamma_3 + \sin 2(\beta_k - \beta_m)\Gamma_4)]$$

$$A_{km}^{21} = 2\mu[2\sin^2(\beta_k - \beta_m)\Gamma_1 + \sin 2(\beta_k - \beta_m)\Gamma_2 - \overline{y}(\cos 2(\beta_k - \beta_m)\Gamma_3 + \sin 2(\beta_k - \beta_m)\Gamma_4)]$$

$$A_{km}^{22} = 2\mu[-\Gamma_2 + \overline{y}(\sin 2(\beta_k - \beta_m)\Gamma_3 - \cos 2(\beta_k - \beta_m)\Gamma_4)]$$

where:

$$\overline{x} = (x_k - x_m)\cos\beta_m + (y_k - y_m)\cos\beta_m$$

$$\overline{y} = -(x_k - x_m)\sin\beta_m + (y_k - y_m)\cos\beta_m$$

x_k and y_k are the coordinates for the midpoint of the element k, while x_m and y_m are the corresponding coordinates for the midpoint of element m. Angles β_k and β_m are measured with respect to the system of reference fixed to the solid. The Γ terms are given by:

$$\Gamma_1 = \frac{1}{4\pi(1-\nu)}\left[\frac{\overline{y}}{(\overline{x}-a)^2+\overline{y}^2} - \frac{\overline{y}}{(\overline{x}+a)^2+\overline{y}^2}\right]$$

$$\Gamma_2 = \frac{1}{4\pi(1-\nu)}\left[\frac{\overline{x}-a}{(\overline{x}-a)^2+\overline{y}^2} - \frac{\overline{x}+a}{(\overline{x}+a)^2+\overline{y}^2}\right]$$

$$\Gamma_3 = \frac{1}{4\pi(1-\nu)}\left[\frac{(\overline{x}-a)^2-\overline{y}^2}{(\overline{x}-a)^2+\overline{y}^2} - \frac{(\overline{x}+a)^2-\overline{y}^2}{(\overline{x}+a)^2+\overline{y}^2}\right]$$

$$\Gamma_4 = \frac{2\overline{y}}{4\pi(1-\nu)}\left[\frac{(\overline{x}-a)}{(\overline{x}-a)^2+\overline{y}^2} - \frac{(\overline{x}+a)}{(\overline{x}+a)^2+\overline{y}^2}\right]$$

The parameter a represents the half length of the linear element.

Once the system (4-4) has been solved for the D_m^1 and D_m^2, we can find the displacements at the midpoints of the elements, forming a system of equations for the displacements which is given by:

$$\begin{aligned} u_s\rfloor_k &= \sum_{m=1}^{N} B_{km}^{11} D_m^1 + \sum_{m=1}^{N} B_{km}^{12} D_m^2 \\ u_n\rfloor_k &= \sum_{m=1}^{N} B_{km}^{21} D_m^1 + \sum_{m=1}^{N} B_{km}^{22} D_m^2 \end{aligned} \qquad (4-5)$$

$$\text{for } k = 1 \text{ to } N$$

and:

$$\begin{aligned} B_{km}^{11} &= [(1-2\nu)\sin(\beta_k-\beta_m)\Gamma_5 + 2(1-\nu)\cos(\beta_k-\beta_m)\Gamma_6 \\ &\quad - \overline{y}(\sin(\beta_k-\beta_m)\Gamma_1 + \cos(\beta_k-\beta_m)\Gamma_2)] \\ B_{km}^{12} &= [-(1-2\nu)\cos(\beta_k-\beta_m)\Gamma_5 + 2(1-\nu)\sin(\beta_k-\beta_m)\Gamma_6 \\ &\quad - \overline{y}(\cos(\beta_k-\beta_m)\Gamma_1 - \sin(\beta_k-\beta_m)\Gamma_2)] \\ B_{km}^{21} &= [(1-2\nu)\cos(\beta_k-\beta_m)\Gamma_5 - 2(1-\nu)\sin(\beta_k-\beta_m)\Gamma_6 \\ &\quad - \overline{y}(\cos(\beta_k-\beta_m)\Gamma_1 - \sin(\beta_k-\beta_m)\Gamma_2)] \\ B_{km}^{22} &= [(1-2\nu)\sin(\beta_k-\beta_m)\Gamma_5 + 2(1-\nu)\cos(\beta_k-\beta_m)\Gamma_6 \\ &\quad + \overline{y}(\sin(\beta_k-\beta_m)\Gamma_1 + \cos(\beta_k-\beta_m)\Gamma_2)] \\ \Gamma_5 &= \frac{1}{4\pi(1-\nu)}[\ln\sqrt{(\overline{x}-a)^2+\overline{y}^2} - \ln\sqrt{(\overline{x}+a)^2+\overline{y}^2}] \\ \Gamma_6 &= -\frac{1}{4\pi(1-\nu)}[\tan^{-1}\frac{\overline{y}}{\overline{x}-a} - \tan^{-1}\frac{\overline{y}}{\overline{x}+a}] \end{aligned}$$

where the B terms represent the influence coefficients for the displacement equations. Notice that the values for the displacement discontinuities D_m^1 and D_m^2 in (4-4) and (4-5) are the same. Then, the displacements u_s and u_n can be calculated by using just the values for the D terms found in (4-4). Also, we can make use of

(4-4) and (4-5) to find the stresses and displacements at any point (exterior to the cavity) within the solid.

At the beginning of this section, it was pointed out that our main goal is to compute the deformation of a cavity (pore) embedded in an elastic solid. This kind of formulation is called the exterior problem. But the above formulation is also employed to solve another type of physical situation known as the interior problem, which describes the elastic behavior of the internal points of a finite solid subjected to an external field. The finite solid can possess any shape and its contour might be subjected to boundary conditions in the same way that the cavity of the exterior problem is. But how can we distinguish between interior and exterior problems?. It can be shown *(Crouch and Starfield, 1983)* that the influence coefficients for both problems are essentially the same except for the diagonal of the B terms which is given by:

$$B_{kk}^{12} = B_{kk}^{21} = 0$$

$$B_{kk}^{11} = B_{kk}^{22} = \begin{cases} -1/2 & \text{(for interior points)} \\ +1/2 & \text{(for exterior points)} \end{cases} \qquad (4-6)$$

Then, using the appropriate influence coefficients we can determine what kind of problem we are dealing with.

5. SYMMETRY CONDITIONS

The formulation we have described so far, applies to arbitrary pore shapes and it leads to a system of $2N$ linear equations with $2N$ unknowns. However, if the pore presents one or several axes of symmetry, we can use this condition to reduce the number of linear equations to solve. This can be accomplished by the fact that a line of symmetry acts as a mirror of one portion of the shape. Then we can include the effect of the image element in the influence coefficients. As an example, let us consider a problem where the lines of symmetries are $x = 0$ and $y = 0$ as shown in figure 5-1. The normal components of the displacement discontinuity for the real and image elements are the same, but the shear components change sign each time a line of symmetry is crossed. These symmetry conditions can be incorporated into the influence coefficients so we actually need to consider just one quadrant (for instance $x, y \geq 0$). Then the number of linear equations reduces to $2N/4 = N/2$. The introduction of symmetry conditions has tremendous repercussion in the numerical efficiency of the boundary element method. Reducing a system of linear equations by half will decrease the processing time by a factor much larger than $1/2$ because the number of arithmetic operations involved in this process decreases more rapidly than in a geometric progression. Also, the memory required to hold both the program and data is reduced substantially as well. Fortunately, pores that we observe in most rocks can be very well modeled by cavities that present at least one axis of symmetry. As an example, figure 5-2a shows a SEM * picture of a crack in a sample of Coconino Sandstone. This pseudo star shape is formed by the space left when the surfaces of four grains are in contact with each other. Since sandstones are formed mainly by the association of granular matter, this star shape is very representative of the kind of pore we have to use to model that type of rock. Figure

* Scanning Electronic Microscope.

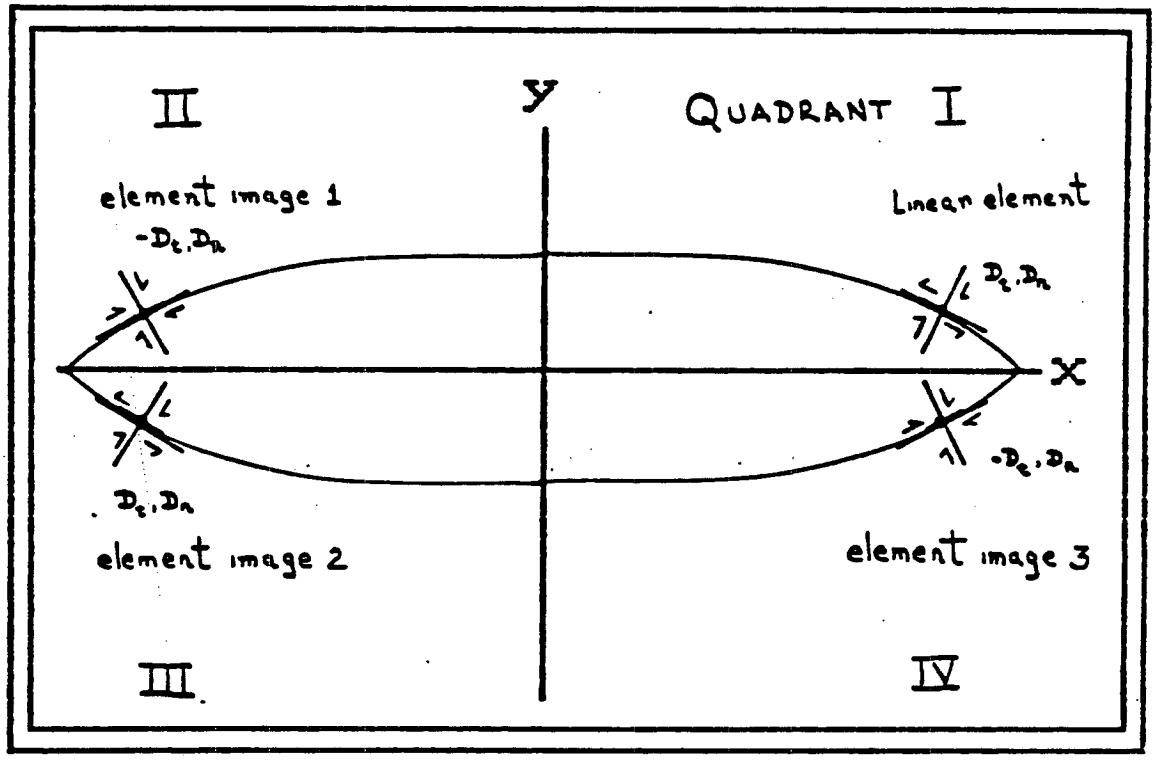

Figure 5-1. Representation of the symmetry conditions in a pore. The x and y axes are lines of symmetry. Notice that the portion of the pores in quadrants II, III and IV are images of the portion which lays in quadrant I. The magnitudes for the D_t and D_n at the particular elements shown, are exactly the same. However, their signs changes as indicated in the figure. Then, the influence coefficients can be re-written so they reflect the sign changes of the displacement discontinuity perturbations at every quadrant and for every element.

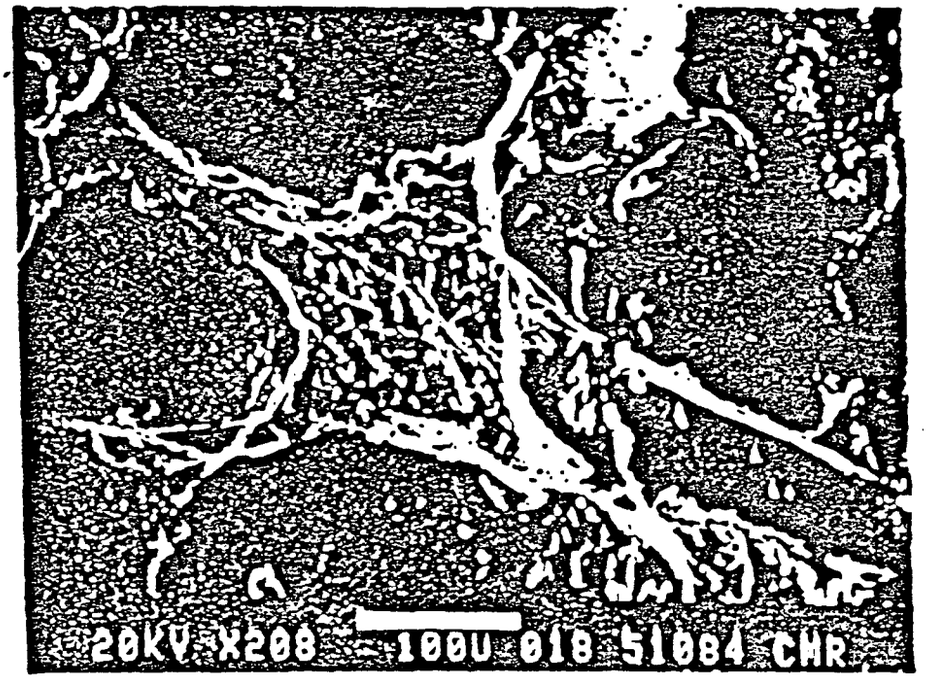

(a)

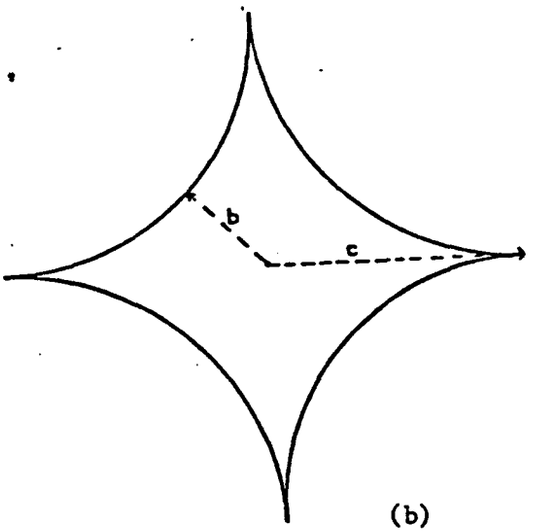

(b)

Figure 5-2. a) SEM microphotograph of a sample of Coconino sandstone. The star shape in the middle of the photo is a pore. The white line at the bottom represents 100 microns. The pore space has been filled with epoxy so it can be easily seen against the black background. b) Representation of a star-shaped pore. Notice the similarities between the pore in (a) and the star-shaped pore.

5-2b sketches a tentative model for a pore that can be used to represent pore spaces in sandstone. This pore presents two axes of symmetry and it can be studied in the context of the boundary elements method, by just discretizing 1/4 of its shape.

6. ANALYSIS OF THE PORE DEFORMATION

In the last sections, we have made a general revision of the boundary elements method. In this section, we will use that technique to study the deformation of a pore embedded in an elastic solid under the influence of external forces. The study of such deformation can help us to get a better picture of the real behavior of pores as individual entities instead of obtaining some average values as the self-consistent approach does (*O'Connell and Budiansky, 1974*). Also, we can use that information to compute other physical parameter, for example the strain energy, variation of porosity, elastic moduli and seismic velocities, hydraulic and electrical conductance, among others. We will discuss more in detail how to compute some of these parameters in a later section.

Although in the last section we did not compute the deformation of the walls of a pore, we did learn how the displacements can be calculated. In particular, the boundary elements method gives us the displacements of the midpoints of each element used to discretize the walls of the cavity. Since the initial shape (i.e. the shape of the pore when no stresses have been applied) is known, then we use the values for the displacements to predict the new spatial location of the midpoints. Therefore, we reconstruct the new shape of the pore by interpolating the new positions of the midpoints. Although this procedure seems to be very simple, in practice it leads to some difficulties that we will analyze next.

The first problem has to do with the magnitude of the stress applied to obtain a specific deformation. In the last section we did not make any comment about

the limits for which the numerical method is valid. However, we did mention that the process is valid only under the context of linear elasticity. In other words, the equations have to obey Hook's law which says that at every point of a linearly elastic body, the components of the stress tensor are linearly related to the components of the strain tensor. This is mostly true when the magnitude of the stress is small. But the question of how small a stress magnitude has to be in order to follow Hook's law must be answered experimentally by plotting the strain-stress relation for different solids. So, before we use a technique like the boundary elements method as discussed here, we must have a clear picture of the elastic response of the solid we wish to analyze. Especially, we are concerned about the elastic behavior of sandstones. *Yale (1984)* and *Mendoza (1985)* have used the concept of linear elasticity to study a variety of sandstones at pressures up to 500 bars without noticing an appreciable nonlinear behavior. In this study, we will be conservative so external pressure will not be considered beyond 250 bars. Nevertheless, most of the important changes in the hydraulic, electrical and elastic properties of sandstones have been observed for the first 100 bars *(Han and Nur, 1986)*.

Another aspect we have to consider in order to obtain the deformation of the walls of the cavity has to do with the symmetry of pore space. Let's suppose that a particular pore holds a line of symmetry which lies on the x axis, so we only need to describe the upper portion. If an external stress is acting parallel to the y axis, the pore is going to reduce in size as its upper walls approach the x axis as shown in figure 6-1a. Eventually the walls will touch the x axis but they can not cross it, because in that case there would be an overlap between the upper and lower walls of the pore as shown in figure 6-1b. To avoid a possible overlap, we have to implement some constraints which forbid the walls of the pores to overlap. In general, the use of constraints introduces those physical aspects of the problem that math leaves out.

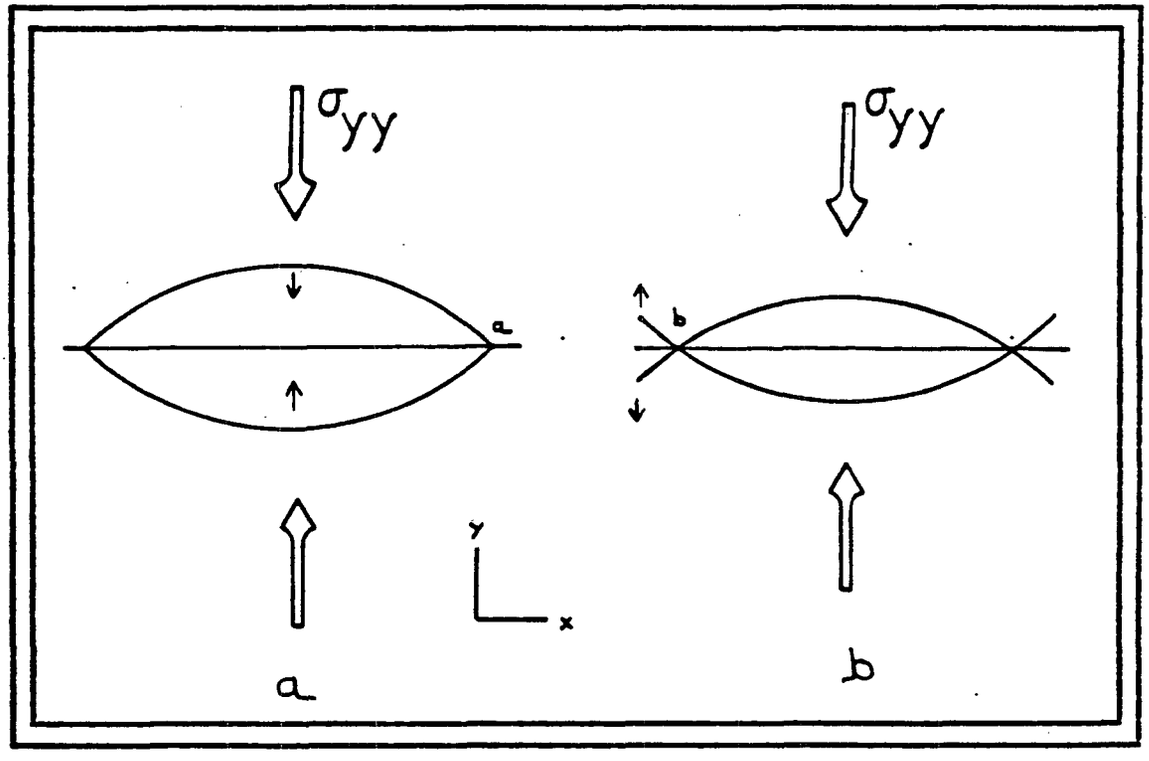

Figure 6-1. a) Representation of the deformation of a pore under uniaxial stress σ_{yy}. The walls of the pore start to collapse in the direction shown by the inner arrows. b) Without boundary constrains, the walls of the pore eventually overlap. This situation is physically impossible.

In our case, we introduce the constraints by impossing the condition that whenever an element touches a line of symmetry to overlap its image, it will be fixed to the point at least in the direction of the overlapping.

The last aspect that we discuss has to do with the discretization of the surface of the pore. Unlike analytical formulations, numerical methods deal only with a finite number of points because of the storage limitations in a digital computer. The numerical procedure used here gives us information only at the midpoints of each element. But what about the other points? We can approximate this problem by saying just that the other points inside an element behave in the same way the midpoint does. In real situations this kind of approximation does not have to be necessarily true but it represents a good starting point. We can always improve the resolution of the method by choosing a shorter element, but reducing the size of the element will decrease the efficiency of the algorithm because it will require more processing time and more memory to store the corresponding system of equations. So it is necessary to balance resolution and efficiency according to the class of problem we are solving and the type of computer available. Next, we will apply the numerical procedure to some well known geometrical shapes for which analytical solutions already exist. These examples will serve to clarify the three aspects previously discussed.

As a first example, we analyze the classic problem of a circular cavity embedded in a linearly elastic solid under the influence of hydrostatic pressure. Solutions for this problem are widely available in the literature (*Sokolnikoff, 1956; Timoshenko and Goodier, 1970; Muskelishvili, 1953*). The first step is to determine the symmetry conditions. Since a circle has a radial symmetry, we co-locate its center in such a way that it coincides with the origin of a cartesian system of reference as shown in figure 6-2. Then the lines $x \geq 0$ and $y \geq 0$ are lines of symmetry because the piece

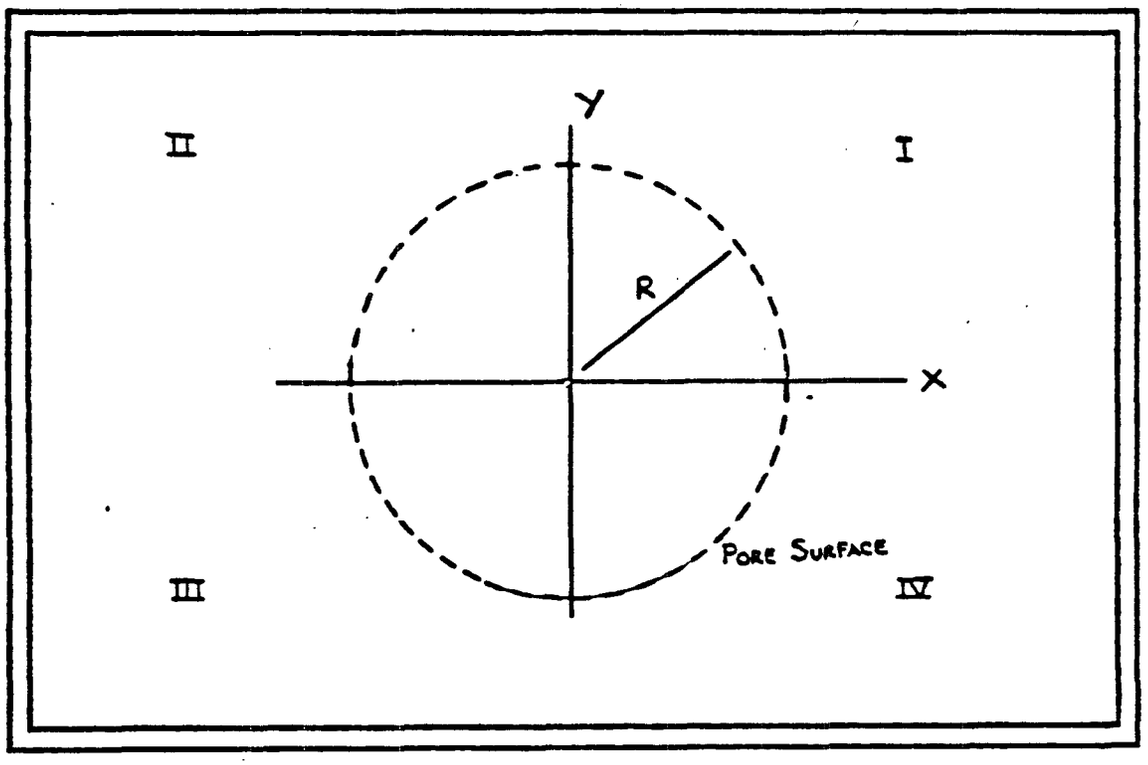

Figure 6-2. Circular pore centered at the origin of a system of coordinates. The radius of curvature of the pore is given by R. The x and y axes are lines of symmetry so the quadrants II, III and IV are images of quadrant I.

of the circle which lies on the first quadrant has its corresponding images in the other quadrants. From the time being, we only work with the 1/4 of circle contained in the first quadrant. The second step is to approximate the circular shape by a set of linear elements. We will start using a poor discretization, then the number of elements will be increased to improve resolution. The numerical results for the deformation will be plotted against the theoretical solution which is given by:

$$R(p) = R_0(1 - \frac{2p(1-\nu^2)}{E\sqrt{2}}) \qquad (6-1)$$

where $R(p)$ indicates the new radius of curvature of the circle for a pressure p. R_0 is the initial radius. ν and E are respectively the Poisson's ratio and Young's modulus of the matrix. Since the circle is pushed by hydrostatic pressure, the deformation is uniform along its surface.

The first discretization consisted of four linear elements distributed uniformly along the surface as indicated in figure 6-3a. In this case, what we have is a 16-sided polygon. Figure 6-4 shows the 'radius of curvature' of the polygon (plus symbols), measured at the midpoints, as a function of applied pressure in bars, compared to the theoretical results (solid line). Notice that although the discretization is not very good, the numerical results are similar to those found by using the analytical solution. The second discretization consisted of seven elements as shown in figure 6-3b. The numerical results obtained by this type of discretization are indicated with stars in figure 6-4. As we expected, the results improve as the length of the elements becomes smaller. The next discretization consisted of 13 elements as shown in figure 6-3c. For this particular model, the resultant polygon resembles very well the circular cavity. The numerical results for this model are plotted with triangles in figure 6-4. These results show a little improvement with respect to those obtained by using seven elements. Increasing even more the number of

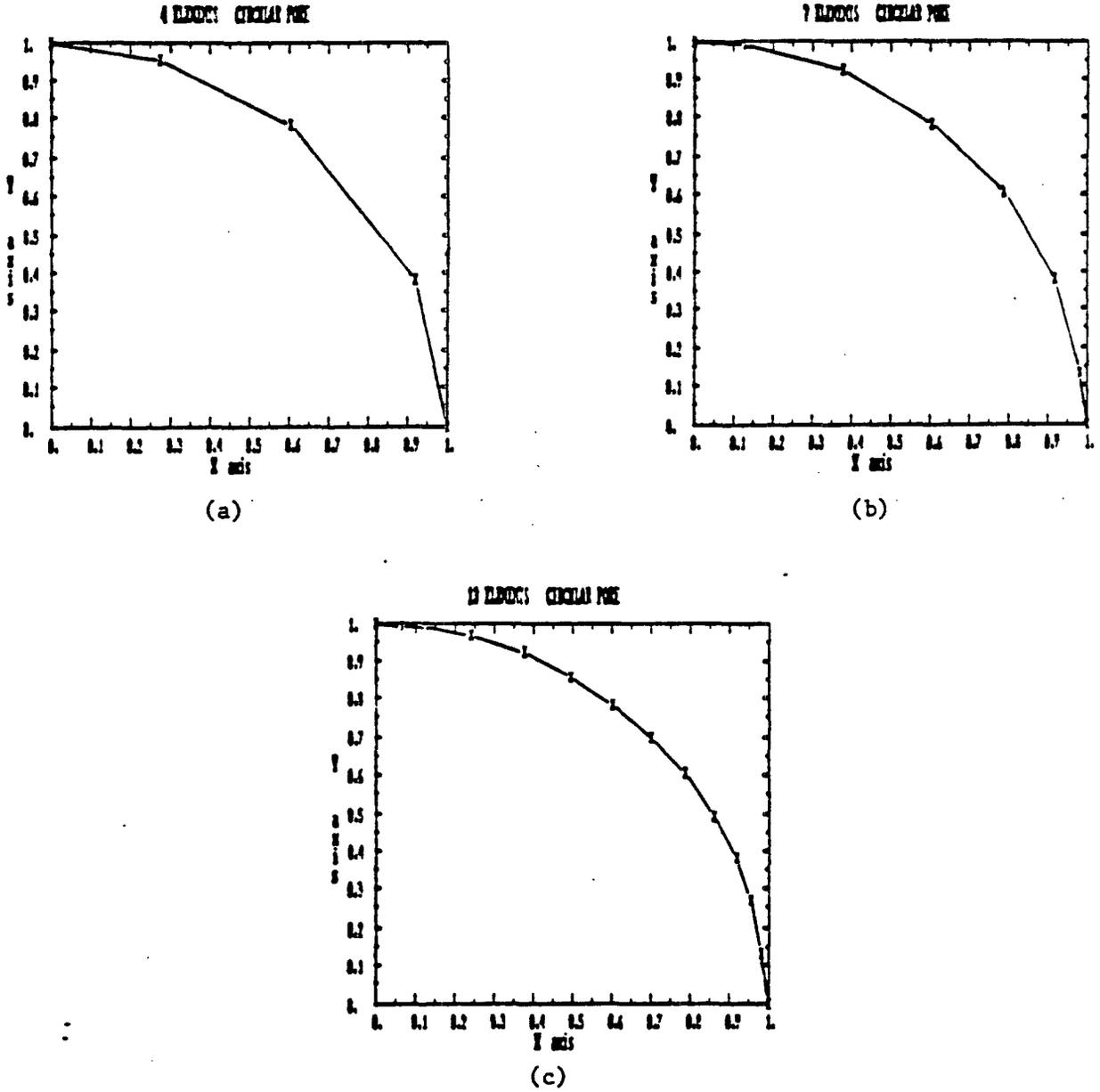

Figure 6-3. a) Discretization for a four elements circular pore. b) A seven elements circular pore. c) A thirteen elements circular pore. Notice how well this discretization resembles a circular arc.

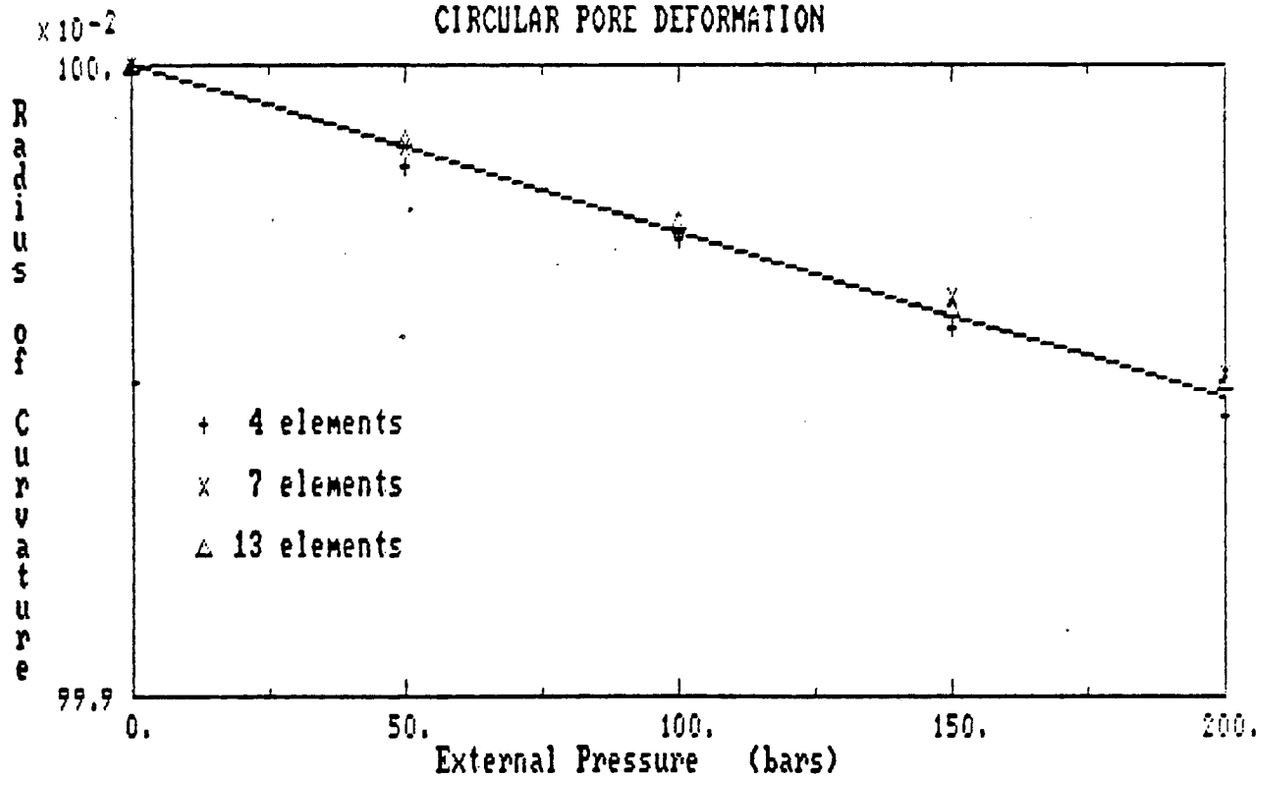

Figure 6-4. Figure represents the results for the deformation of a circular pore model, using the displacement discontinuity method under hydrostatic pressure. The pressure goes from 0 to 200 bars. The line indicates the results predicted by the theoretical equation (6-1). Plus symbols represent the 4 elements model. Stars indicate the results for the 7 elements model and triangles represent the 13 elements model results.

elements leads to smaller improvement of the numerical results, indicating that we have almost reached the maximum resolution of the algorithm. Nevertheless, the maximum difference between numerical and theoretical results for both the seven elements model and the 13 elements model was less than 0.05% which is very small indeed and therefore it is more than acceptable for most applications. The main reason why the circular shape was very well modeled by a small number of elements is due to the fact that such shape represents a very stiff structure and then its deformation is very small and uniform at every point of its surface. Because there are not abrupt changes on the walls of the cavity, even when it is subjected to large stresses, the behavior of the internal points of each element can be very well represented by the motion of their midpoints. Figure 6-5 shows the deformation of a single element for the 13 elements model subjected to an external pressure that goes from 0 to 250 bars. Notice how small the displacements are, compared with the length of the element.

Besides the deformation of the walls of the cavity, there is another physical factor that can be used to help decide what is the minimum number of elements necessary to obtain a satisfactory numerical model. That factor is the internal area of the cavity. This area can be calculated by just integrating the discretized points of the cavity surface. Table 6-1 shows the undeformed areas for the three numerical models, compared with the area of the circle. Notice that although the seven elements model seems adequate to model the deformation of the pore, its corresponding area can represent roughly the internal surface of the circle. This fact tells us that the seven elements model is not very realistic and we must consider a more complex model.

The circular cavity was useful to illustrate the principles involved in the boundary elements method. However its solution is simple and smooth and then, it does

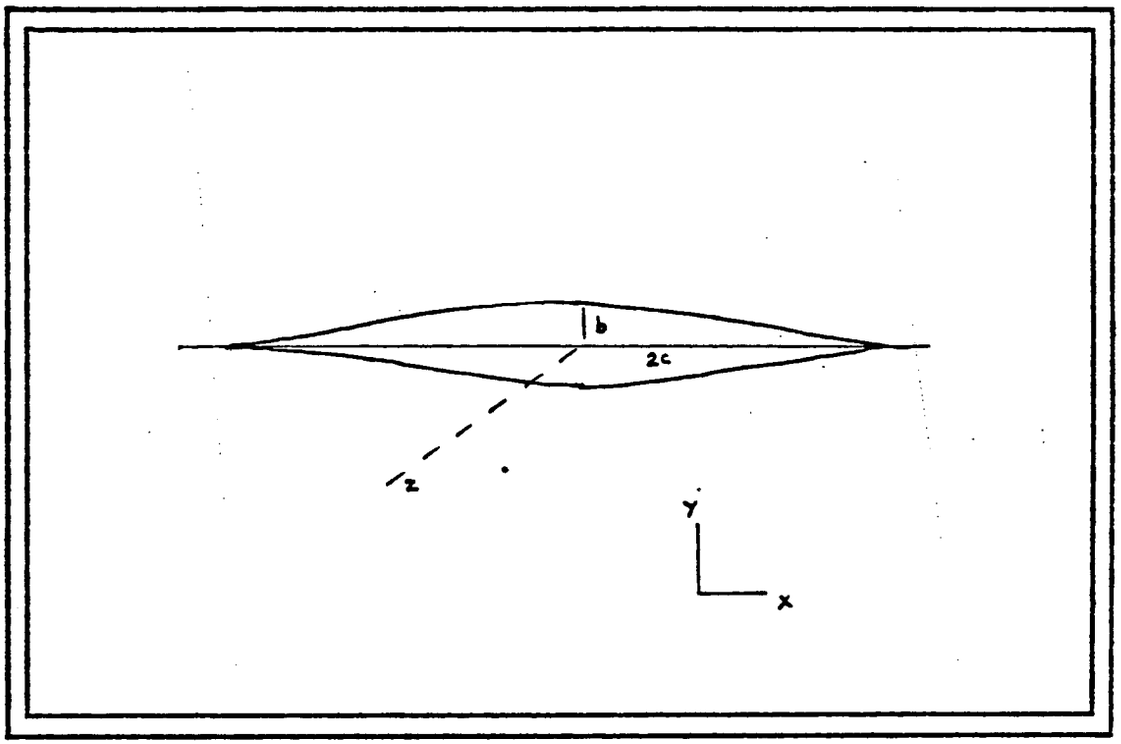

Figure 6-6. Schematic representation of a tapered pore. $2c$ is the length of the pore, b is the half width and z is the length of the pore into the page. The aspect ratio is defined as $\alpha = b/c$. Notice how sharps are the tips of the pore.

take advantage of the symmetry of the pore shape. This can be accomplished by considering the center of the cavity as the origin of the system of coordinates. Then the figure is rotated until the tapered edges are pointing in the direction of the x axis (fig. 6-6). As for the circular shape, it is only necessary to analyze just one quarter of the pore since the other three quarters are the images of the first one.

Now let's assume that the aspect ratio of the pore is $\alpha = 0.002$ which is much less than one. Also, the pore will be subjected to a hydrostatic stress. The next step is to discretize the surface of the cavity. We start with five linear elements as shown in figure 6-7a. The results for this pore model are shown in figure 6-8, where the plus symbols indicate the model results and the solid line indicates the predicted results obtained by using (6-2). As we see, the numerical results are not consistent with the theoretical model. Now we double the number of elements to 10 as shown in figure 6-7b. The numerical results are indicated by stars in figure 6-8, which again are not consistent with (6-2) but they represent an improvement over the five elements model. For a larger number of elements, the solution improves just a little bit until the model reaches 18 linear elements (fig. 6-7c). Then a big improvement in the results can be noted. The results for an 18 elements model are indicated by squares in figure 6-8. As we can see, the numerical results fit the theoretical model fairly well. Figure 6-9 shows the deformation of the walls of the 18 elements model for different pressures. In this model, we have used smaller elements to discretize the pore tips. This obeys to the fact that we are interested in modelling the tips deformation very accurately. Using a uniform discretization along the surface leads to inaccurate results for the deformation of the tips. Increasing the number of elements beyond 18 does not improve the results appreciably. Triangles in figure 6-8 indicate the results for a model of 20 elements, while the resulting of a 40 elements model are represented by squares. Notice that the results for the

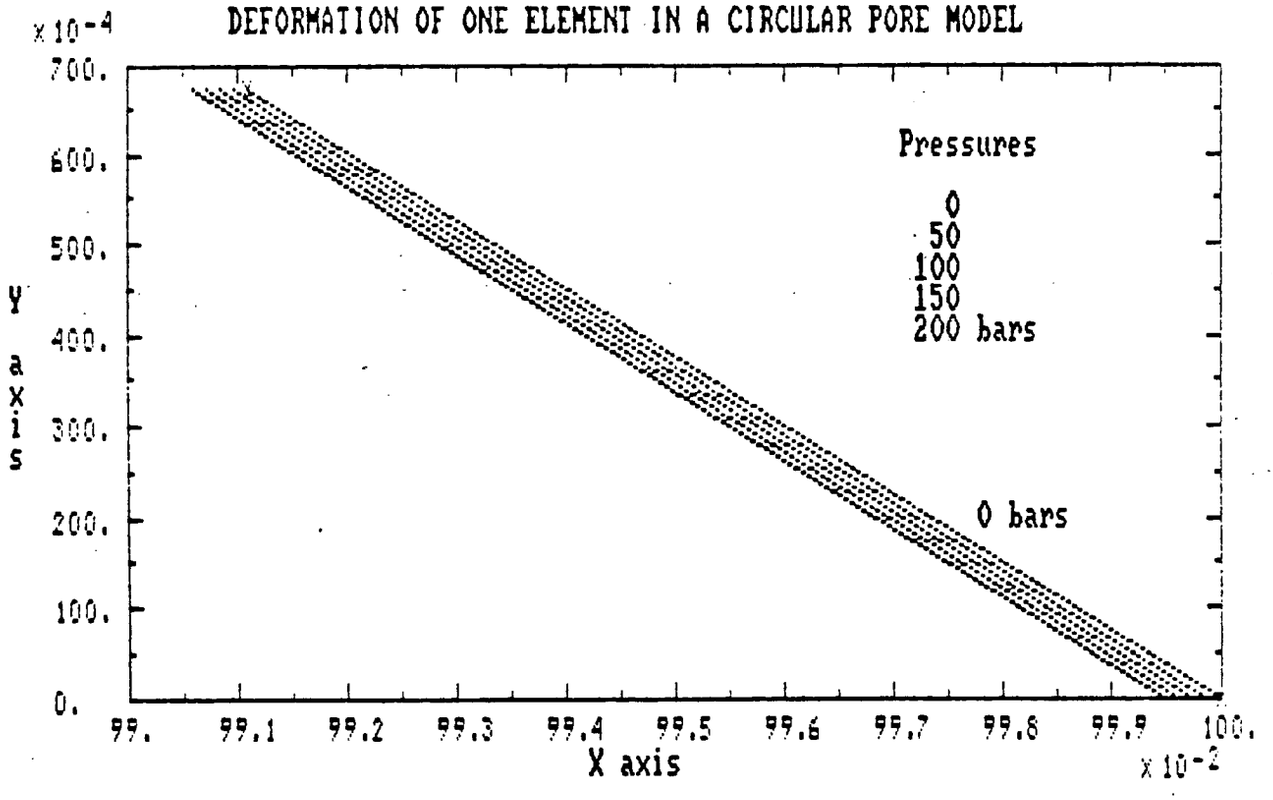

Figure 6-5. Representation of the deformation for a single element in the 13 elements circular model. Hydrostatic pressure goes from 0 to 200 bars. Notice how small is the displacement of the element for the range of pressures used.

TABLE 6-1

FIGURE	AREA (um^*)
circle	3.14
4 elements	2.90
7 elements	3.01
13 elements	3.12

* units of measure

not represent an excellent example to demonstrate the advantages and limitations of the algorithm. Nevertheless, a circular pore is a type of structure we have to include in a realistic model for sedimentary rocks because as *Yale (1984)* has pointed out, most of the porosity in sandstone is concentrated within very stiff structures. Next, we shall consider a more complex pore geometry. Instead of modelling elliptical pores which are unrealistic representations of pore space in sedimentary rocks (*Mavko and Nur, 1978*), we will examine the behavior of a broad class of two dimensional nonelliptical cavities known as tapered pores. The deformation for this class of structure has been obtained by *Mavko and Nur (1978)* using the well-developed theory of elastic dislocations (*Landau and Lifshitz, 1959; Bilby and Eshelby, 1968; Delameter, 1974*). A sketch of the geometry for this type of pore is presented in figure 6-6. Let c_0 be the half length of the pore and b its half width. Then the aspect ratio is defined as $\alpha = b/c$. We will consider only noninteracting, flat planar cracks with aspect ratio $\alpha \ll 1$. Under the above assumptions, we can write the deformation of the half length as a function of applied pressure p as:

$$c(p) = c_0\left(1 - \frac{4p(1-\nu^2)}{3\alpha E}\right)^{1/2} \qquad (6-2)$$

The first step is to choose a convenient system of reference so that we can

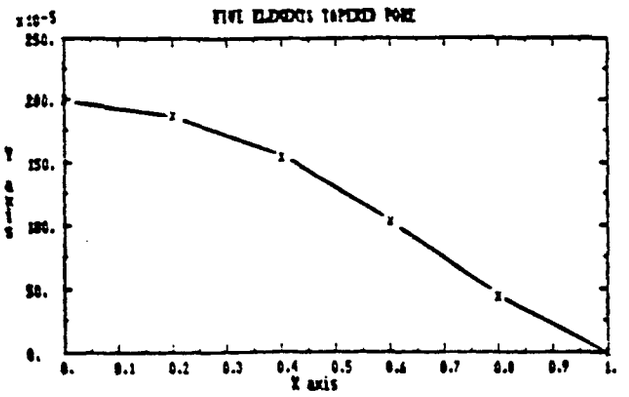

(a)

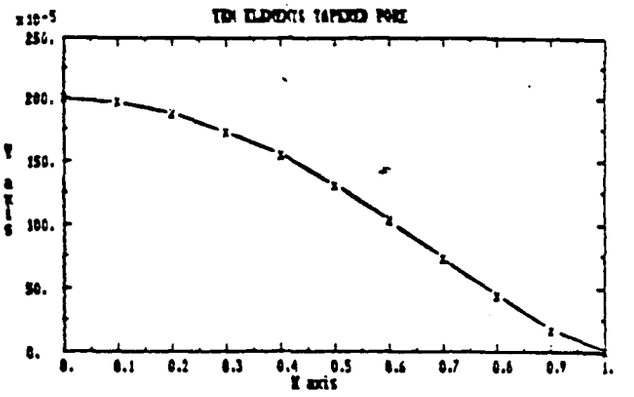

(b)

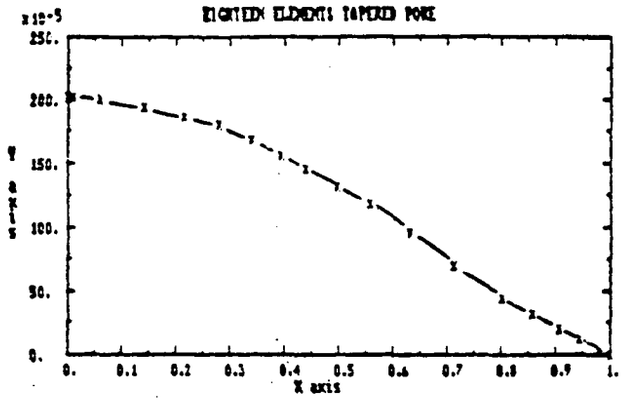

(c)

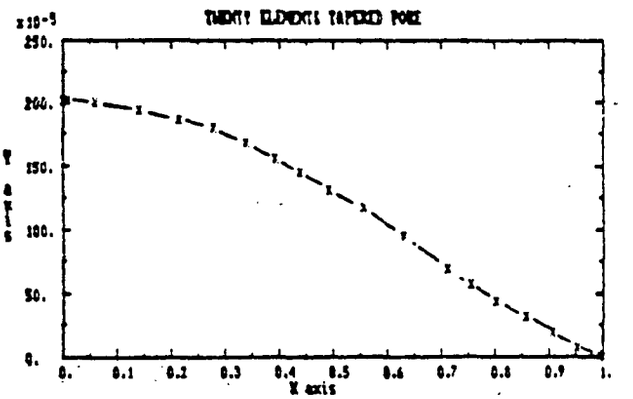

(d)

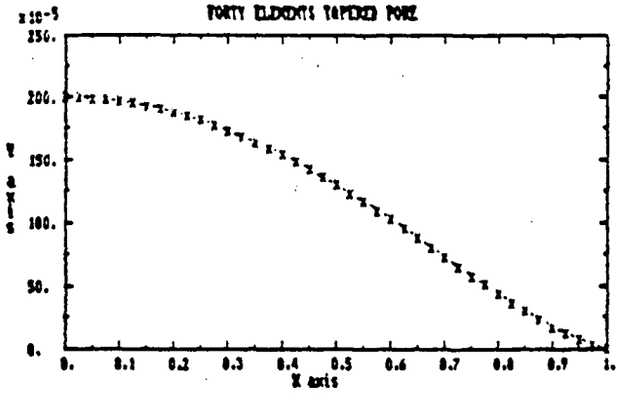

(e)

Figure 6-7. a) Figure represents a discretization for a five elements tapered pore. b) A ten elements tapered pore. c) A eighteen elements pore. d) A twenty elements pore and e) a discretization for a forty elements pore. Notice that small tip elements have been used in the eighteen and twenty elements model to increase the accuracy of the deformations at such points.

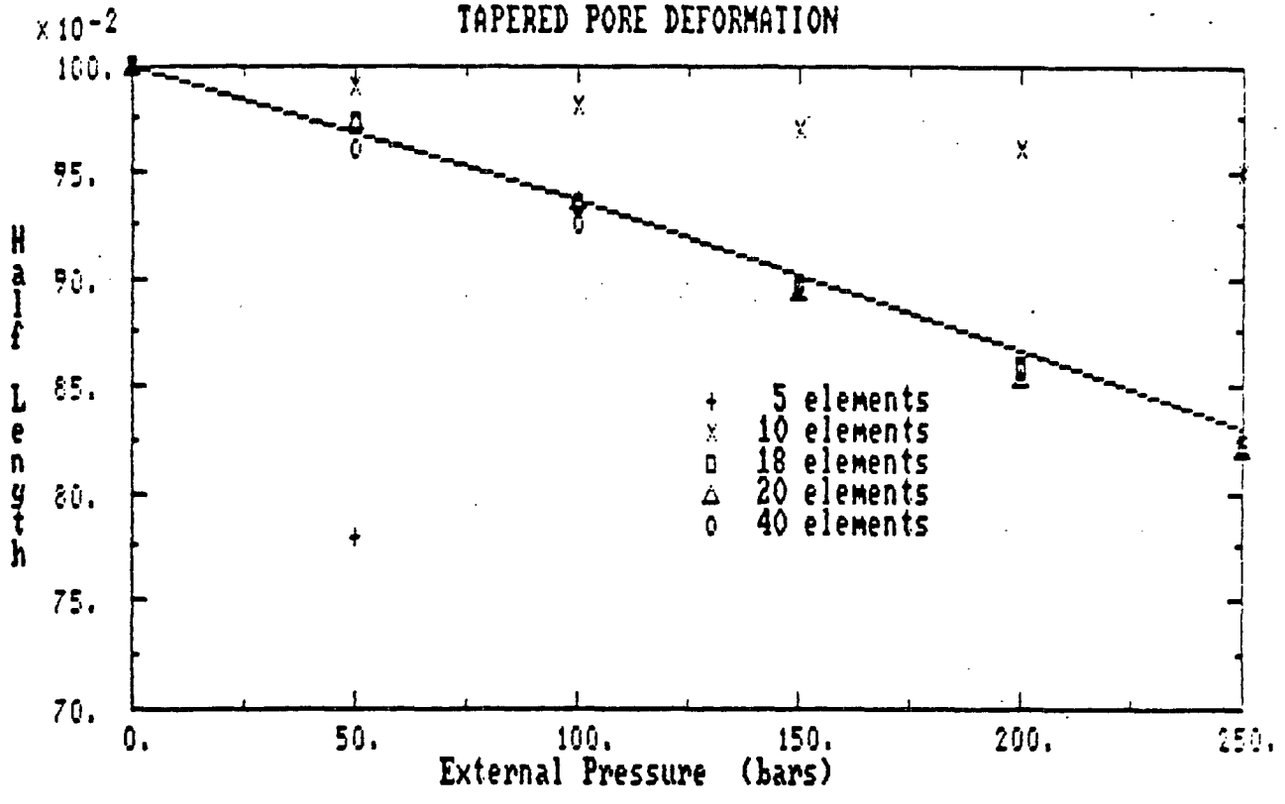

Figure 6-8. The figure represents the results for the deformation of a tapered pore model, using the displacement discontinuity method under hydrostatic pressure. The pressure goes from 0 to 200 bars. The line indicates the results predicted by the theoretical equation (6-2). The plus symbol represents the 5 elements model result. Notice that only one point is represented. The other points fell far below the graphic scale. Star symbols indicate the results for the ten elements model. Squares represent the 18 elements model. Triangles indicate the 20 elements model and circles represent the 40 elements model results. Notice the good agreement presented by the 18, 20 and 40 elements models, with respect to the theoretical prediction.

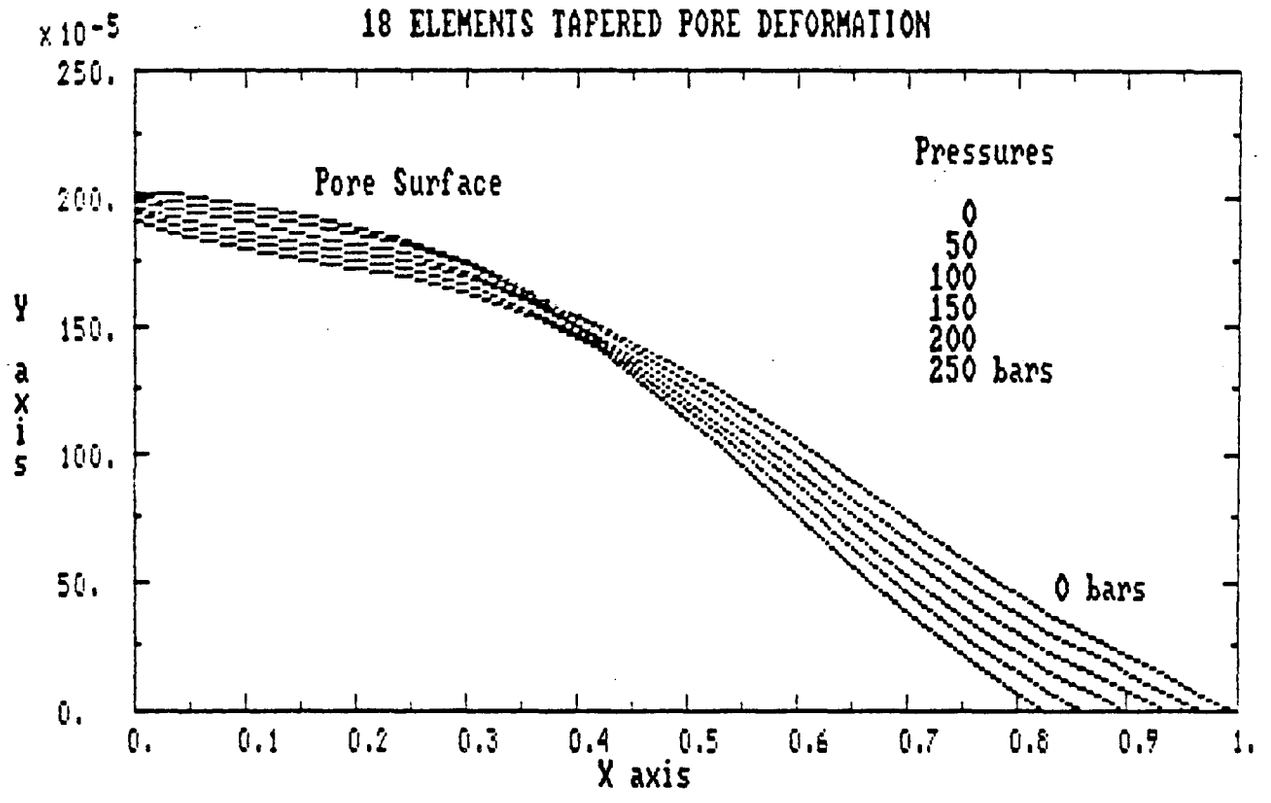

Figure 6-9. Representation of the deformation of the walls for an 18 elements tapered model under hydrostatic pressure. For simplicity, only the deformation of the first quadrant is shown. Notice how the deformation decreases near the rounded part of the pore surface. This portion is much more rigid than the rest of the pore surface.

20 and 40 elements models are very close to both the 18 elements model and the theoretical prediction. Also notice that the discretization of the pore surface for the 40 elements model is very uniform, because the length of each element is very small compared with the pore dimensions (fig. 6-7e). This type of behavior was also observed for the case of the circular shape. For a small number of elements, the numerical results are far away from the theoretical model. Increasing the number of elements improves the results a little bit. But once a certain number of elements has been reached, the results suddenly converge close to the real (theoretical) solution. Beyond that number, the solution seems to stabilize. Let us call that minimum number of elements 'the resolution number.' We can say that before the resolution number is reached, there is not enough information available to produce a stable result but once we pass that number, the information becomes redundant and it is not possible to resolve the system in more detail.

From the above results we deduce that the resolution number is proportional to the complexity of the shape. The more complex the shape is, the more information will be required to properly model it. We can determine the resolution number empirically by observing the changes in the numerical results as a function of the number of elements. The number of elements for which the solution tends to stabilize will represent the resolution number. It is important to point out that the resolution number is only an auxiliary parameter which serves as an indicator of the convergence of the method and it does not have real physical meaning.

The numerical method as described in this paper is only valid under the context of linear elasticity. Unfortunately, there are problems in elasticity which may not be solved by using just linear equations. For such problems it is necessary to utilize nonlinear elements to discretize the surface. Although the principles involved in this type of problem are similar to those treated in section 3, the resulting

system of equations may not be linear and other numerical techniques must then be considered. We will not be concerned with that class of problems in this paper.

So far we have been concerned with the accuracy of the solution but we have not discussed much about the efficiency of the algorithm. It is important to recall that most of the strength of a numerical method lies in its efficiency. After all, a computer program that produces very precise results but takes a very long time to converge can be as bad as a fast program that produces wrong answers. To study the efficiency of the algorithm, we will explore two major areas: memory consumption and processing time.

Let's considering the memory consumption. The program implemented in this work is less than 40 kilobytes long. But besides the program length, it is necessary to consider the amount of memory used to hold the data. Basically the program has to solve a system of linear equations and most of the memory is consumed by holding the coefficients of a squared matrix. For a 50 linear elements model, 64 kilobytes of memory are required. From the examples presented above, a discretization containing 50 linear elements seems to be more than adequate to represent very complex pore structures. Then, program and data take less than 120 kilobytes which is in the range of today's microcomputers. Notice that the size of the system of equations required to solve a similar problem by using the finite elements method must be considerably bigger, because the mesh points have to cover the interior and exterior points of the cavity.

The second point has to do with the processing time involved in the calculations. Again, most of the processing time is consumed by solving the system of equations. The smaller the system, the faster the processing time. We can expect a tremendous saving in computing time in a boundary elements method. Table 6-2 presents some comparative processing times against the number of elements used.

Those results were obtained with an IBM PC † microcomputer. The combination of small memory requirement and fast processing makes the boundary elements method a powerful tool to study boundary value problems in different physical disciplines. However, there are some limitations we have to consider. These limitations will be discussed in a later section.

TABLE 6-2

NUMBER OF ELEMENTS	TIME (sec)
5	3
10	9
20	38
40	159

† IBM is a registered trademark of International Business Machines Corporation.

7. MEASUREMENTS OF THE STRESS CONCENTRATION

In the last section we used the boundary elements technique to compute the displacements of the surface of a cavity. But as it was pointed out in sections 3 and 4, we can also compute the stresses and displacements induced by the pore on the solid matrix. The study of the behavior of local stresses around pores can lead to very important practical applications. Among others, the computation of the stresses around cracks is of capital importance for the design of engineering structures because it can help us to determine the limits of tolerances for which a particular structure will not crack. But it can also serve to help understand the way that pores interact inside rocks.

Inglis (1913) was perhaps the first to show that local stresses in an elastic solid tend to concentrate in the vicinity of holes, notches, reentrant corners and other types of geometric discontinuities. Such concentration raises the magnitude of the stresses to a level several times that of the applied stress. It thus became apparent that even submicroscopic flaws might be potential sources of weakness in solids. Figure 7-1 shows the ratio between the stress field in the y direction, and the applied stress σ_p, near the tip of an elliptical hole. This ratio is called *the elastic stress concentration factor*. In the case of a flat planar elliptical pore the ratio is given by (*Inglis, 1913*):

$$\frac{\sigma_{yy}}{\sigma_p} \approx \sqrt{2(c/\rho)} \qquad (7-1)$$

where b and c represent the half width and half length of the pore respectively. ρ is the radius of curvature at the tip. The magnitude of the stress concentration factor is inversely proportional to ρ which means that we may expect very high stress concentration around very sharp pore tips. It follows from figure 7-1, that the stress concentration factor rises to a sharp peak near the tip of the cavity. However, the

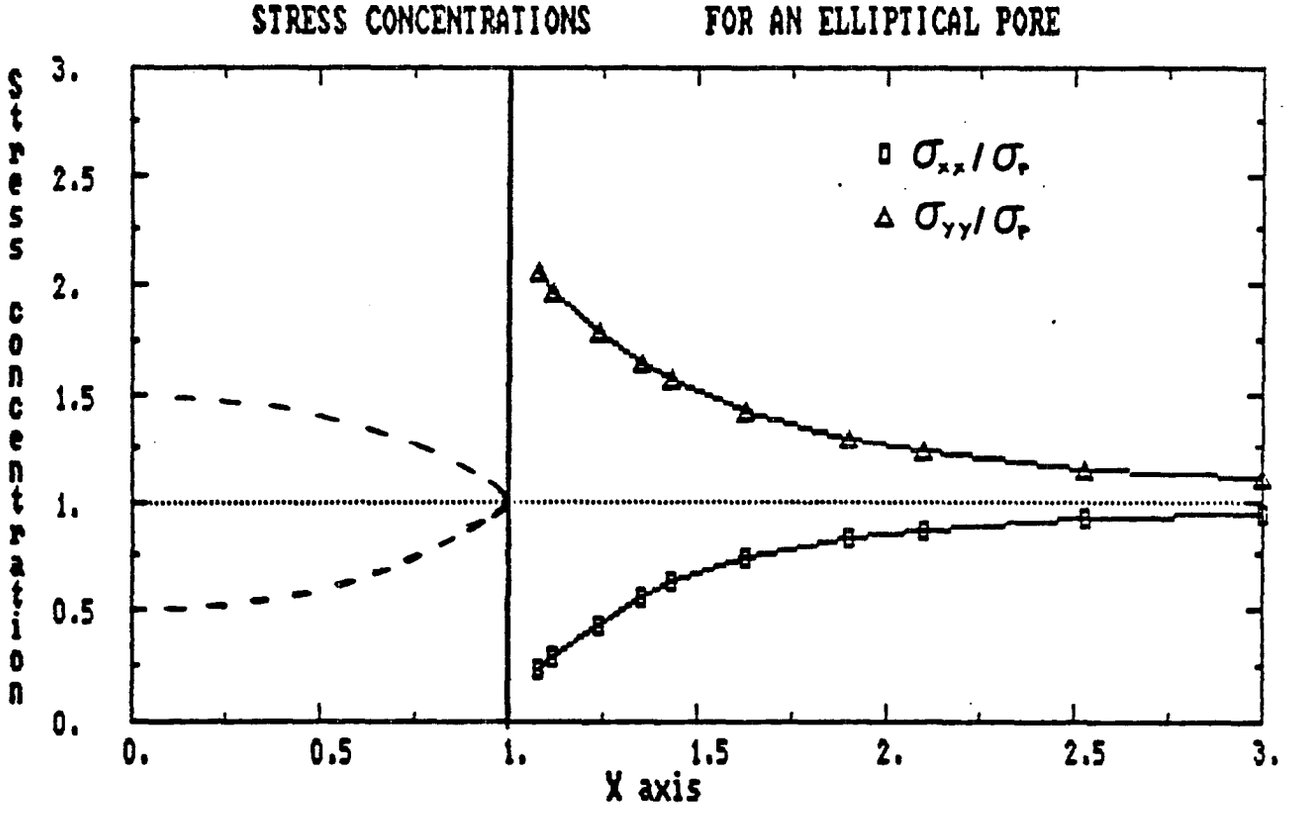

Figure 7-1. X and Y components for the stress concentration factor near the tip of an elliptical pore with aspect ratio $\alpha = .002$ and subjected to hydrostatic pressure. The location of the elliptical pore is indicated by the dashed lines (The half width is not at scale). Notice how small the stress concentration becomes at a distance of c (half length) along the x axis.

stress drops rapidly along the x axis and away from the tip, and at a distance c (the half length of the pore) measured from the tip, the stress concentration factor has decayed to a value approximately equal to one, which means that the local stress at that point is almost equal in magnitude to the applied stress. Therefore, the perturbation produced by the induced stress at that point is negligible.

For most complex shapes, the calculation of the stress concentration factor becomes very complicated and an adequate analytical solution is difficult to find. However, we can use a boundary elements method (for instance the displacement discontinuity method) to compute the magnitude of the stress field outside of the pore. In this way, the stress concentration factor can be calculated over a discrete number of exterior points. As an example, let us compute the external stress field 'induced' by a tapered pore. The tapered pore will consist of 20 linear elements. The aspect ratio α is 0.002 and the pore is subjected to hydrostatic pressure. Figure 7-2 shows the stress concentration factors for the components of the stress field σ_{xx} and σ_{yy} along the x axis. Again, the stresses reach a peak near the tip of the crack, dropping along the axis and becoming negligible at a distance equal to c. The only major difference between figure 7-1 and 7-2 is that the magnitude of the peak for the tapered pore is much greater than in the elliptical pore. This is an expected result since the tips of the tapered pore are very sharp. Figure 7-3 shows the stress concentration factors for the components σ_{xx} and σ_{yy}, computed along the y axis. In this case, the magnitude of the induced stress field is less than in figure 7-2, because the surface of the pore is very smooth at that location. However, some studies have shown *(Olson, 1986)* that stacking several pores along the y axis causes a strong interaction between the pores. We will not consider that case in this study.

Having in mind the above results, we locate a second pore on the x axis in such

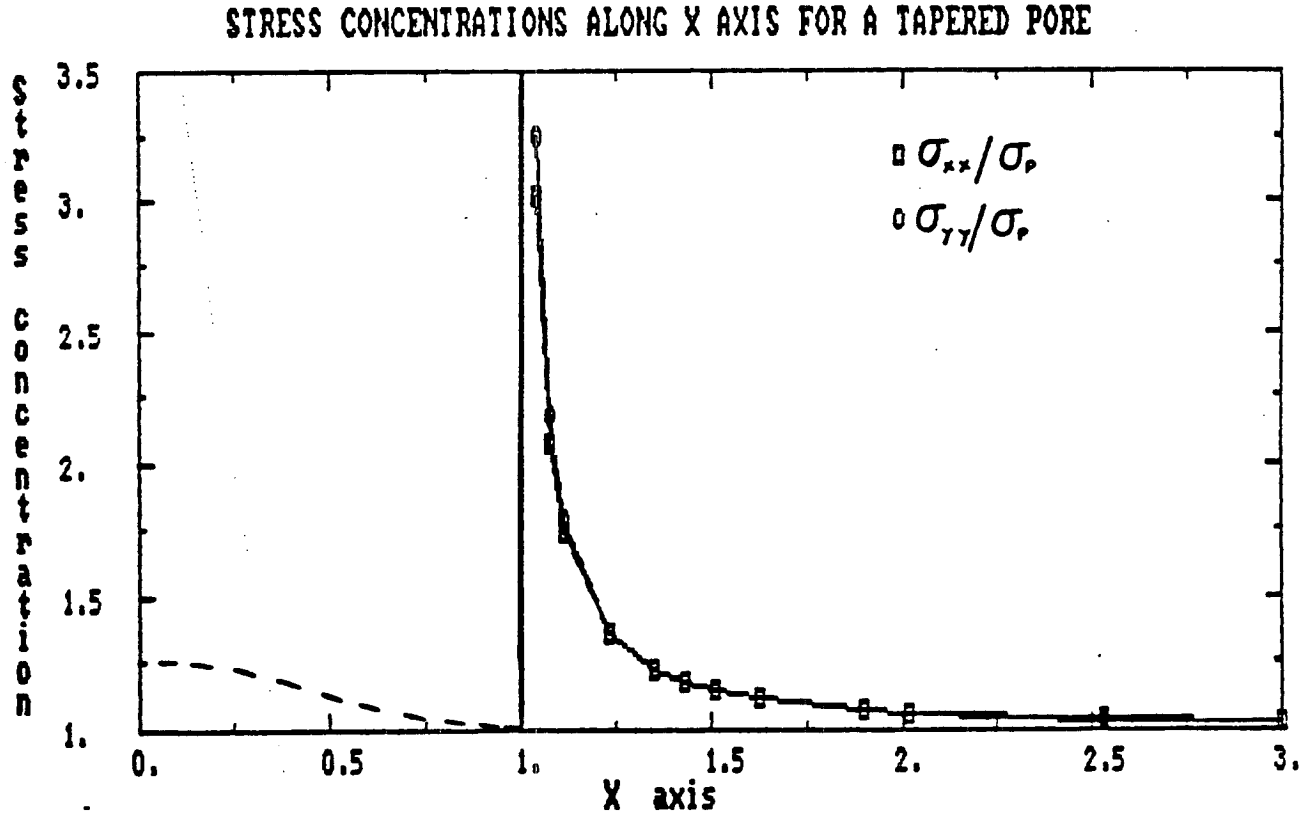

Figure 7-2. X and Y components for the stress concentration factor near the tip of a tapered pore with aspect ratio $\alpha = .002$ and subjected to hydrostatic pressure. The location of the tapered pore is indicated by the dashed lines (The half width is not at scale). Notice how small the stress concentration becomes at a distance of c (half length) along the x axis. Also notice that the magnitude of the stress concentration is bigger than the presented by the elliptical pore. However, the stresses drops more rapidly along the x axis.

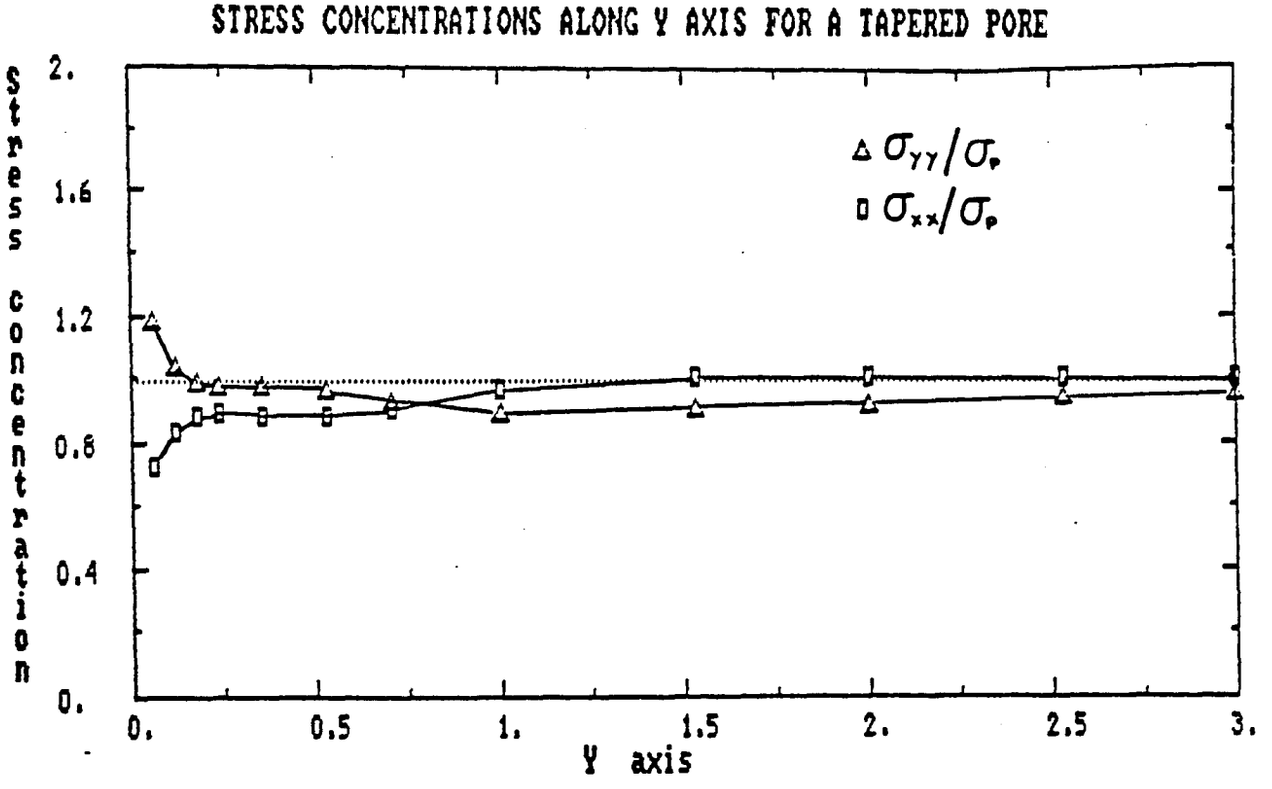

Figure 7-3. *X* and *Y* components for the stress concentration factor along the *y* axis of a tapered pore. Notice how small are the stresses compared with those presented in figure 7-2.

a way that the tips of either pores are separated by a distance $2c$. For simplicity, the two pores are identical in shape and size. Because the stress concentration induced by one pore is very small at the position of the second pore, their mutual interactions can be considered negligible. (We have assumed here that the surfaces of the pores do not hold any charge, neither are they magnetized, so that they can be considered free from other perturbations. The only way that the two pores can interact is through the stress field.) But when the separation becomes shorter than $2c$, the surface of the pores will be affected not only by the external stress field but also by the stress concentration induced by each one of the pores. As we expect, the magnitude of the stress concentration is not constant, therefore the surfaces of the pores are exposed to a non-homogeneous resulting stress field with its maximum strength acting on the portions of the two pores which face up.

The resulting stress field acting on the surfaces of the pores depends mainly on two factors: the shape of the pores and the separation between them. In most cases, the resulting stress field exhibits a complex form and consequently, an analytical formulation that describes such interactions is very difficult to find. Again, we can use a boundary elements method to study the effect of such interactions. As a practical example, let's consider two identical tapered pores as shown in figure 7-4. Since the pores are self-similar, we can choose the x and y axes as lines of symmetry. Therefore, the pore on the left becomes the image on the pore of the right so that it is only necessary to consider the section of one pore that falls into the upper right quadrant. There is nothing in the equations of sections 3 and 4 that prohibits analyzing a system of two or more pores, as long as their surfaces are subjected to specific boundary conditions. For this case, every element on the surface of both pores will be exposed to the external stress field and the stress field induced by the other elements. Figure 7-5 presents a sequence of images for the deformation

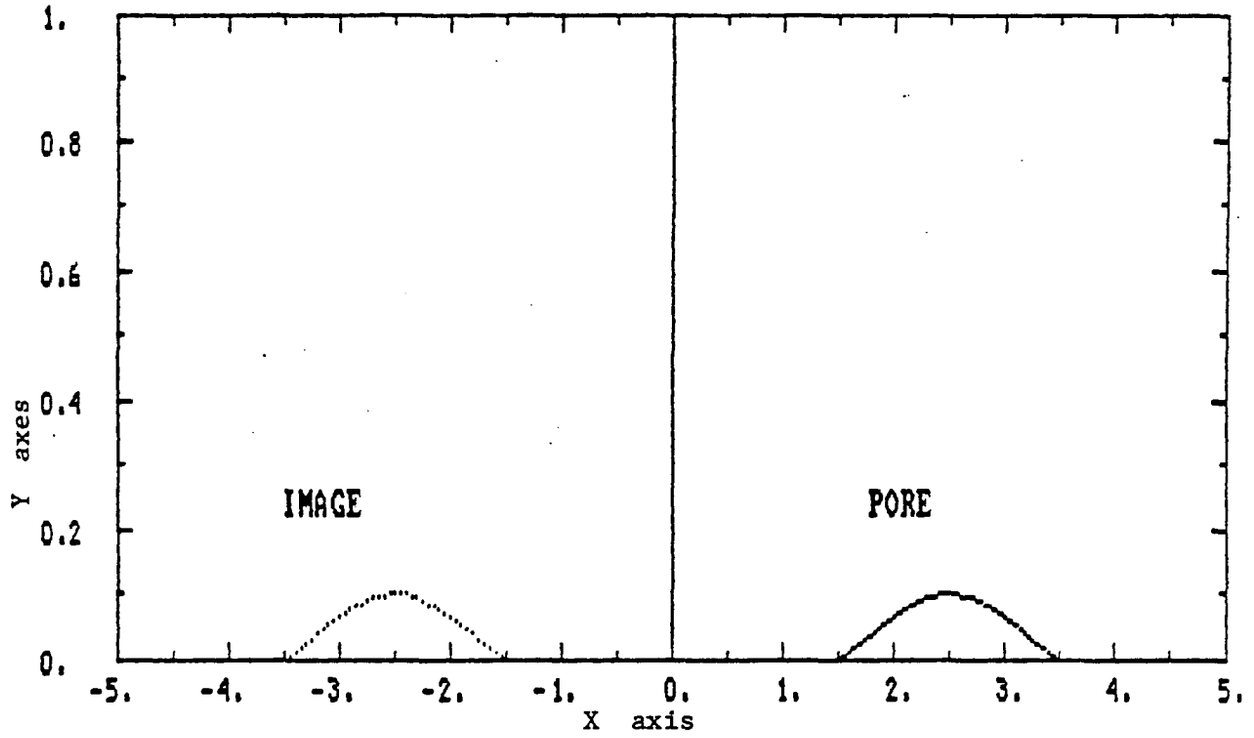

Figure 7-4. Representation of the upper parts of two identical tapered pores. Since the pores are self similar and the x and y axes are lines of symmetry, the pore of the left becomes the image of the pore of the right.

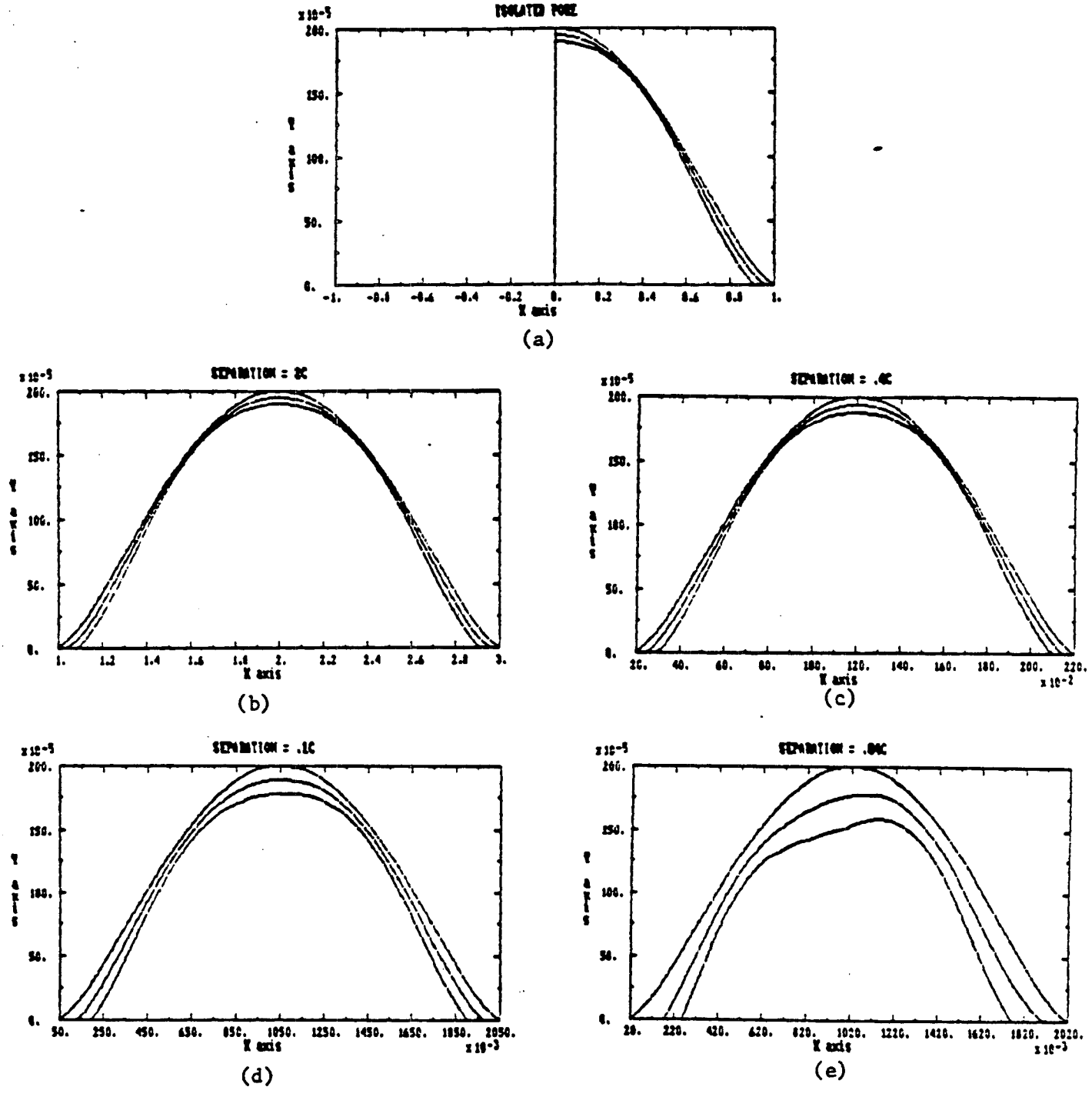

Figure 7-5. Deformation of the two self similar tapered pores considerate in figure 7-4. The pores surfaces are subjected to hydrostatic pressure (0, 50 and 100 bars). For simplicity, only the upper part of the pore of the right is shown. a) Deformation of an isolated pore. This pore deformation is used as a reference. b) Deformation for a separation of 2c between the two pores. c) Deformation for a separation of .4c. d) Deformation for a separation of .1c. Notice the abnormal deformation caused by the mutual interactions. e) Deformation for a separation of .04c. Now, the interaction between the two pores is very clear, causing a strong deformation on the walls of the pore.

of a system formed by two tapered pores located along the x axis. For simplicity only the deformation of the pore on the right is plotted for three external pressures (0 bars, 50 bars and 100 bars). As a reference, figure 7-5a shows the deformation of a single isolated pore. Figure 7-5b shows the deformation for a separation of $2c$. At this distance, the interaction of the pores is almost negligible. Figure 7-5c presents the deformation for a distance of $0.4c$. The interaction of the pores is still very small. Figure 7-5d shows the deformation of the pore for a separation of $0.1c$. At this distance, the effect of the interaction start to become noticeable. Figure 7-5e shows the deformation for a distance of $0.04c$. At this point, the interaction between the two pores is very clear, causing a strong deformation on the walls of the cavity. Notice that the left part of the pore is much more deformed that the right part because of its proximity to the second pore. The effect of the interaction will have serious repercussions on the elastic behavior of a porous rock, because as we will show in the next section, the deformation of a crack will govern the exhibited values for the elastic moduli and the seismic velocities of the rock.

The boundary elements method is not limited to analyzing the interaction of two similar cavities. We can also use two or more irregular pores subjected to any sort of external stress. However, the use of irregular shape may reduce the symmetry of the problem. Concomitantly with this, the memory requirements and the processing time will increase noticeably.

8. ELASTIC MODULI AND STRAIN ENERGY

Potential theory predicts that any vectorial field (electric, gravitational, elastic) stores energy. In particular, the stress field generated by external forces acting on an solid stores potential energy. This type of energy is known as strain energy. For an isotropic, homogeneous elastic solid that energy is distributed uniformly over the matrix. But for a cracked material, part of the energy is stored in the pore spaces. Then the pores act as springs which store potential energy when they suffers deformations caused by applied forces.

The pore spaces are responsible for the lack of rigidity in a cracked material. This lack of rigidity causes a reduction in the magnitudes of the elastic moduli. However, the matrix of the solid still conserves its original values for the elastic moduli. But what we measure in the lab is not just the magnitude of local elastic constants but the average values over the whole material. Then, for an external observer, the solid behaves like a homogeneous body, holding 'effective' elastic moduli which are lower in magnitude than those exhibited by the uncracked material.

When a porous material is subjected to external stresses, pores start to store additional strain energy. (There is an initial amount of energy stored in the pore at the moment of its creation.) While the pores reduce in size, there is a general increment in the values of the effective moduli. Once the pores close completely, they are no longer able to store more energy and the effective elastic moduli reach their maximum values which correspond to those held by the elastic matrix. By studying the variations of the strain energy stored in the pores, we may be able to calculate the variations of the effective elastic moduli in cracked bodies.

In order to find some useful relationships between the elastic moduli and the strain energy of a porous material, we will make use of a well known theorem of the

theory of elasticity. This is known as the reciprocal or reciprocity theorem. The theorem states that for an elastic body acted upon separately by two sets of tractions, the work done by the first set of tractions acting through the displacements produced by the second set of tractions is equal to the work done by the second set of tractions acting through the displacements produced by the first set of tractions. The reader interested in a rigorous proof of the theorem is referred to *Timoshenko and Goodier (1970)*. To better visualize the scope of the theorem, let us consider the problem of an elastic solid under the influence of one set of given stresses σ_n and σ_s which produce the displacements u_n and u_s. Both stresses and displacements are known. Let's supposes that the same elastic solid is subjected to another given set of stresses σ'_n and σ'_s, which produce a set of displacements u'_n and u'_s for which their magnitudes are unknown. Then the theorem states that the work done by σ_n and σ_s on the displacements u'_n and u'_s is equal to the work done by σ'_n and σ'_s on the displacements u_n and u_s. Mathematically, this can be written as:

$$\oint_C (\sigma_n u'_n + \sigma_s u'_s) da = \oint_C (\sigma'_n u_n + \sigma'_s u_s) da \qquad (8-1)$$

where the integral is performed over the whole area of the solid.

The solution for the primed displacements is then given by an integral equation. Solution for this equation may become cumbersome especially for a complex boundary value problem. In that case, a numerical method is required. If the theorem is applied to an embedded cavity whose boundaries have been divided into small rectilinear elements, the integral equation can be used as the starting point for another type of boundary elements method known as the direct boundary integral method (*Crouch and Starfield, 1983*). We will avoid such formulation by dealing with two simple physical situations.

First of all, let us consider an elastic solid with a volume V. The solid contains

just one pore. Then, the solid is loaded by an external uniaxial stress σ_{yy}. Suppose that the pore faces hold a stress which is equal in magnitude to σ_{yy} but acting in the opposite direction as shown in figure 8-1a, so that the pore surface is in equilibrium with the external force. In this case, the deformation of the solid is due only to a reduction in the dimensions of the matrix, so the system behaves like an uncracked body.(This situation is useful to represent the behavior of an effective solid.) Now let's consider a second situation where the solid is loaded with the same uniaxial stress but the pore faces are stress free as shown in figure 8-1b. Then both the matrix and the pore exhibit a deformation. The displacements along the x axis do not produce work because they are perpendicular to the applied stress and the work is defined as the dot product between the force and the displacement. Applying the reciprocity theorem to the system of figure 8-1 and after making some simplifications (*Walsh, 1965*) we end up with:

$$\frac{1}{E_f} = \frac{1}{E_0} + w \qquad (8-2)$$

where:

$$w = \frac{z}{V} \oint_C \frac{\partial U(C, \sigma_{yy})}{\partial \sigma_{yy}} dC \qquad (8-3)$$

Equation (8-2) links the effective Young's modulus E_f with the Young's modulus of the matrix E_0. The parameter w is related only to the pore and it was derived by considering just the strain energy stored in the crack shape. The function $U(C, \sigma_{yy})$ describes the crack shape. z is the length of the pore into the page of figure 8-1 and it is fixed because of the plain strain approximation. The integral is taken over the whole surface of the pore.

Now let's suppose that the solid considered in figure 8-1 is subjected to hydrostatic pressure P. In this case, the displacements along the x and y axes produce

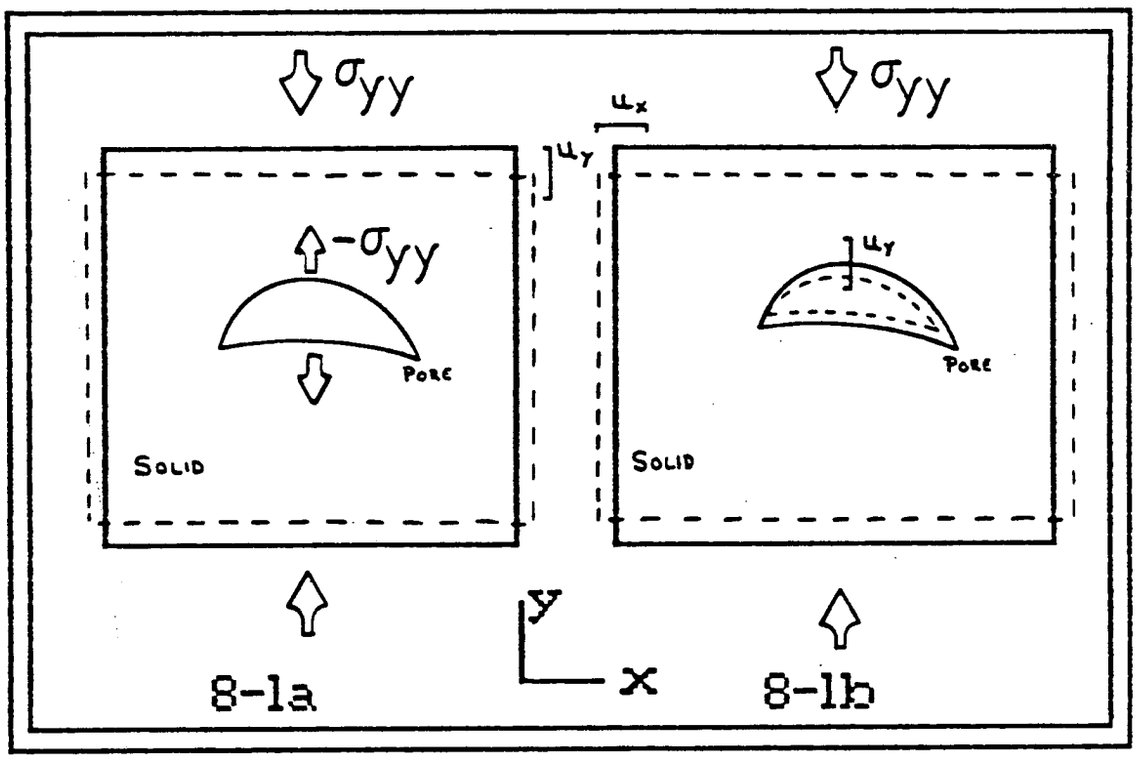

Figure 8-1. Resulting displacements of a porous solid subjected to an uniaxial stress σ_{yy}. a) The walls of the pore are subjected to the same applied stress but it is acting in opposite direction. b) The walls of the pore are stress free.

mechanical work. Then applying the reciprocity theorem and after making some simplifications (*Mavko and Nur, 1978*) we have:

$$\frac{1}{K_f} = \frac{1}{K_0} + w \qquad (8-4)$$

where:

$$w = \frac{z}{V} \oint_C \frac{\partial U(C, \sigma_p)}{\partial \sigma_p} dC \qquad (8-5)$$

Equation (8-4) links the effective bulk modulus K_f of the solid with the bulk modulus of the matrix K_0 and the pore factor w. Equation (8-5), although similar to (8-4) does not produce the same result because the deformation of the pore is now due to hydrostatic pressure which pushes its surface from any direction.

We can evaluate the pore factor w for an arbitrarily oriented crack, if the variation of the shape $\partial U/\partial \sigma$ is known. However, the functional form of the pore factor w as given in equation (8-3) or (8-5) can be even more simplified by the introduction of convenient symmetry conditions. Let's represent the integral term in equation (8-3) and equation (8-5) as:

$$\oint_C \frac{\partial U(C, \sigma)}{\partial \sigma} dC \qquad (8-6)$$

Now we make the assumption that the pore has at least one line of symmetry as shown in figure 8-2. Also, the shape of the pore which is represented by $U(x, \sigma)$ is a continuous function of x (there are no gaps on its surface). Using the symmetry conditions, (8-6) can be written as:

$$2 \int_{-c(\sigma)}^{c(\sigma)} \frac{\partial U(x, \sigma)}{\partial \sigma} dx \qquad (8-7)$$

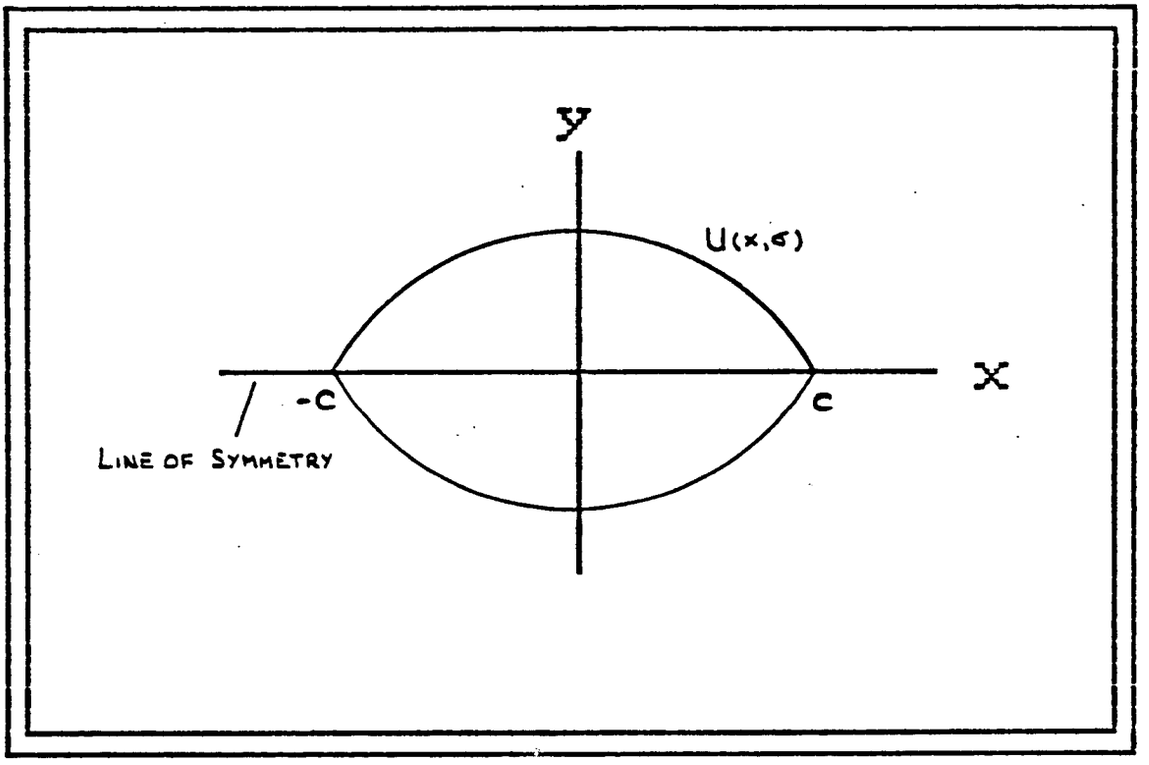

Figure 8-2. The figure shows a pore exhibiting a line of symmetry along the x axis. The function $U(x, \sigma)$ is used to represent the pore surface.

But the function $U(x,\sigma)$ touches the x axis at the locations of the pore tips, i.e. $U(\pm c,\sigma) = 0$. Using this condition, the partial derivative in (8-7) can be taken outside the integral, becoming a total derivative. Hence (8-7) can be written as:

$$2\frac{d}{d\sigma}\int_{-c}^{c} U(x,\sigma)dx \qquad (8-8)$$

where the integral term in (8-8) is nothing more than the internal area of the pore. For simplicity, let us write the integral in equation (8-8) as:

$$\int_{-c}^{c} U(x,\sigma)dx = A(\sigma) \qquad (8-9)$$

where $A(\sigma)$ represents the internal area of the pore as a function of the applied stress σ. Finally, the pore factor w can be written as:

$$w = 2\frac{z}{V}\frac{dA(\sigma)}{d\sigma} \qquad (8-10)$$

From a numerical point of view, equation (8-10) leads to a more convenient and stable way to compute the pore factor w, because the number of derivatives necessary to evaluate has been reduced to just one. Computing numerical derivatives is not a very stable process, especially when a very fine discretization is not currently available. On the other hand, computing the integral of a discrete function is a straightforward process. Values for the internal area of the pore as a function of external stresses can be calculated by the displacement discontinuity method, because the discrete shape $U(x,\sigma)$ is evaluated from the displacements of the elements at the midpoints. Once the internal area is known, the pore factor w can be calculated by discretizing equation (8-10) in terms of a finite difference given by:

$$w(\sigma) \approx 2\frac{z}{V}\frac{A(\sigma+\delta\sigma) - A(\sigma-\delta\sigma)}{2\delta\sigma} \qquad (8-11)$$

The value for the stress increment $\delta\sigma$ in (8-11) must be adjusted empirically for the type of pore considered. We can expect to use a large value for $\delta\sigma$ if the walls of the pore deform smoothly (stiff structures). On the other hand, we must use a small value if the function $U(x,\sigma)$ changes abruptly with pressure. Once equation (8-11) is evaluated, we can compute the effective bulk modulus and Young's modulus of the solid by plugging the pore factor w in equations (8-2) and (8-4).

Equations (8-2) and (8-4) were derived for a single pore embedded in an elastic solid. However, a typical rock is made of a large number of pores. Then we can superimpose the results obtained for several different types of pores to build a general solution for the effective elastic response of the rock. Because the values of the elastic moduli in the matrix do not change, we only need to substitute the w term in (8-2) and (8-4) by a summation over the N pores used to model the rock:

$$w \longrightarrow \sum_{i=1}^{N} w_i \qquad (8-12)$$

This superposition is also valid for interacting pores as long as we include all the w terms associated with those pores.

In conclusion, to determine the elastic constants in a porous rock model, we need to run two separate numerical simulations. In the first simulation, the pores are subjected to a uniaxial stress. Then (8-2) will be used to obtain the effective Young's modulus of the model. In the second simulation, the pores will be subjected to a hydrostatic pressure. For this case, equation (8-4) is used to compute the effective bulk modulus of the model. But once two elastic constants are determined, we can use their values to compute other moduli because only two elastic constants are independent (*Sokolnikoff, 1956*). Table 8-1 shows some of the relationships between the elastic constants and seismic velocities.

TABLE 8-1

Shear Modulus:	$\mu = \frac{3KE}{9K-E}$
Poisson's Ratio:	$\nu = \frac{3K-E}{6K}$
P velocity:	$V_p = \sqrt{\frac{3K}{\rho}\frac{3K+E}{9K-E}}$
S velocity:	$V_s = \sqrt{\frac{1}{\rho}\frac{3KE}{9K-E}}$

9. EXTENSIONS AND LIMITATIONS.

So far, we have described the basis for the boundary elements method. We have also applied that method to solve the problem of the deformation of a cavity as well as the stress and strain fields induced by that cavity on the elastic solid. Then, we have used these results to infer other elastic properties of the solid like the stress concentration factor and the effective elastic moduli.

It was pointed out in section 2 that the basic principles used to develop the numerical method can also serve as the starting point to study many other physical situations involving boundary value problems. The applicability of the boundary elements method can be better visualized by giving the algorithm a simple structural form. Such structure is characterized by the following modules:

1) Formulate of the problem and specify the related boundary conditions.

2) Find a convenient elementary solution for which the influence coefficients can be computed.

3) Discretize the region where the boundary conditions are de-

fined.

4) Calculate functional forms for the influence coefficients by applying coordinate transformations.

5) Set up the system of linear equations by considering the boundary conditions at each element.

6) Compute other responses in the system, using the values for the perturbation factors obtained in step 5.

This type of structure warrants that most of the computer code written for a particular boundary elements program can be used to implement other boundary elements programs. The main difference will be in the module which contains the functional form for the influence coefficients. Then we can move from one application to the other by exchanging these modules. There are further advantages of writing a modular program but perhaps the most important is that the process of maintaining of the computer code becomes straightforward.

Most of the limitations found in the boundary elements method can be solved and extended by rewriting a few modules. For instance, we can deal with nonlinear elastic problems by including a module (or group of modules) that solves a nonlinear system of equations. Problems in inhomogeneous bodies can be treated by discretizing the lines of separation between homogeneous regions. Then the numerical technique is applied on selected points on those lines. A complete discussion on the implementation of modules for different types of problems in linear elasticity, including inhomegeneous and anisotropic bodies, is presented by *Crouch and Starfield (1983)*.

There are other aspects that can be incorporated into the context of our formulation, for example the effect of water saturation on the elastic moduli and seismic

velocities in porous materials. The general approach we followed in section 8 is only applicable to dry pores, i.e. the internal region of the cavity is totally empty. (This treatment can also be used for air filled pores, because in this case the surface of the pore behaves almost like a free surface.) However, an interesting situation occurs when the pore spaces are completely filled with fluid (water, oil). We can solve this problem by assuming that the surface of the pore acts as a boundary of two inhomogeneous regions (fluid and solid). However, a rather simple solution can be found within the low frequency limit by using the Gassman's relation (*Gassman, 1955*). This relation links the bulk modulus of a dry sample with the corresponding bulk modulus of the fully saturated sample. The general expression is given by:

$$\frac{1}{K_s} = \phi/(\frac{K_d K_0 \phi}{3(K_0 - K_d)} + \frac{K_d K_f}{K_d - K_f}) \qquad (9-1)$$

where Ko, Kd, Ks and Kf are the bulk modulus of the solid matrix, the modulus of the dry rock, the modulus of the saturated rock, and the modulus of the fluid which fills the cavity. ϕ indicates the porosity of the rock.

However, equation (9-1) is not valid for the Young's modulus. To determine the value for the saturated modulus, we use the relation between the dry and saturated values for the shear modulus. This relation says that the shear modulus is independent of the degree of saturation of the sample. Using this fact, the Young's modulus for the saturated sample is given by (*Mendoza, 1985*):

$$E_s = 1/(\frac{1}{9K_s} + \frac{1}{E_d} - \frac{1}{9K_d}) \qquad (9-2)$$

In this way, both the bulk and Young's moduli of a saturated sample can be determined by using their corresponding dry values given by equations (8-2) and (8-4).

There are other areas of application for the numerical technique, for example the calculation of the hydraulic and electrical properties of rocks, because such properties are basically controlled by the geometry of pore spaces. In future research,

we will try to combine most of the petrophysical properties of sedimentary rocks in a unified model.

There are evidences "in situ" (*Nur, personal communication*) that systems of active faults act as domains which may influence the creation of new faults. The study of the interactions between cracks can be extended to macroscopic scales so that the effect of the stress field induced by a system of active geological faults under the influence of tectonic stresses can be better understood.

10. CONCLUSIONS

A numerical scheme has been developed for the analysis of deformations of arbitrarily shaped cavities embedded in a elastic matrix under the influence of arbitrarily applied stresses. The scheme is based on the boundary elements method where single linear elements are used to generate solutions around the cavity which satisfy the prescribed boundary conditions. The technique as formulated in this paper is applied to two-dimensional pores but it can be extended to cover more general formulations. The method has been applied to solve the problem of the effective elastic constants and seismic velocities in rocks as well as the study of the interaction between closed pores. It has also been suggested that the numerical algorithm is suitable for the study of crack propagation, hydraulic and electric properties in porous material, as well as the study of geological faults under the influence of tectonic stress. Therefore, the method can serve as the starting point for the study of more complex problems in areas of elasticity, rock physics, seismology and other related sciences.

The scheme is efficient in terms of processing time and memory consumption compared with other well-known numerical techniques such as the finite elements method, and can be implemented in microcomputers like the IBM PC.

REFERENCES

Bilby, B. A., and J. D. Eshelby, 1968, Dislocations and the theory of fracture. *Fracture: An Advanced Treatise, vol 1, edited by H. Liebowitz, Academic, New York.*

Brebbia, C. A., 1980, New developments in boundary element methods. *Southampton: CML Publications.*

Chang Y. P., C. S. Kang, and D. J. Chen, 1973, The use of fundamental Green's functions for the solution of problems of heat conduction in anisotropic media. *Int. J. Heat Mass Transfer, vol 16.*

Cole, D. M., D. D. Kosloff and J. B. Minster, 1978, A numerical boundary integral equation method for elastodynamics. *Int. Bull. Seismol. Soc. Am., vol 68.*

Crouch, S. L., and A. M. Starfield, 1983, Boundary element methods in solid mechanics.*Edited by George Allen & Unwin, London.*

Delameter, W. R., 1974, Weakening of elastic solids by arrays of cracks, *Ph.D. dissertation, Dep. of Appl. Mech., Stanford Univ., Stanford, Ca.*

Gassmann, F., 1951, Uber die elastizitat poroser medien, *Vierteljahresschr. Nalurforsch. Ges., Zuerich, vol 96.*

Han, D., and A. Nur, 1986, Effects of porosity and clay content on velocities of sandstones. *Geophysics. in print.*

Inglish, C. E., 1913, Stresses in a plate due to the presence of cracks and sharp corners. *Trans. Inst. Naval Archit. vol 55.*

Landau, L. D., and E. M. Lifshitz, 1959, Theory of Elasticity. *Addison-Wesley, Reading, Mass.*

Malbéqui, P., S. M. Candel and E. Rignot, 1986, Application of the integral equation method to the calculation of acoustic scattering by a space launcher. *J. Acoustic. Soc. Am. Suppl. 1, Vol. 79.*

Mavko, G., and A. Nur, 1978, The effect of nonelliptical cracks on the compressibility of rocks. *J. Geophys. Res., vol 83.*

Mendoza, J., 1985, Modelling seismic velocities and elastic constants in rock using a pore space network. The reciprocity approach.*Stanford Rock Physics Report vol. 25.*

Muskelishvili, N. I., 1953, Some basic problems of the mathematical theory of elasticity. *4th ed., Trans. JRM Rodok Groningen, Noordhoff*

Nur, A. Personal communication. *Dep. Geophys. Stanford University, Stanford Ca.*

O'Connell, R. J. and B. Budiansky, 1974, Seismic velocities in dry and saturated cracked solids. *J. Geophys. Res., vol 79.*

Olson, J., 1986, Fracture mechanics applied to jointing problems in sedimentary rock. *Stanford Rock Physics Report vol. 27.*

Rizzo, F. J. and D. J. Shipply, 1971, An application of the correspondence principle of linear viscoelasticity theory. *SIAM J. Appl. Math., vol 21.*

Sokolnikoff, I. S., 1956, Mathematical theory of elasticity. *2nd edn. McGraw-Hill, New York.*

Timoshenko, S. P., and J. N. Goodier, 1970, Theory of elasticity. *3rd edn. McGraw-Hill, New York.*

Walsh, J. B., 1965, The effect of cracks on the uniaxial elastic compression of rocks. *J. Geophys. Res., vol 74.*

CHAPTER III

MODELLING POROSITY AND THE STATIC BULK MODULUS IN SEDIMENTARY ROCKS

1. INTRODUCTION

The last chapter described in detail how the boundary elements technique can be applied to calculate the deformation of pores caused by external stresses, and also to use that information to infer the elastic moduli of porous materials. In this section, we will apply that numerical technique to explore the elastic behavior of several arbitrary pore shapes. Then, based on such results, we construct a theoretical model which explains the observed changes in porosity and bulk modulus with pressure for selected samples of sandstones.

The theoretical model will consist of a discrete distribution of pores shapes. Only a few pore shapes will be considered, although the number of pores for each shape is not restricted. There are two reasons to consider only a small number of pore shapes instead of a broad distribution. First, we are interested in identifying which geometries are responsible for the main trend observed in the bulk modulus and porosity, rather than fitting the data highly accurately; and second a forward model will be used to simulate the changes in porosity and bulk modulus. In a forward simulation, the pore parameters must be changed by hand (and common sense). Therefore, the process of matching the experimental data becomes cumbersome when the number of parameters and pore geometries increases. Results from this study will serve to better understand the importance of the pore geometry in the behavior of the elastic moduli. Also, they will be the starting point for most complex simulations.

2. EXPERIMENTAL DATA

The theoretical treatment presented in the last chapter is applicable only to the study of static elastic constants. This imposes a limitation on the type of data that may be used, because it is well known that the behavior of the elastic constants may be severely affected by the frequency used to measure them *(Biot, 1955; Simmons et al., 1965; Winkler, 1983)*. This means that the elastic moduli derived by velocity data measured at high frequencies can be up to an order of magnitude different than the elastic constants measured at zero frequency. We do not intend to discuss the nature of such observations here but rather to use that fact to restrict our present analysis to a particular range of frequencies (i.e., zero frequency).

Data for several types of sandstones listed in the SRP rock catalog *(SRP, 1986)* were available in the form of porosity as a function of applied pressure. All of the samples used are composed of fine grains which are very well-consolidated and very well-cemented, with porosities that oscillate between 9% and 20%. The clay content in the solid matrix and pores is low. We restrict our present analysis to dry rocks. A list of the sandstones and their corresponding porosities is presented in the next table.

TABLE 2-1

SAMPLE	POROSITY (%)
Fontainebleau A	15.9
Fontainebleau B	20.0
Santa Barbara	12.2
Nugget	10.0
Tory	14.7

The changes in bulk modulus can be computed from the porosity data by means of a simple mathematical procedure:

The bulk compressibility is defined as:

$$\beta = -\frac{1}{V}\frac{dV}{dp} \qquad (2-1)$$

In a porous solid, the total volume V is given by:

$$V = V_m + V_p \qquad (2-2)$$

where V_m indicates the volume of the matrix and V_p represents the volume occupied by the pores.

Assuming that the volume of the matrix V_m does not change appreciably when pressure is applied to the solid, the total change in volume with respect to pressure can be expressed as:

$$\frac{dV}{dp} \approx \frac{dV_p}{dp} \qquad (2-3)$$

Now, the porosity of the material is defined as:

$$\phi = \frac{V_p}{V} \qquad (2-4)$$

Then, the change in porosity with pressure is:

$$\frac{d\phi}{dp} = \frac{\frac{dV_p}{dp}V - V_p\frac{dV}{dp}}{V^2} \qquad (2-5)$$

Substituting (2-3) in (2-5) and using the definition of porosity (2-4):

$$\frac{d\phi}{dp} = \frac{1}{V}\frac{dV_p}{dp}(1-\phi) \qquad (2-6)$$

and using the definition of bulk compressibility (2-1), we finally obtain:

$$\frac{1}{K} = \beta = \frac{-\frac{d\phi}{dp}}{1-\phi} \qquad (2-7)$$

where K represents the bulk modulus of the solid.

In this way, the bulk modulus can be calculated if the changes in porosity with pressure are known. In practice, the application of this procedure imposes some limitations which will be discussed next.

If the porosity data are represented by a finite number of points, then the derivative in (2-7) must be computed using an approximated numerical technique as in the case of the finite differences. Then the accuracy of the results will depend mainly on the behavior of the function, as well as on the number of points used to represent the porosity data. Figure 2-1 shows a typical plot of porosity as a function of pressure for the Fontainebleau A sample. Since the points in figure 2-1 tend to form a smooth curve, they were interpolated by a continuous function given by:

$$a_1 e^{(a_2(1-e^{(-\frac{P}{a_3})}))} \qquad (2-8)$$

where:

$$a_1 = 102$$

$$a_2 = -.06$$

$$a_3 = 1594$$

Porosity plots for the other samples look quite similar. The next table shows the coefficients of the interpolating functions for the other samples used in this study.

TABLE 2-2

SAMPLE	a_1	a_2	a_3
Fontainebleau B	101	-.05	1588
Santa Barbara	101	-.02	1789
Nugget	102	-.07	1385
Tory	109	-.30	1073

The use of a function to represent the porosity and the fact that the data are relatively smooth, help to obtain stable values for the bulk modulus. Figure 2-2

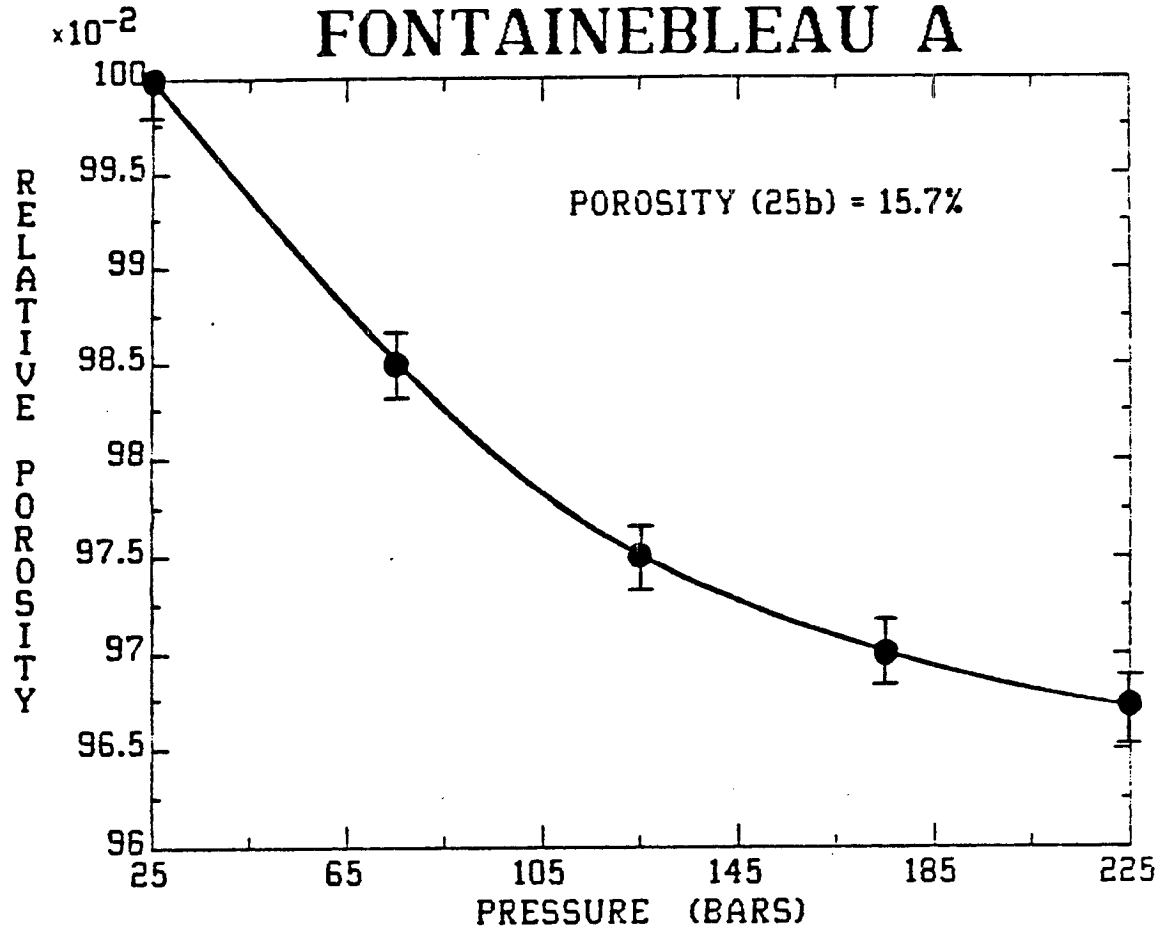

Figure 2-1: The figure shows a typical plot of the relative porosity as a function of pressure for the Fontainebleau A sample. The magnitude of the porosity at 25 bars is 15.7%.

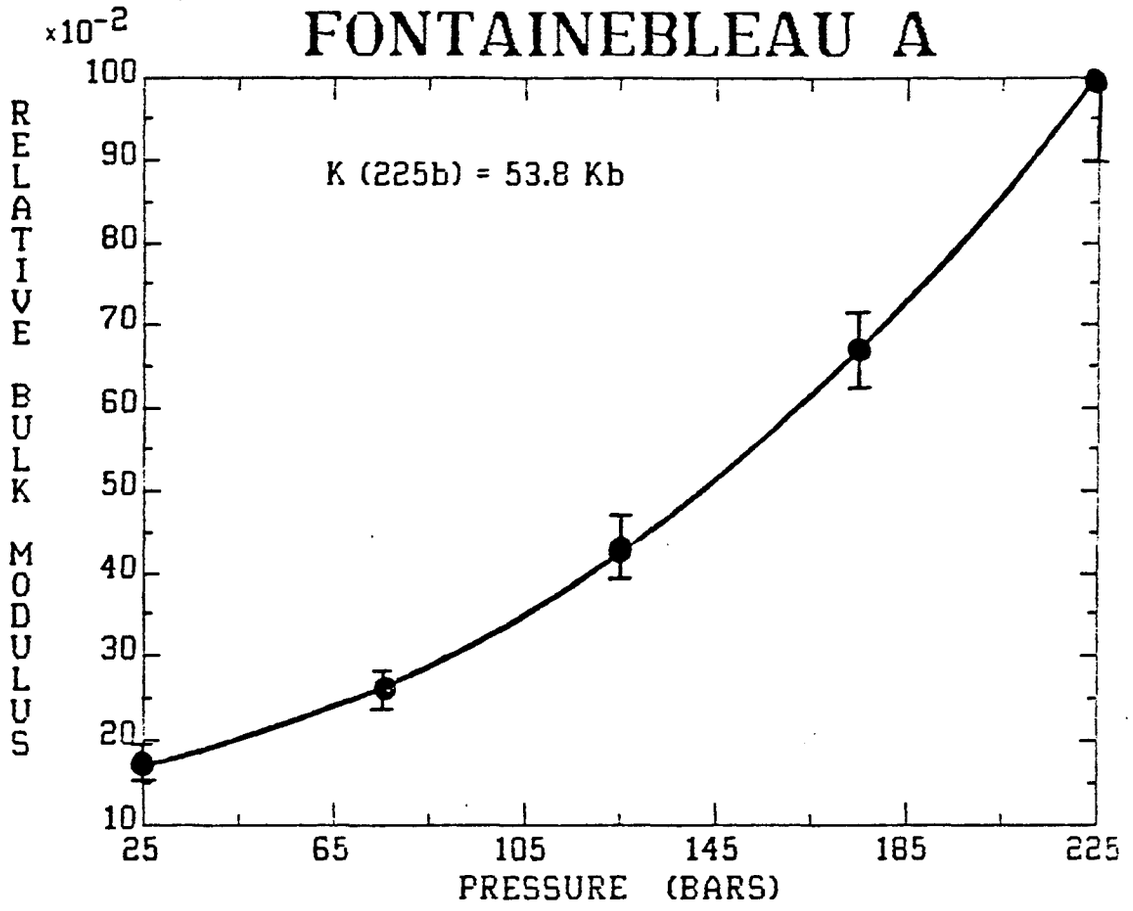

Figure 2-2: The figure shows a plot of the relative bulk modulus as a function of pressure for the Fontainebleau A sample. The magnitude of the static bulk modulus at 225 bars is 53.8 kilobars. Notice the huge change in the relative value for the bulk modulus between 25 and 225 bars.

shows the bulk modulus for the Fontainebleau A sample as a function of pressure. The bulk modulus for the other samples follows a similar pattern.

To obtain a better idea about which pore geometries are more appropriate to model the porosity and bulk modulus of the samples, we must get some preliminary conclusions from the behavior of the curves in figures 2-1 and 2-2. The first thing to note is that the change in bulk modulus from 25 bars to 225 bars is about 80%. This is a large change which is observed only in static measurements and is mostly due to the closing of pore spaces. It is clear that very stiff geometries like those shown by circular and starlike pores will not be able to explain such large change in the bulk modulus. (we will discuss these geometries in detail in a later section.) However, ellipsoidal pores with small aspect ratios *(Toksöz et al., 1976; Mavko et al., 1978)* are more suitable to explain larger changes, although not as large as the ones shown in figure 2-2. On the other hand, low aspect ratio cracks, can account for porosities only between 0% and 1% which are too low for most sandstones. The stiff geometries can easily account for much higher porosity.

These facts tell us that in principle we should try to combine large aspect ratio geometries, which take care of the magnitude of the porosity, with low aspect ratio geometries, which take care of the relative changes in bulk modulus, to model the samples.

3. THEORETICAL MODELS

The theoretical basis to compute the pressure dependence of the elastic constants for a particular pore geometry was explained in the last chapter. In that section we found that most of the elastic properties of the solid (including porosity and bulk modulus) are governed by the internal area of the pore $A(\sigma)$. In particular, the bulk modulus of a solid containing N pores is given by:

$$\frac{1}{K_f} = \frac{1}{K_0} + 2\sum_{i=1}^{N} \frac{z_i}{V} \frac{dA_i(\sigma)}{d\sigma} \qquad (3-1)$$

and the porosity as:

$$\phi = \frac{1}{V} \sum_{i=1}^{N} A_i(\sigma) z_i \qquad (3-2)$$

These equations are also valid for groups of interactive pores as long as they hold mirror symmetries, so that they can be treated as one large and complex pore.

We first compare the results for well known geometries (circular and tapered) with the porosity and bulk modulus obtained from the samples in order to figure out in what direction we need to go to obtain new pore geometries which can explain such data. All the computations were made assuming that all the applied stresses are hydrostatic. The first shape to try is the circular pore. The equation for circular pores shown in the last chapter is:

$$R(\sigma) = R_0(1 - \frac{2p(1-\nu^2)}{E\sqrt{2}}) \qquad (3-3)$$

This equation gives us the pressure dependence of the internal radius of the circle $R(\sigma)$ if the original radius (at zero pressure) R_0 is known. Then, the internal area is given by:

$$A(\sigma) = \pi R^2(\sigma) \qquad (3-4)$$

Using the values of 0.23 for the Poisson's ratio ν and 4×10^5 bars for the Young's modulus of the matrix, the bulk modulus and porosity for the circular pore compared with the data from the Fontainebleau A sample is plotted in figure 3-1. We

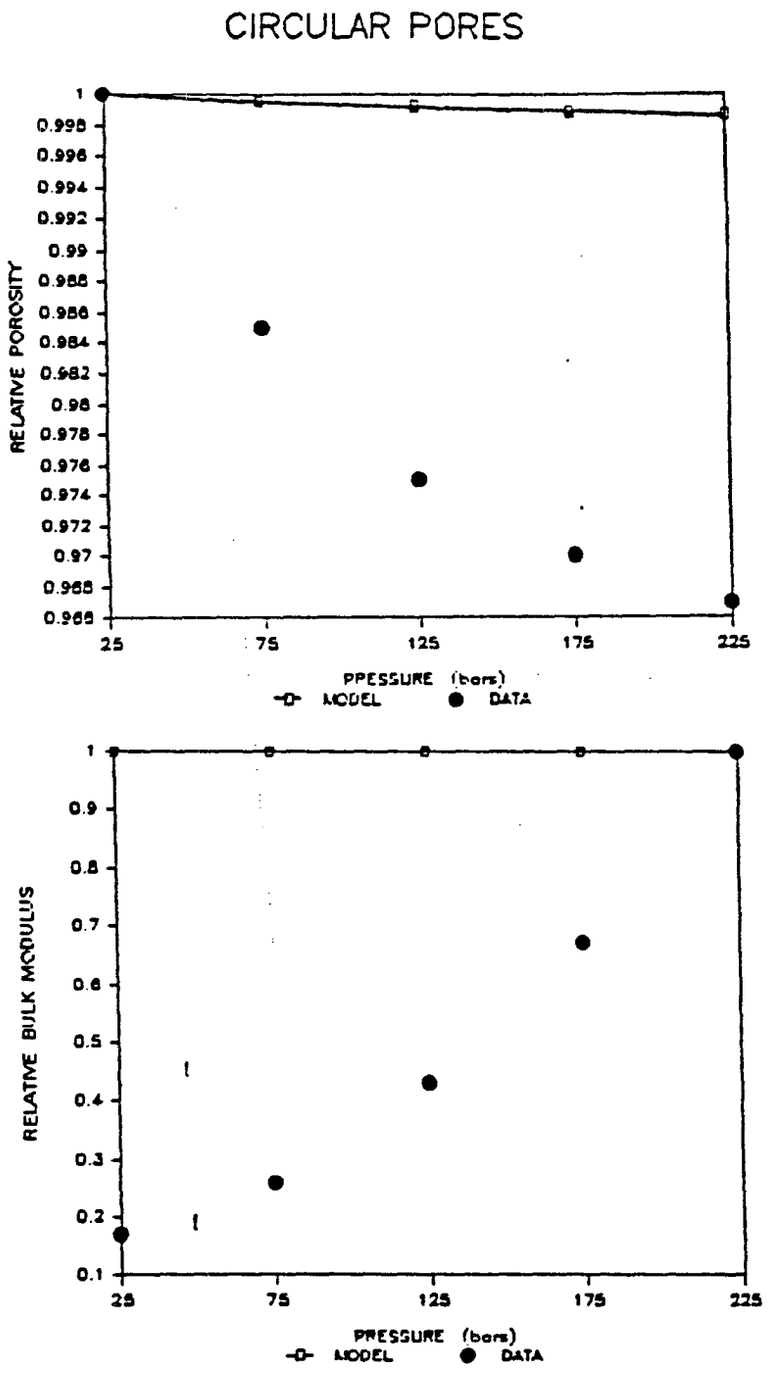

Figure 3-1: The figure shows a model results for a group of circular pores against the data from the Fontainebleau A sample. Line with squares represents the model results; black circles represent the experimental data. The number of pores has been adjusted to reflect a match in the magnitude of the porosity for the model and sample at 25 bars. Two populations of circular pores were used: The first one consisted of 480 pores with a $R_0 = 1.4um$ and $s = 5um$ and the second was of 100 pores with $Ro = 1um$ and $s = 3$. The magnitude of the bulk modulus at 225 bars was about 209 kbars.

have adjusted the number of pores N to reflect a match in the magnitude of the porosity for the model and sample at 25 bars. As was expected, the changes in bulk modulus for the circular pore are negligible, because the variations in its internal area with pressure are very small. However, this geometry has the advantage of keeping porosity high because of its great internal area.

Let us now compare the results from a tapered pore with the data from the Santa Barbara Sandstone sample. This sample also presents a large change in bulk modulus from 25 to 225 bars (about 80%). A very low aspect ratio ($\alpha = 0.001$) was used for the pore model to try to match the large changes in bulk modulus and porosity. The results are shown in figure 3-2. The number of pores was adjusted to match the magnitude of the porosity at 25 bars. As we can see, the change in bulk modulus for the tapered pore is small compared with the data. The magnitude of the bulk modulus turned out to be very small as well. If we tried to match the magnitude of the bulk modulus, we would obtain an insignificant value in porosity. This is due to the small internal area presented by the pore.

The next geometry to try is the cruciform crack or star-shaped crack. This type of shape has been studied by several authors *(Rooke and Sneddon, 1969; Kutter, 1970; Williams, 1971)* and as it was pointed out in the last chapter, this geometry is very representative of the kinds of pores we expect to see in sandstones. The elastic response for the star-shaped pore becomes quite similar to that found in circular pores when the number of spikes is greater than two *(Kutter, 1970)*. For these results, we have assumed that the number of spikes in the pore is even and all of the spikes have the same length. The same kind of results can also be found for a more irregular type of star-shaped pore for which the lengths of the different spikes are not the same, as long as the differences in length are small. (This result can be obtained by analyzing the pore by means of the boundary elements technique

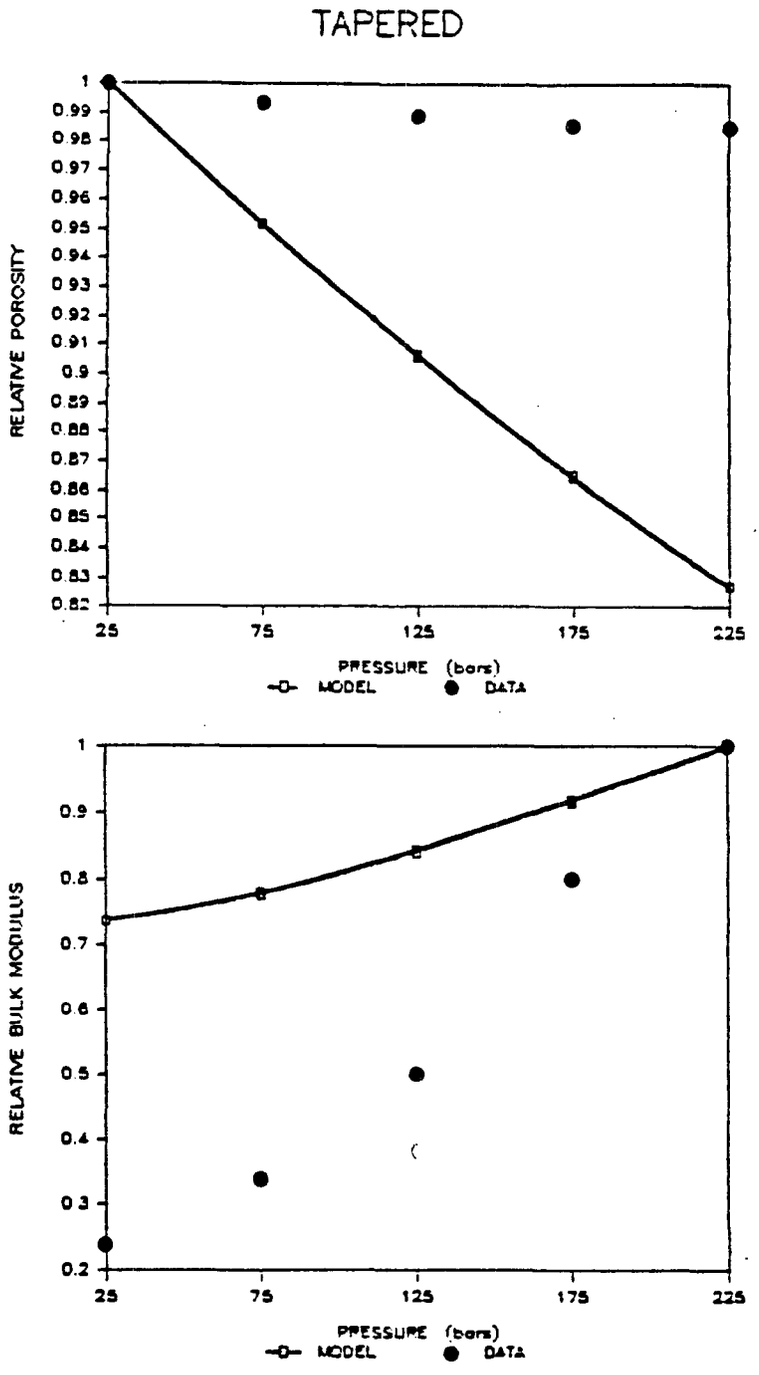

Figure 3-2: The figure shows model results for a group of tapered pores against the data from the Santa Barbara sample. Line with squares represents the model results; black circles represent the experimental data. The number of pores has been adjusted to reflect a match in the magnitude of the porosity for the model and sample at 25 bars. One population of tapered pores with aspect ratio of 0.001 and $z = 12um$ was used. The magnitude of the bulk modulus at 225 bars was about 5600 bars.

described in the last chapter.) Figure 3-3 shows a four spikes star-shaped crack and its internal deformation with pressure. As we expect, the change in bulk modulus for this geometry presents the same characteristics as the circular pore. However, the amount of porosity due to this type of pore is much smaller because of its reduced internal area. The deformation of the pore with respect to applied pressure can be increased if we group two or more pores close to each other so that they are allowed to interact. Such a technique was also discussed in the last chapter. This type of geometrical disposition is observed in sandstones where a group of at least two star-shaped pores are in close association. Figure 3-4 shows the internal deformation presented by the same pore shown in figure 3-3, but when it interacts with a self-similar crack located at a distance of $0.01c$ where c is the length of the pore measured from opposite spikes. As we see, the deformation is bigger for an interactive crack, but still it is not big enough to explain by itself the large change in bulk modulus observed in the data. Figure 3-5 shows a model of star-shaped cracks compared to the data from the Fontainebleau A sample. Again, the number of pores N has been adjusted to match the magnitude of the porosity at 25 bars.

At this point, one may ask the reason why the star-shaped pore with an even number of spikes of four or more becomes very rigid (the two spike case becomes a tapered pore). What happens is that in a star-shaped pore with more than two spikes, the stresses around the pore can thus be approximated by those around a circular, 'equivalent' hole of a radius equal to that of the crack spikes *(Kutter, 1970)*. In the case of two spikes, the stress pattern is not symmetric and it makes the walls of the cavity less stiff. So far, our analysis has been restricted to an even number of spikes. An odd number of spikes can also be treated by a boundary elements method but due to the lack of two axes of symmetry (there is only one), its analysis becomes more complex. We will not examine that case in this study.

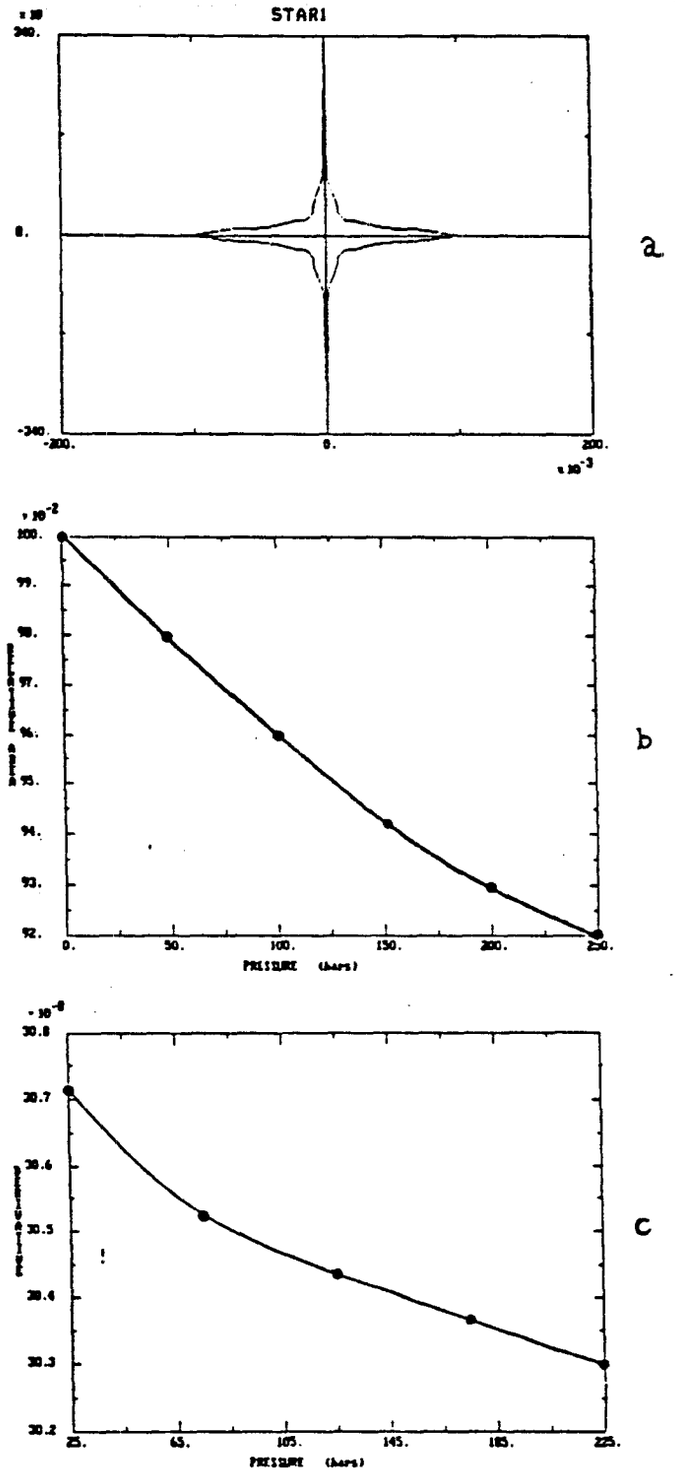

Figure 3-3: a) Four-spike star-shaped pore or STAR1. Notice that the y axis is one order of magnitude lower than the x axis. b) Relative change of internal area or deformation of the STAR1 pore from 0 to 250 bars. c) Derivative of (b) as a function of pressure.

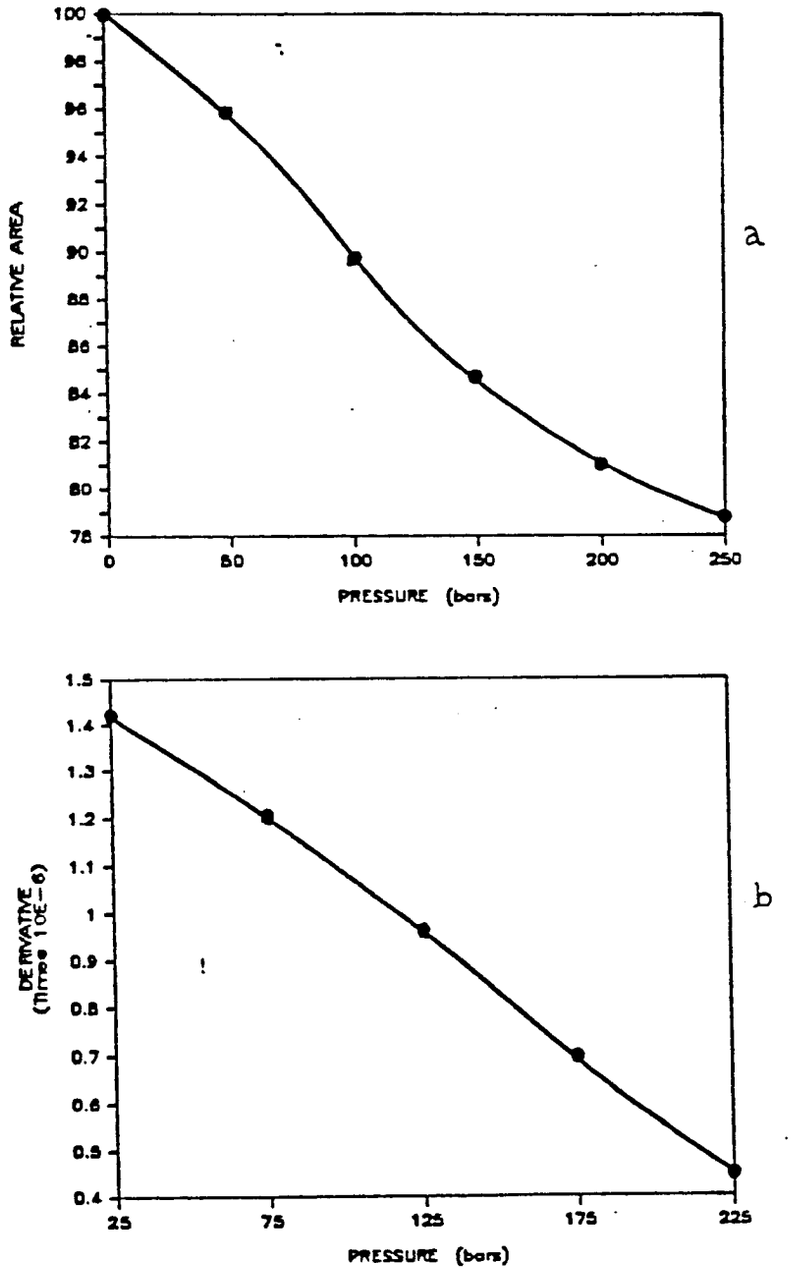

Figure 3-4: a) Relative change of internal area and b) derivative of (a) for an interactive STAR1 pore. The separation of tips between the two pores was of 0.01c.

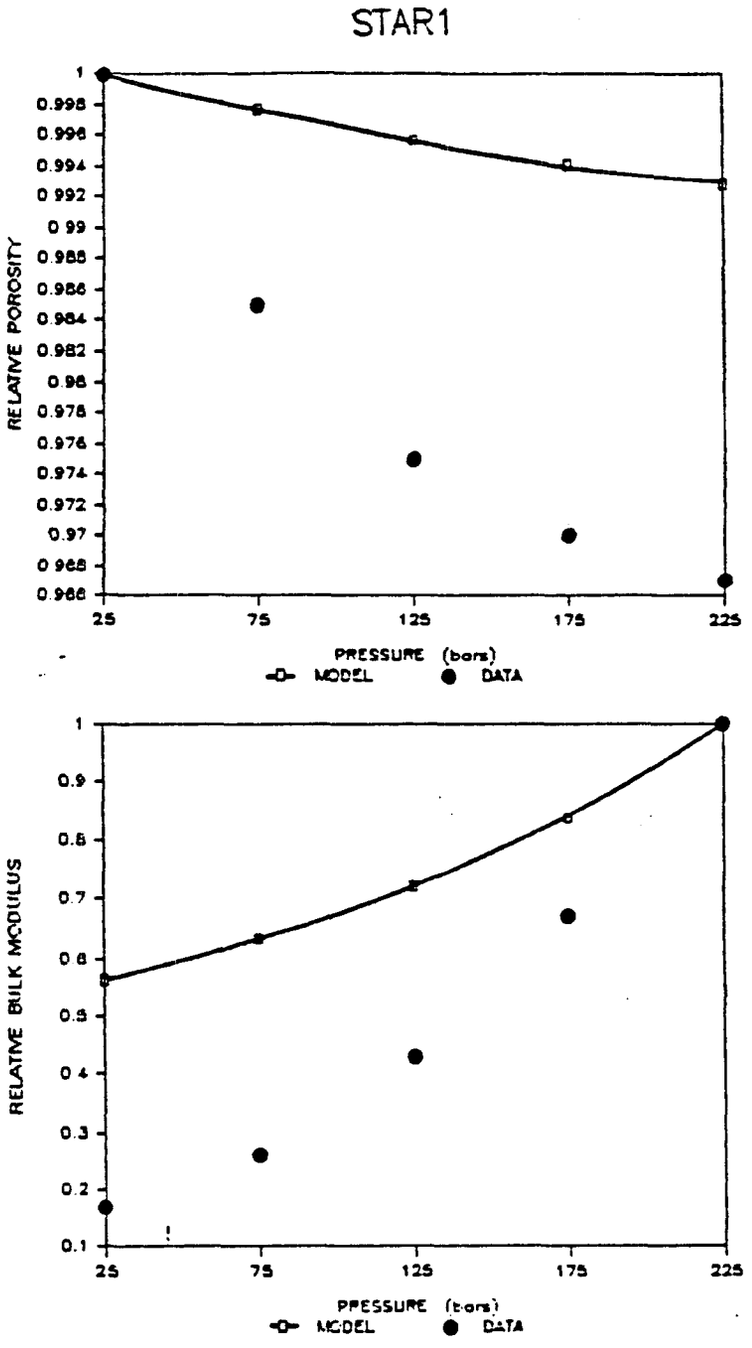

Figure 3-5: The figure shows model results for a group of STAR1 pores against the data from the Fontainebleau A sample. Line with squares represents the model results; black circles represent the experimental data. The number of pores has been adjusted to reflect a match in the magnitude of the porosity for the model and sample at 25 bars. One population of 9850 STAR1 pores with $s = 17um$ was used. The magnitude of the bulk modulus at 225 bars was about 89.6 kbars.

We will now review an intermediate type of pore which is in between the tapered and the star-shaped geometry. For simplicity, let's refer to this particular family of geometries as the pseudo-tapered (we could also use the term pseudo-star). This geometry can be visualized as the space left by four quasi rectangular grains as shown in figure 3-6.

Figures 3-7 to 3-10 show the deformations and their corresponding derivatives for four different pseudo-tapered pores. The main differences between those pores is the length of the spike parallel to the y axis. Notice that the slopes held by the derivatives are much steeper than those presented by other shapes. The decompensation in the stress field due to the incipient spike is responsible for the great change in internal area of the pseudo-tapered pore. Once the spike becomes large (about 0.1 times the length of the larger one), the resultant stress field around the pore becomes more symmetric and regular and the elastic response of the pore resembles that presented by the circular and star-shaped pores.

The large variation in the internal area held by the pseudo pore, is responsible for the large change in the bulk modulus of the solid which contains these cavities. This large change is big enough to be compared with that presented by the Fontainebleau A sample as well as the other samples available. Figure 3-11 shows a tentative model for the Fontainebleau A sample using the PTAPERED1 pore. We have adjusted the number of pores N to match the magnitude and shape of the bulk modulus. However, because the internal area of the pseudo-tapered pore is small, the porosity (magnitude and pressure dependence) could not be matched.

So far we have found four different types of elastic responses which are summarized next:

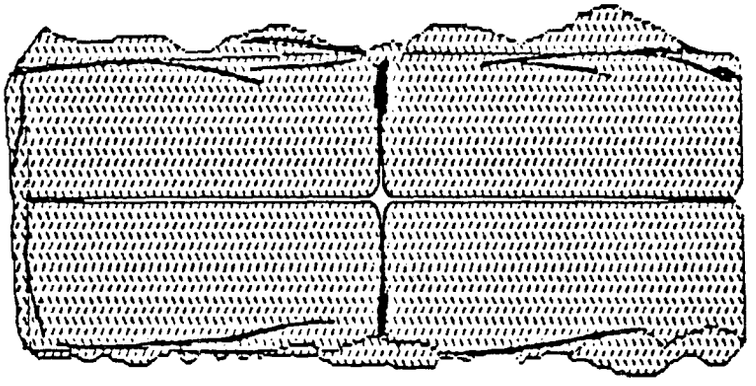

Figure 3-6: The figure shows a sketch of a pseudo-tapered pore. The pore is formed by the space left by the four rectangular blocks. Notice that the aspect ratio of the grains must be much less than 1.

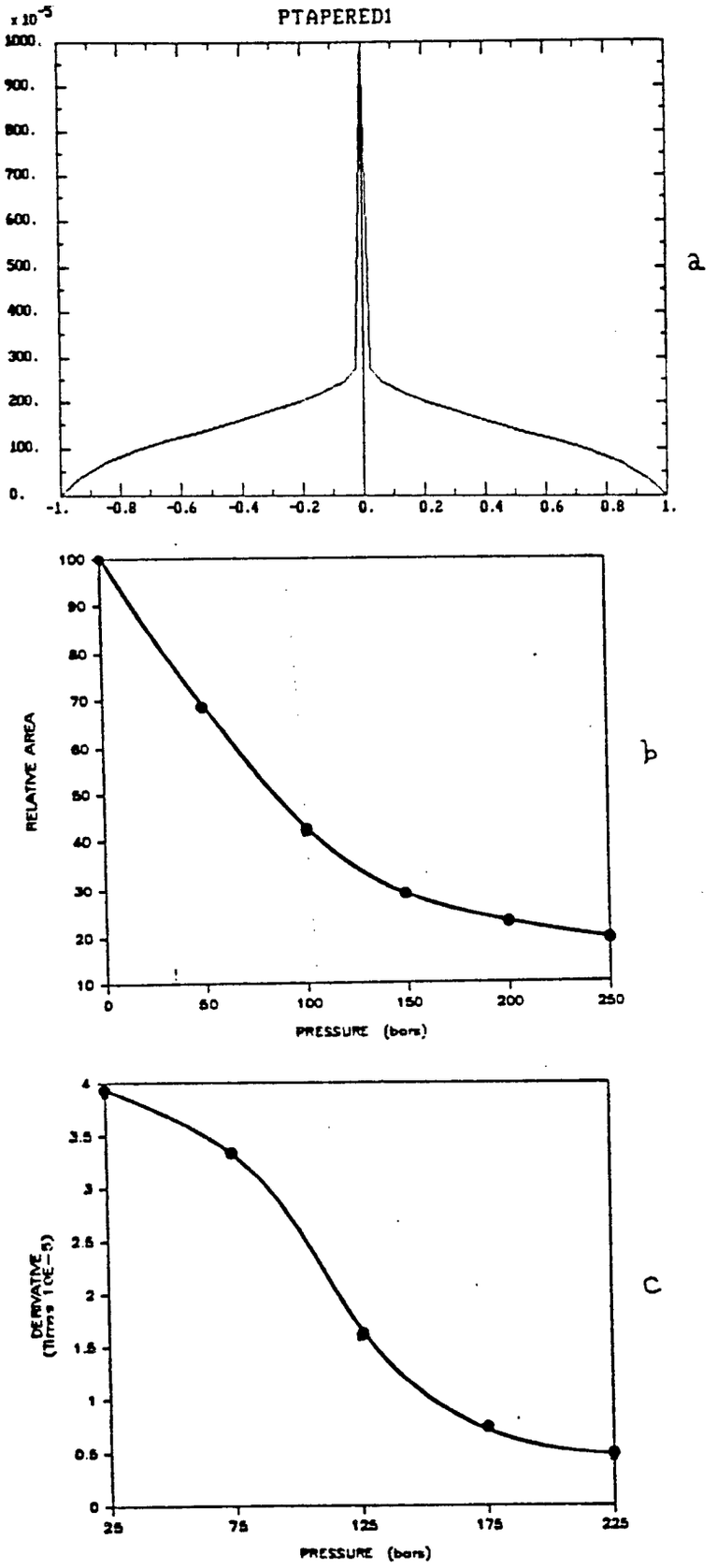

Figure 3-7: a) Upper portion of the pseudo-tapered pore PTAPERED1. b) Relative change of internal area from 0 to 250 bars. c) Derivative of (b) as a function of pressure.

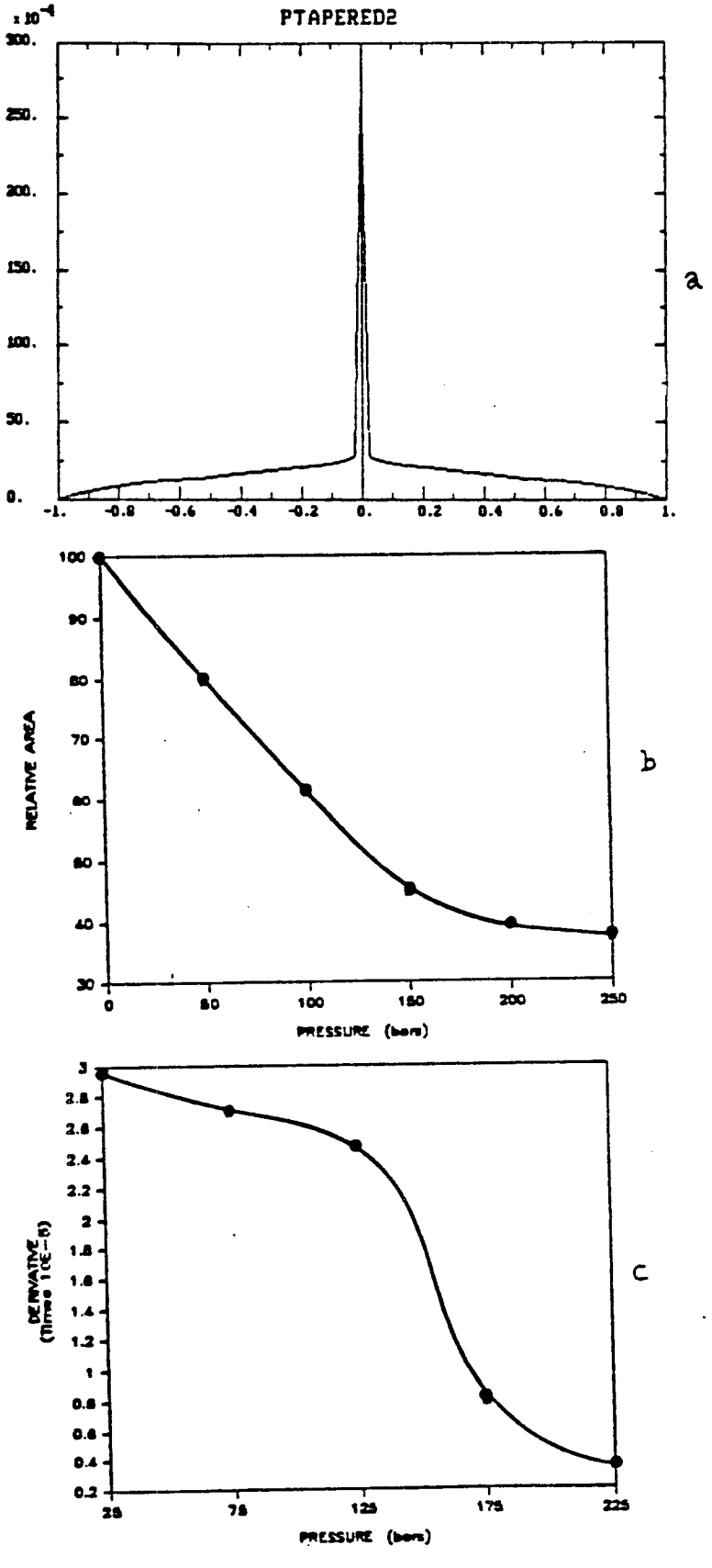

Figure 3-8: a) Upper portion of the pseudo-tapered pore PTAPERED2. b) Relative change of internal area from 0 to 250 bars. c) Derivative of (b) as a function of pressure.

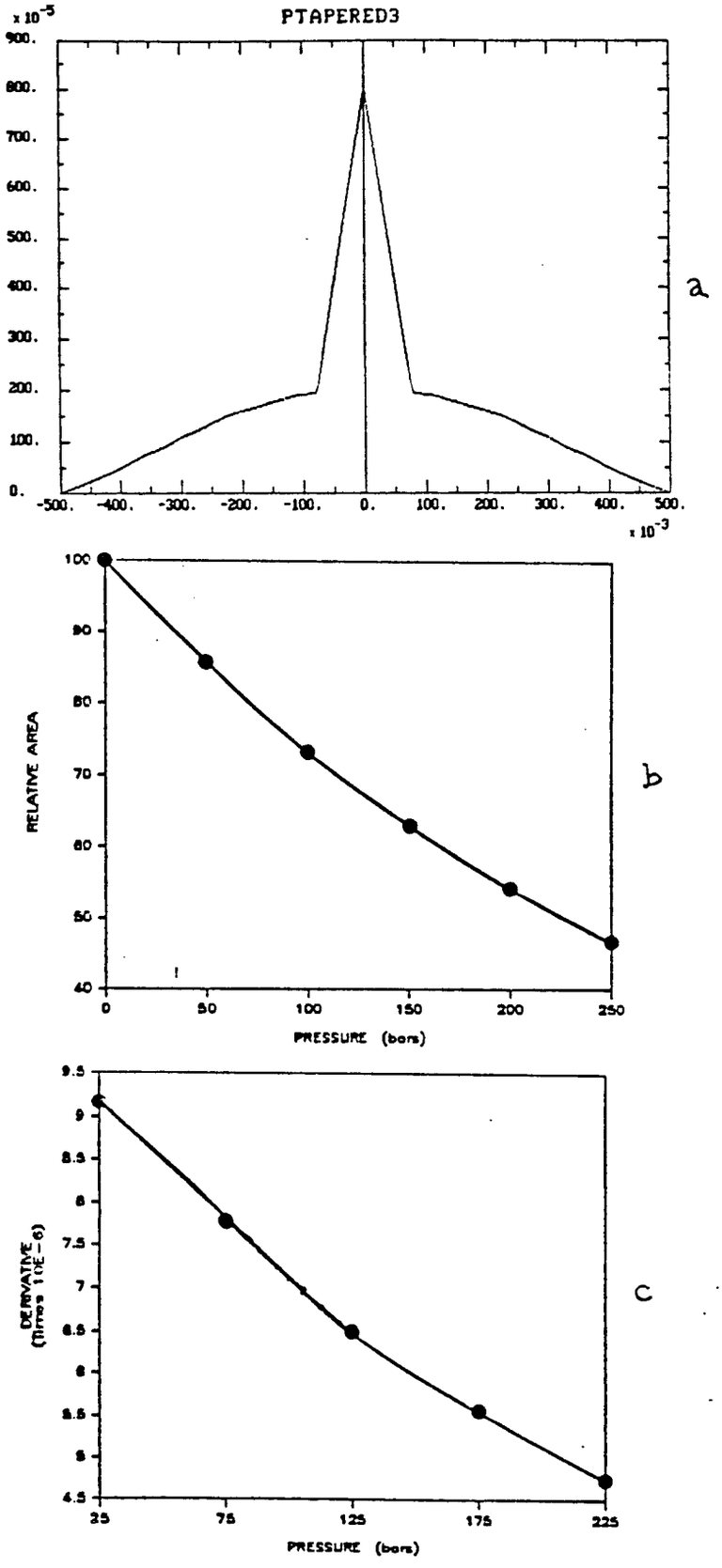

Figure 3-9: a) Upper portion of the pseudo-tapered pore PTAPERED3. b) Relative change of internal area from 0 to 250 bars. c) Derivative of (b) as a function of pressure.

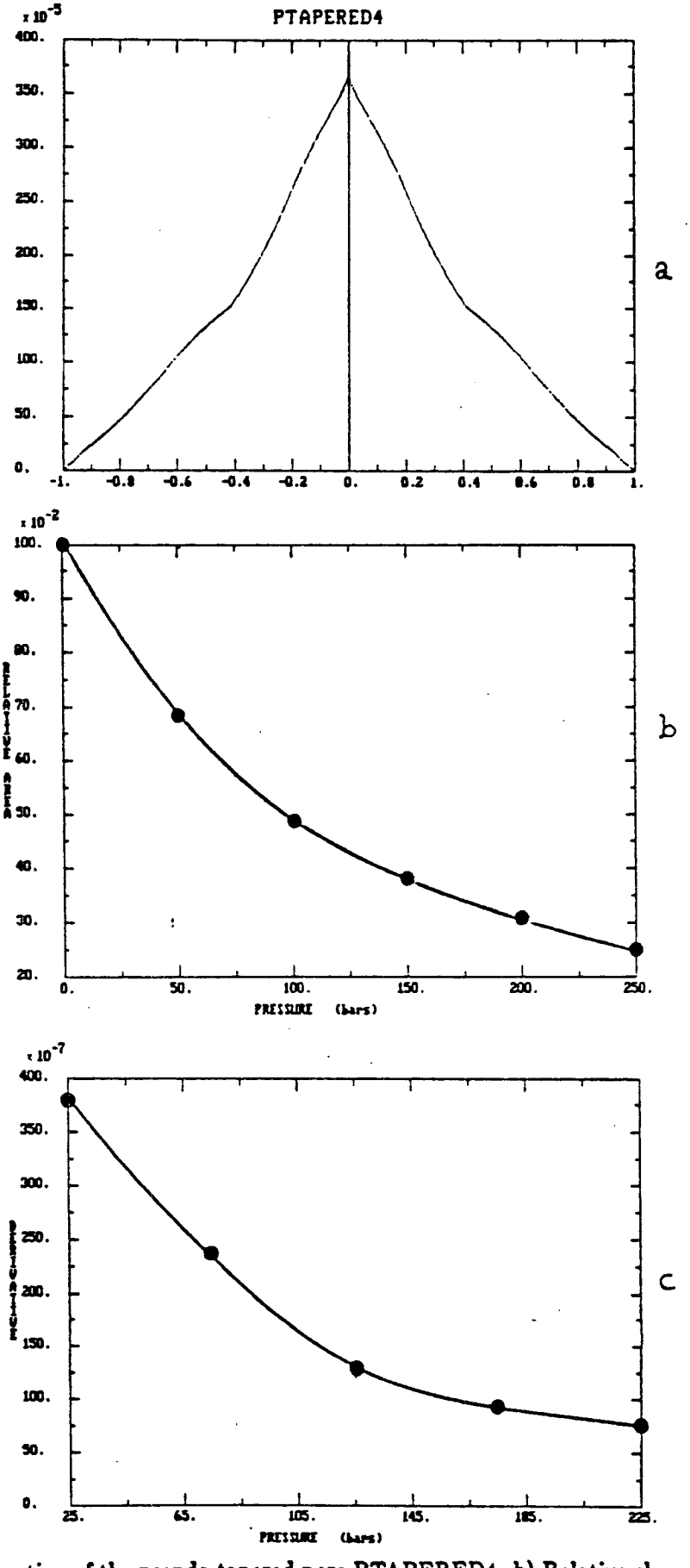

Figure 3-10: a) Upper portion of the pseudo-tapered pore PTAPERED4. b) Relative change of internal area from 0 to 250 bars. c) Derivative of (b) as a function of pressure.

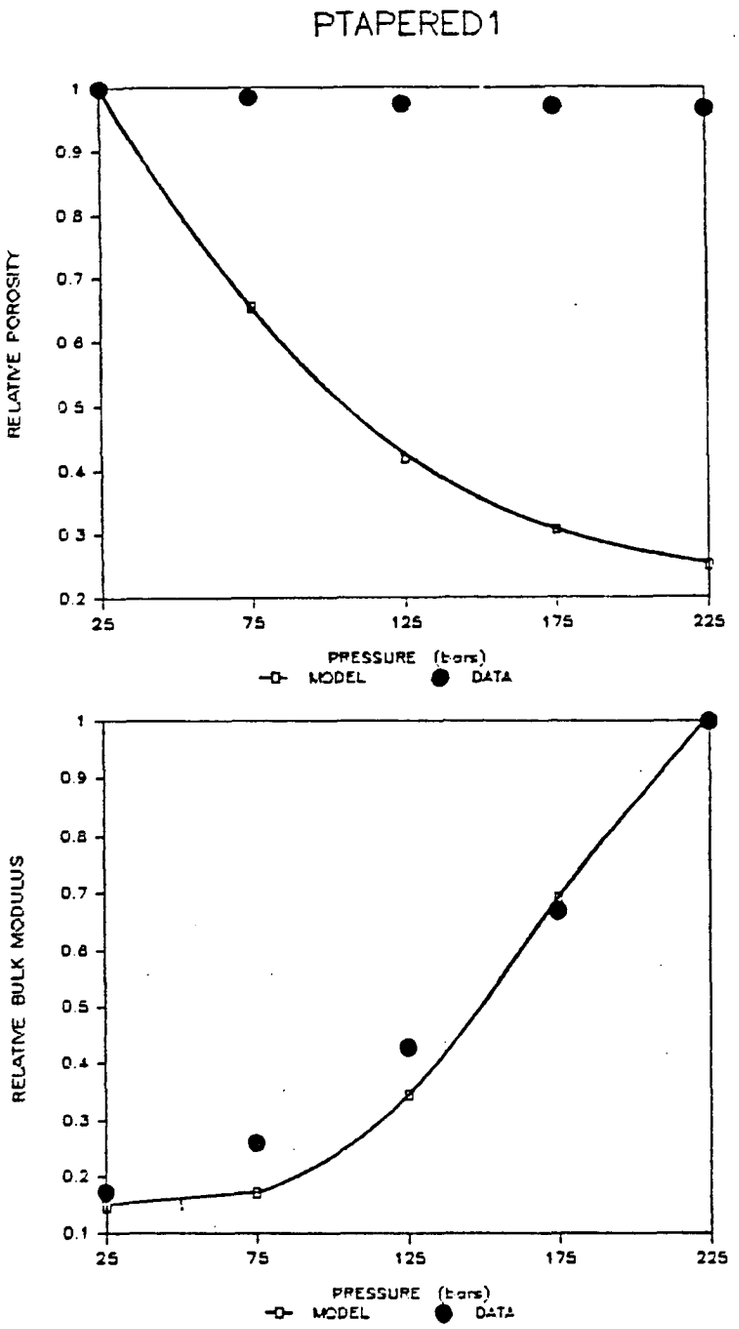

Figure 3-11: The figure shows model results for a group of PTAPERED1 pores against the data from the Fontainebleau A sample. Line with squares represents the model results; black circles represent the experimental data. The number of pores has been adjusted to reflect a match in the magnitude of the bulk modulus for the model and sample at 225 bars. One population of 9738 PTAPERED1 pores with $z = 16um$ was used. The magnitude of the porosity at 25 bars was about 0.8%.

TABLE 3-1

GEOMETRY	CHANGE IN K	INTERNAL AREA
Circular	small	large
Star-shaped	small	medium
Tapered	medium	small
Pseudo-tapered	large	small

From the last table we could conclude that each of the individual pore geometries is not suitable to simulate the bulk modulus and the porosity of the samples by themselves. However, if we mix them together according to some proportion, we may find that the bulk modulus and the porosity of the samples could be modeled, because the elastic responses of some geometries are complemented by others. From a physical point of view, that assumption makes sense because a sandstone is an aggregate of irregular grains which produce pore spaces having many types of shapes and sizes.

4. SCALES

At this point, it is useful to introduce some geometrical relations derived from the discrete representation of the pore space. In the last chapter, we showed that in order to apply the numerical algorithm, we must discretize the shape of the pore as a set of interconnected straight lines. Perhaps, the most interesting consequence of such discretization is that the internal area and the perimeter of a re-scaled pore geometry (i.e. a magnified or diminished pore in which its x and y axes have been multiplied by a constant value) can be obtained from the values of the unscaled pore. If the pore geometry is ellipsoidal, we can then say that the corresponding aspect ratios in both the original pore and the rescaled pore are exactly the same. However, their perimeters and internal areas are different. To derive the relations that link area and perimeter in both pores, we first consider one linear element of the pore walls.

Let $y = ax + h$ be the linear equation which represents one element of the original pore. The area under the straight line for the segment defined by $x_1 \leq x \leq x_2$ is given by:

$$A_0 = \int_{x_1}^{x_2} (ax + h)dx = \frac{a}{2}(x_2^2 - x_1^2) + h(x_2 - x_1) \qquad (4-1)$$

Now, let's multiply the x and y axes by a constant value m. The new equation for the straight line will be given by $y' = ax + mh$. The length of the new segment is now $mx_1 \leq x \leq mx_2$ and the area is given by:

$$A_1 = \int_{mx_1}^{mx_2} (ax + mh)dx = m^2(\frac{a}{2}(x_2^2 - x_1^2) + h(x_2 - x_1)) = m^2 A_0 \qquad (4-2)$$

Then, the new area is the old one multiplied by the square of the magnification term. This result can be extended to all the elements of the pore and by using the superposition principle, we can generalize (4-2) to be valid for the whole internal area of the pore. It is easy to show that (4-2) is also valid for the circular pores

which are made of a polygon of an infinite number of sides. For this case, the internal area of the circle is given by:

$$A_0 = \pi R_0^2 \qquad (4-3)$$

To rescale the pore, we multiply the radius of curvature R_0 by m. Then the new area is:

$$A_1 = \pi(mR_0)^2 = m^2\pi R_0^2 = m^2 A_0 \qquad (4-4)$$

Using similar arguments, one can show that the perimeter of a rescaled pore ($perimeter_1$) can be calculated from the perimeter of the original pore ($perimeter_0$) by:

$$perimeter_1 = m \times perimeter_0 \qquad (4-5)$$

Rescaling a pore produces changes in the magnitude of the internal volume of the cavity and the derivative of its area with respect to pressure. However, the functional form and shape of the derivative for both the original and rescaled pores, remain constant. (The internal area on both pores differs by the square of the factor m which is independent of pressure.) This fact leads to a very important property which will be discused next.

Let's start by writing the equation for the bulk modulus of a homogeneous population of pores, i.e. pores with the same size and only one aspect ratio.:

$$\frac{1}{K_f} = \frac{1}{K_0} + \frac{2m_0{}^2 Nz}{V}\frac{dA}{d\sigma} \qquad (4-6)$$

where m_0 indicates the magnification of the pores within the populations with respect to a reference pore with magnification $m = 1$.

Now, let's assume that the solid contains two populations of pores. Both populations are made of the same type of pores (same aspect ratio) but different

sizes. Calling m_1 the magnification of the first population which contains N_1 pores and m_2 is the magnification of the second population which contains N_2 pores. The bulk modulus for the solid which holds the two populations is given by:

$$\frac{1}{K_f} = \frac{1}{K_0} + \frac{2z}{V}(N_1 {m_1}^2 + N_2 {m_2}^2)\frac{dA}{d\sigma} \qquad (4-7)$$

Now, by picking convenient values for N_1 and N_2, we can see that equation (4-7) produces the same result as equation (4-6). Then, by equating (4-6) to (4-7) we find that:

$$N = \frac{N_1 {m_1}^2 + N_2 {m_2}^2}{{m_0}^2} \qquad (4-8)$$

To get equation (4-8) we have assumed that the length of the pore tubes z is constant for all the populations.

The meaning of equation (4-8) is that a particular population of pores with specific size can be split in many populations of the same type of pores. This conclusion clearly affects the uniqueness of the theoretical model and it will be discussed in more detail in section 6.

As was pointed out before, the shape of an ellipsoidal pore can be characterized by a geometrical relation called the aspect ratio which measured the eccentricity of the ellipse. This description is useful for other regular pore geometries like the circular and tapered pores. However, once the geometries become more irregular, the aspect ratio becomes meaningless. Based on the results obtained in (4-2) and (4-5) we will introduce a new factor that can be used instead of the aspect ratio to characterize more irregular geometries. As with the aspect ratio, this factor must be invariant to changes in the pore scale.

In order to find such a factor, we start looking at the ratio between the external surface of the pore and its internal volume which is known as the surface to volume

ratio. Separating this relation in its primitive components we have:

$$(\frac{S}{V})_0 = \frac{perimeter \times z}{area \times z} \qquad (4-9)$$

The surface to volume ratio for a rescaled pore is then:

$$(\frac{S}{V})_1 = \frac{m \times perimeter \times z}{m^2 \times area \times z} \qquad (4-10)$$

which is clearly not equal to (4-9) due to the factor m in the denominator. Then the surface-to-volume ratio is not invariant to the scaling property. Now, if we define the ratio between the surface and the square root of the volume, we end up with a parameter which is independent of the scale used and still is related to the geometry of the pore. To make it dimensionless, we multiply the internal volume by the length of the pore z. If we call this parameter ψ factor it will be given by:

$$\psi = \frac{perimeter}{\sqrt{area}} \qquad (4-11)$$

We must recall that (4-10) has been introduced only to facilitate the description of irregular shapes and may not have any other physical meaning. (A similar factor was introduced by O'Connel and Budiansky, 1974 to define the pore density in materials containing elliptical cracks. See chapter I.)

The next table contains the ψ factor as well as the aspect ratio (where applicable) for some of the geometries presented in section 3.

TABLE 4-1

GEOMETRY	ASPECT RATIO	ψ FACTOR
Circular R=1	1	3.5
Star1	n/a	16.1
Ptapered2	n/a	46.9
Ptapered1	n/a	50.8
Tapered	.002	57.8

As we can see, the ψ factor is inversely proportional to the aspect ratio.

5. SIMULATIONS

So far we have settled the theoretical basis for modeling the pressure dependence of the bulk modulus as well as the porosity of several samples of sandstones. We have also explored the elastic responses for several pore geometries. In this section we will combine these two aspects to obtain a model which can explain the observed data. As was pointed out in a previous section, we will make use of a forward model so only the most representative pore shapes will be considered. This implies that the model will contain a minimum number of geometries which are able to represent the most remarkable aspects of elastic response (average shape and magnitude).

The first step in the simulation is to establish a working model for the rock. From now on, it will be assumed that the rock can be characterized as a cubic solid filled with an elastic matrix. The volume of the solid is about 10^5 $(um)^3$, where um denotes unit of measure. The reason to use an arbitrary system of measure instead of a standard system like the CGS, is because equations (3-1) and (3-2), which establish the functional form of the bulk modulus and porosity of the rock, are independent of the system of units used to define the pore and rock dimensions as long as these two parameters are measured with the same system of units. The following table summarizes some of the matrix properties.

TABLE 5-1

MATRIX PROPERTY	VALUE
Young's modulus	4×10^5 bars
Poisson's ratio	0.23
Density	2.65
Total volume	10^5 um^3

Other elastic parameters like the matrix bulk modulus are derived from the

values given in the above table.

The elastic matrix is embedded with pores of different shapes. Then the model will be characterized by:

1) Pore shapes

2) Number of pores per shape

3) Length of the pore tubes for each shape

Modifying each one of these parameters, will produce a change in the behavior of the bulk modulus and porosity of the model. Then, to simulate the observed data, it is necessary to keep changing the values of these parameters until the model results match the data.

We start the simulation analyzing the Fontainebleau A sample. Figures 5-1 to 5-3 show the results of the simulation. Figure 5-1 shows the bulk modulus simulation. The solid line represents the model results while the dots represent the data results. Although the plot shows only a match of the relative bulk modulus, it has also been required that data and model coincide in magnitude at a pressure of 225 bars. The biggest differences between data and model are about 4%. This error could not be reduced because of the small and limited number of pore shapes used in the model. Figure 5-2 shows the relative porosity as a function of pressure for both model (solid line) and data (dots). Magnitude of the porosity for model and data was required to coincide at a pressure of 25 bars. Figure 5-3 shows a histogram representing (a) the number of pores used in each geometry (in percent) and (b) the internal volume occupied by all the pores of a given shape (in percent). Two important conclusions can be made from the histogram:

1) Most of the porosity is concentrated in the stiff pores (circular)

2) Pores with bigger ψ factors tend to be more abundant than pores with smaller ψ factors.

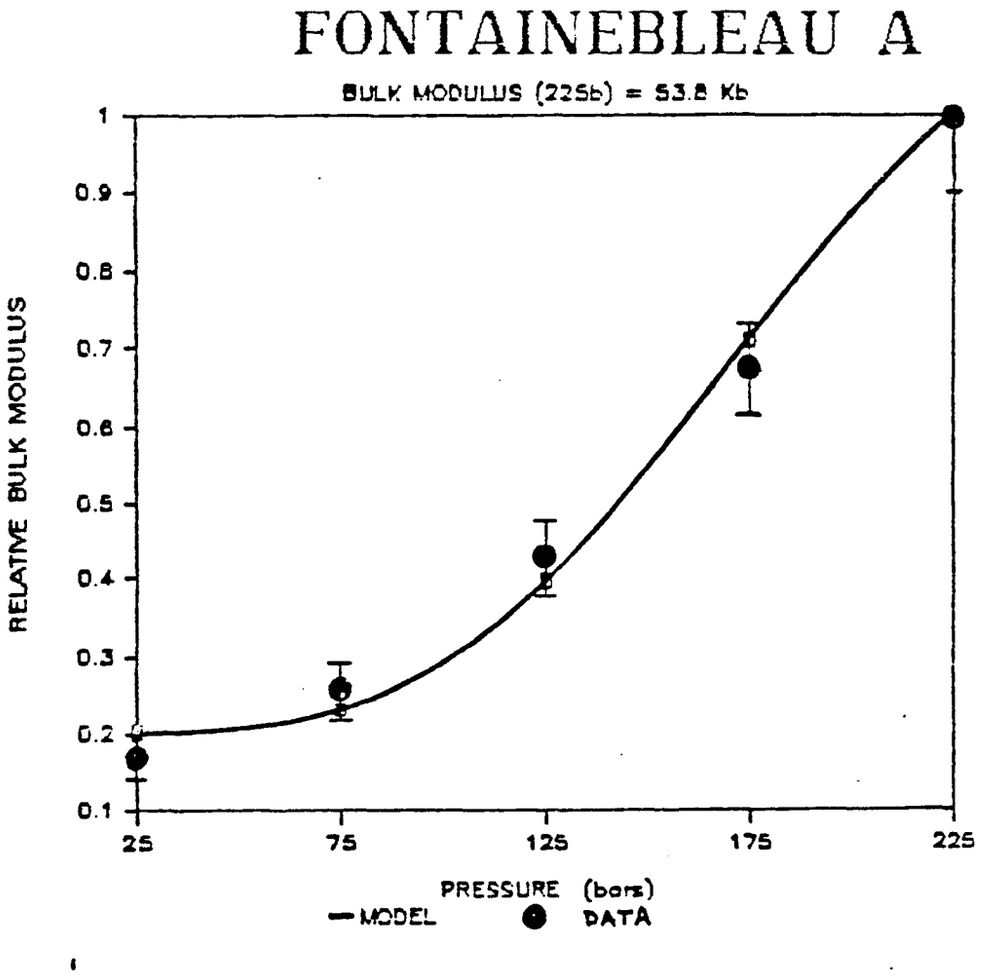

Figure 5-1: The figure shows the results of the relative bulk modulus simulation for the Fontainebleau A sample. Line with squares represents the model results; black circles represent the experimental data. The model parameters were adjusted to reflect a match in the magnitude of the bulk modulus for the model and sample at 225 bars as well as a match in the porosity at 25 bars.

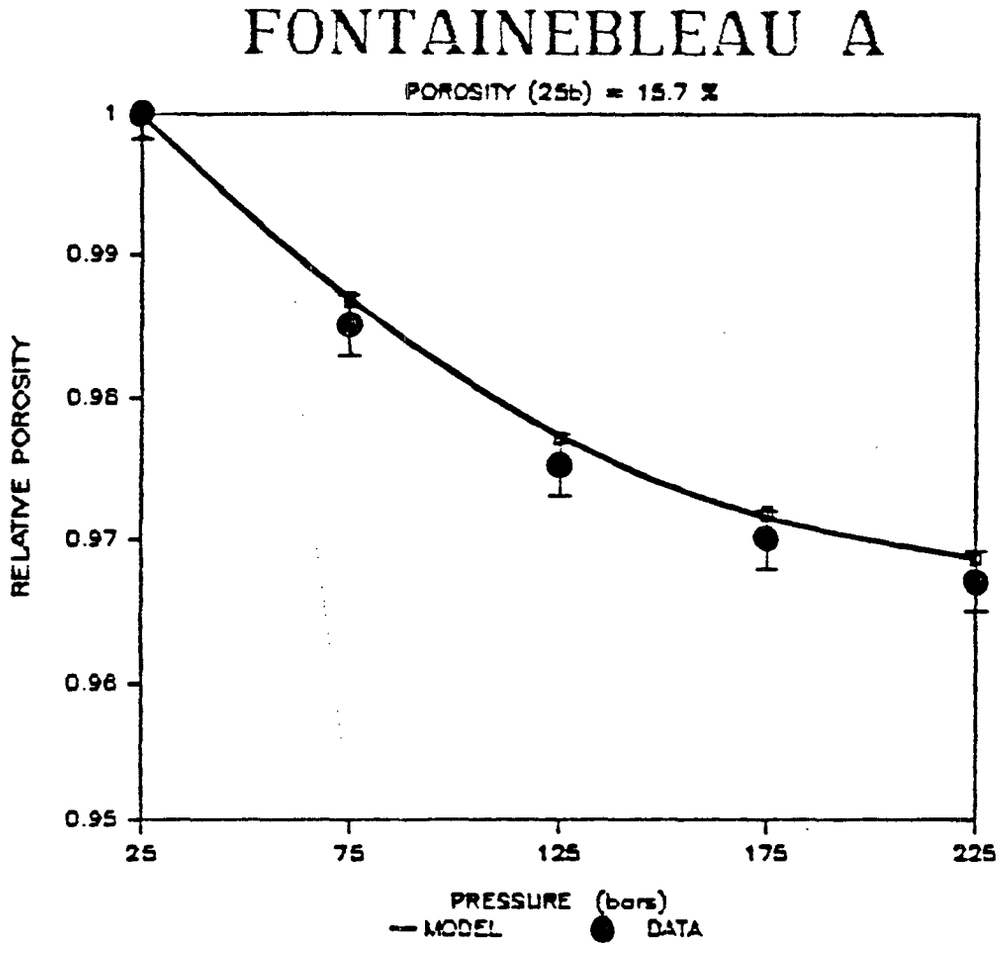

Figure 5-2: The figure shows the results of the relative porosity simulation for the Fontainebleau A sample. Line with squares represents the model results; black circles represent the experimental data. The model parameters were adjusted to reflect a match in the magnitude of the bulk modulus for the model and sample at 225 bars as well as a match in the porosity at 25 bars.

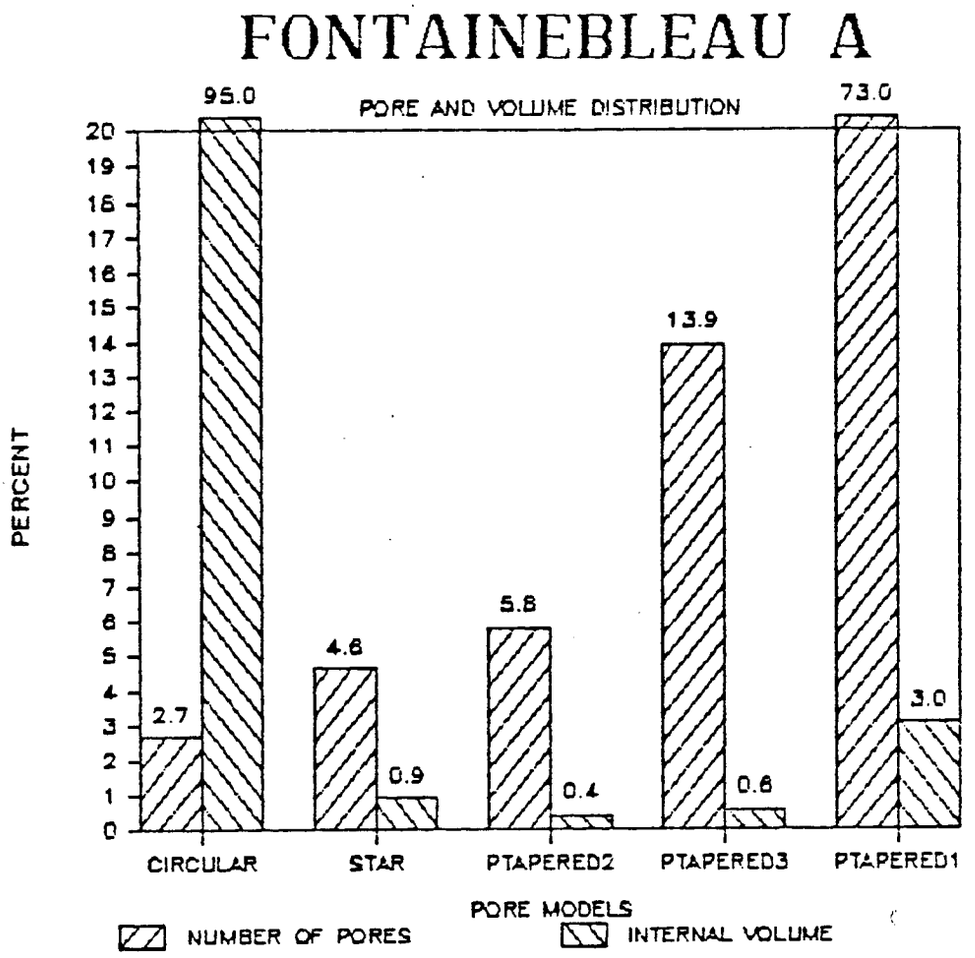

Figure 5-3: The figure shows a histogram representing the percent number of pores used per geometry and the percent volume occupied by all the pores of a given shape to model the Fontainebleau A sample.

Due to the fact that the model was not computed by using an ordinary inversion technique (like the least square method), it is difficult to obtain a quantitative parameter or set of parameters like the resolution and covariance matrix *(Mendoza et al., 1985. See chapter V.)* which describe the contribution and stability of the solution for each of the pore geometries involved in the simulation. However, we can introduce some perturbations by eliminating one geometry and then comparing the new response of the model with respect to the original one. In this way, it is possible to get a good estimate about the role played by a particular shape within the model. Figure 5-4 shows the behavior of the relative bulk modulus generated by a model when each of the geometries has been eliminated. Figure 5-5 is very similar to figure 5-4 but it shows the relative change in porosity. Figure 5-6a shows the variation in magnitude for the bulk modulus at 225 bars while figure 5-6b presents the variation in magnitude for the porosity at 25 bars for the perturbed model. From these figures we can conclude that both the circular pores and the PTAPERED1 pores, are the major contributors to the simulation. The STAR1 pores contribute on a minor scale. Other pores have a minimal contribution to the general trend but they can be used to smooth the curve a little bit more.

Figures 5-7 to 5-9 show the results obtained by modeling the Fontainebleau B sample. Although its elastic behavior is similar to that found in the Fontainebleau A sample, the porosity is now 19.6%. Because the porosity is larger, it was necessary to increase the volume occupied by the circular pores as shown in figure 5-9.

Figures 5-10 to 5-12 show the model results for the Santa Barbara sample, while figures 5-13 to 5-15 present the simulations for the Nugget sample. These two samples have lower porosities (11.7% and 9.3% respectively) and in both cases, the bulk modulus was modeled fairly well. This is probably due to the fact that the lower the porosity the less complex the pore space is and therefore the more easily

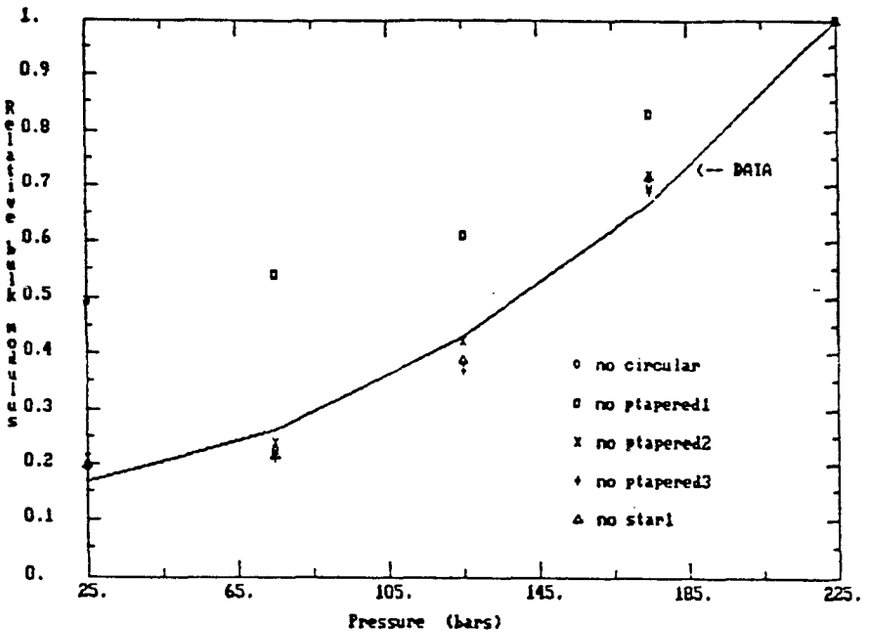

Figure 5-4: The figure shows the behavior of the relative bulk modulus simulation when each of the geometries has been eliminated. The solid line indicates the results of the experimental data. Symbols indicate that all but that particular pore are included in the model. For instance, the open circle indicates that the model contains all the geometries except the circular.

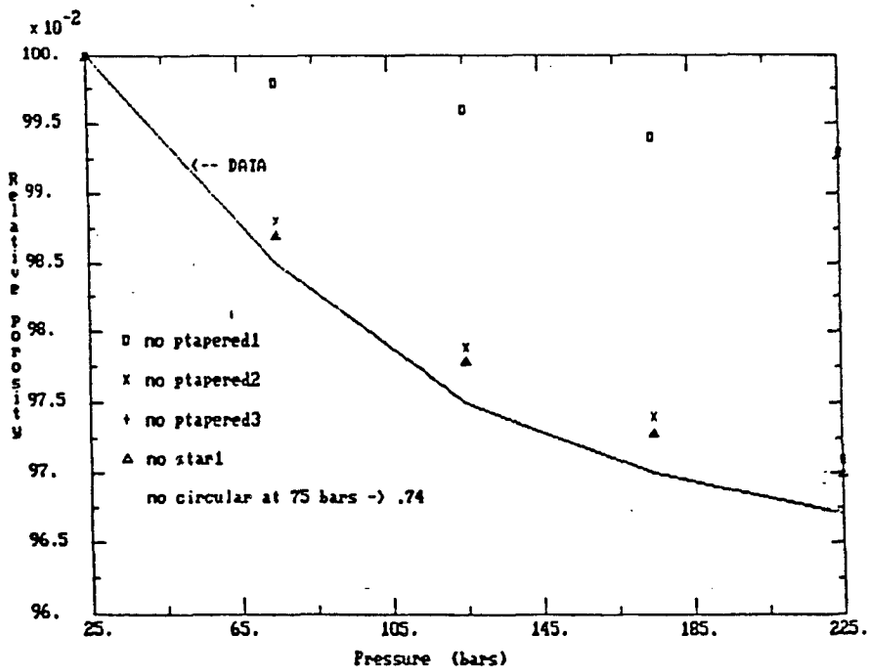

Figure 5-5: The figure shows the behavior of the relative porosity simulation when each of the geometries have been eliminated. The solid line indicates the results of the experimental data. Symbols indicate that all but that particular pore are included in the model.

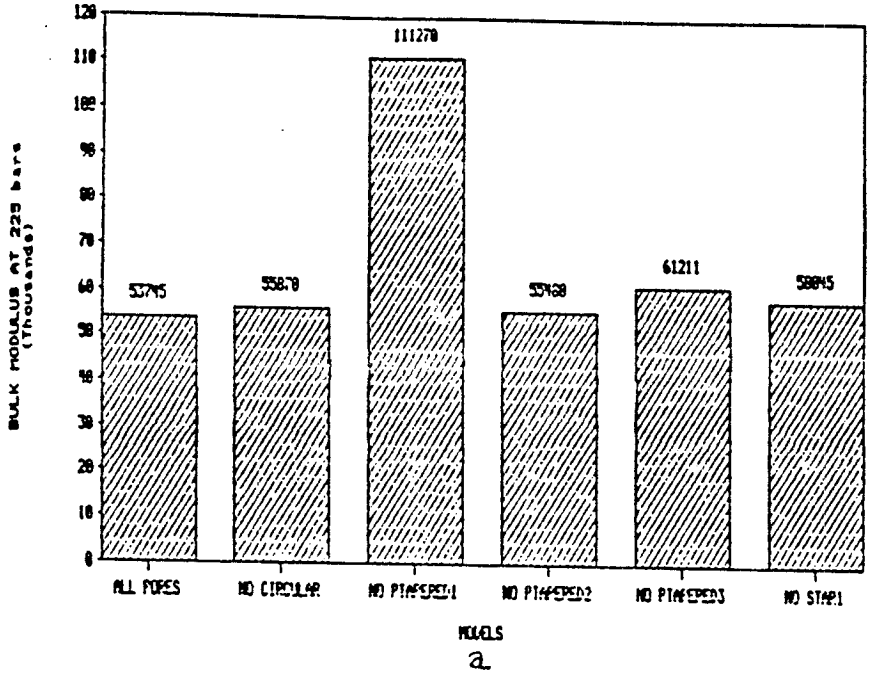

a.

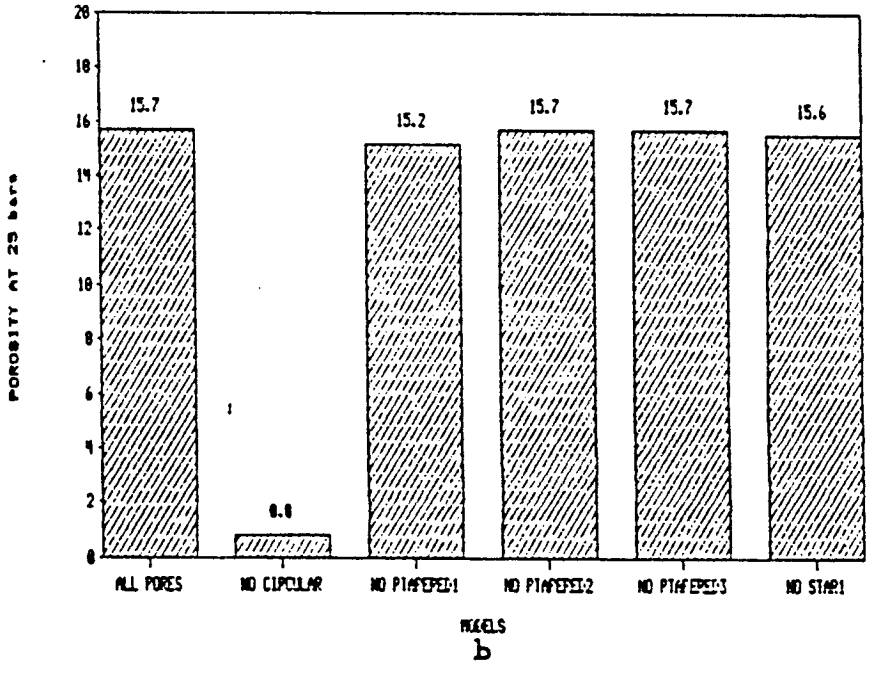

b

Figure 5-6: a) Histogram representing the variation in percent of the magnitude for the bulk modulus at 225 bars in the models presented in figure 5-4. The numbers at top of the bars indicate the magnitude of the bulk modulus for that particular model. b) Histogram representing the variation in percent of the magnitude for the porosity at 25 bars in the model presented in figure 5-5. Numbers at top of the bars indicate the magnitude of the porosity.

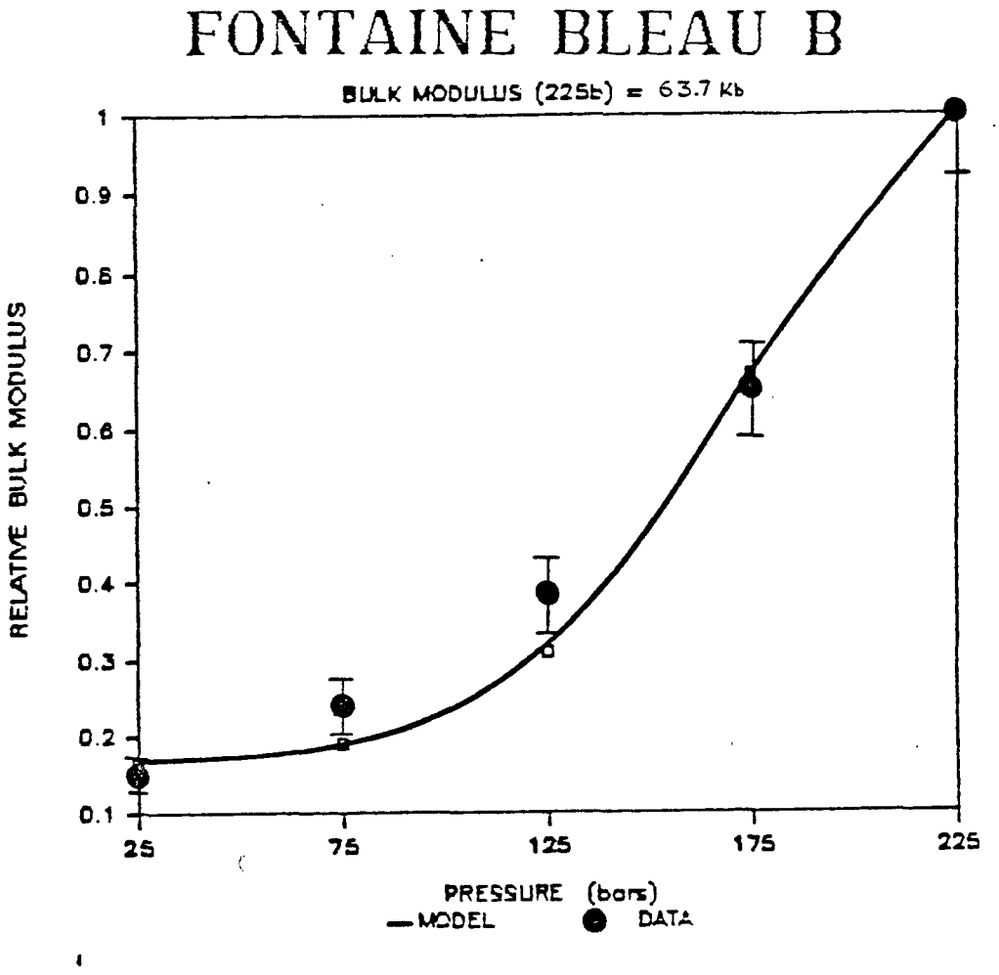

Figure 5-7: The figure shows the results of the relative bulk modulus simulation for the Fontainebleau B sample. Line with squares represents the model results; black circles represent the experimental data. The model parameters were adjusted to reflect a match in the magnitude of the bulk modulus for the model and sample at 225 bars as well as a match in the porosity at 25 bars.

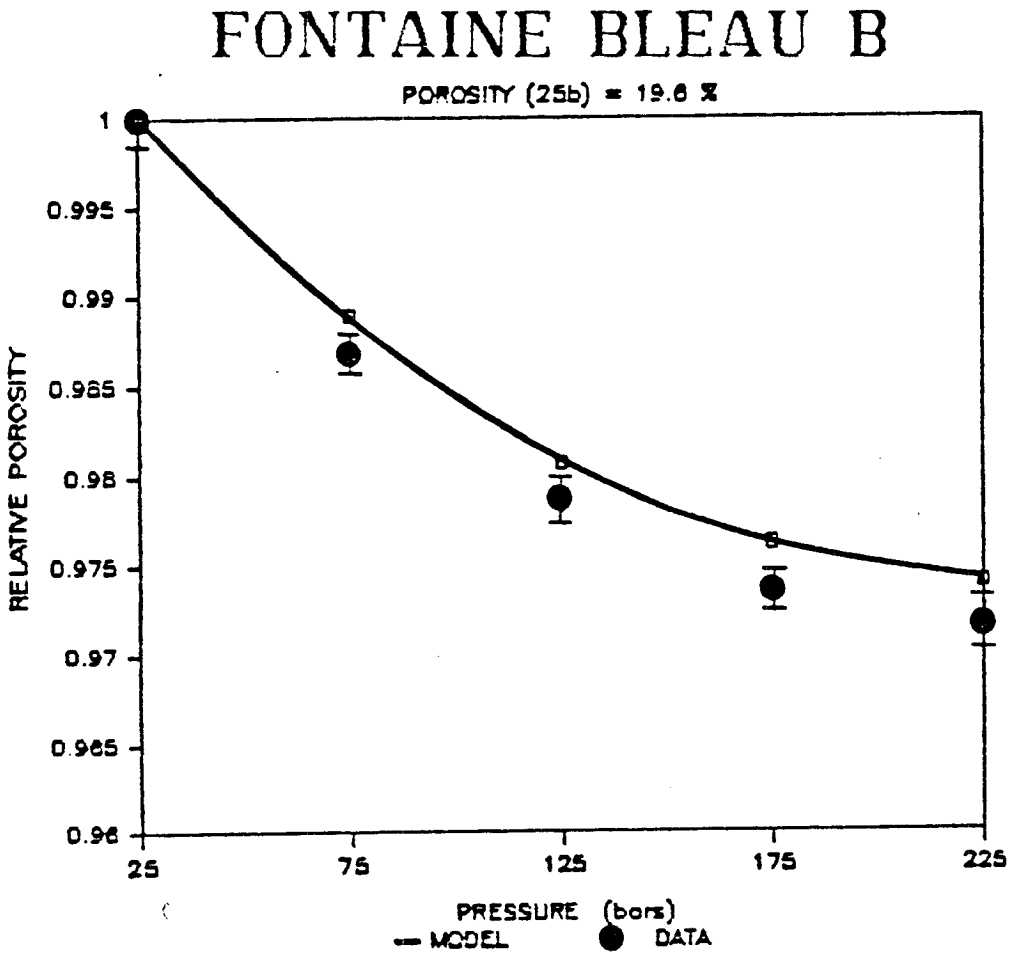

Figure 5-8: The figure shows the results of the relative porosity simulation for the Fontainebleau B sample. Line with squares represents the model results; black circles represent the experimental data. The model parameters were adjusted to reflect a match in the magnitude of the bulk modulus for the model and sample at 225 bars as well as a match in the porosity at 25 bars.

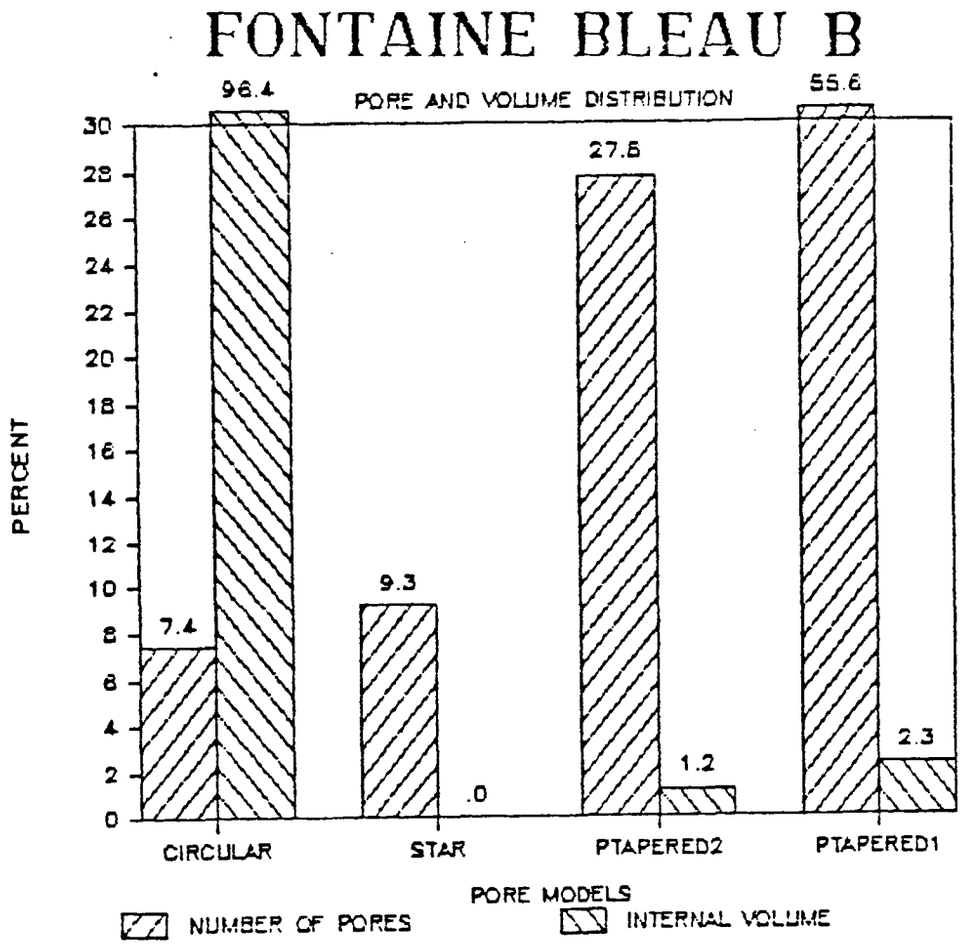

Figure 5-9: The figure shows a histogram representing the percent number of pores used per geometry and the percent volume occupied by all the pores of a given shape to model the Fontainebleau B sample.

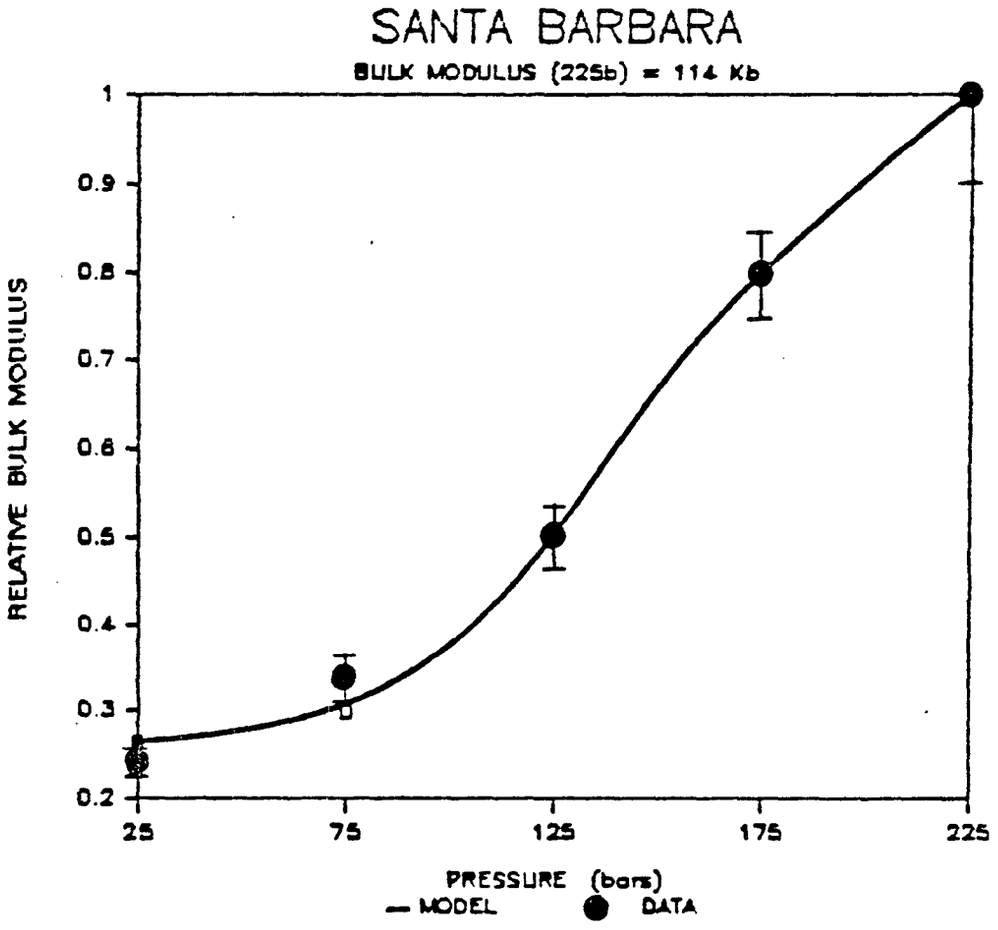

Figure 5-10: The figure shows the results of the relative bulk modulus simulation for the Santa Barbara sample. Line with squares represents the model results; black circles represent the experimental data. The model parameters were adjusted to reflect a match in the magnitude of the bulk modulus for the model and sample at 225 bars as well as a match in the porosity at 25 bars.

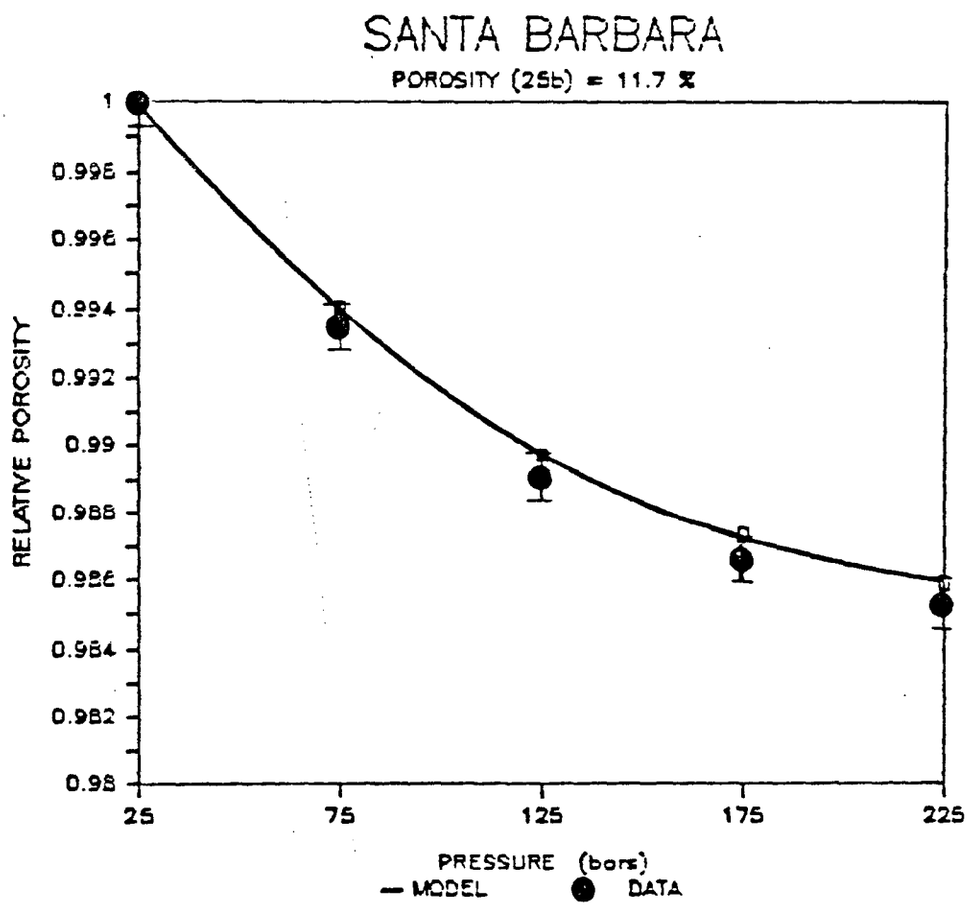

Figure 5-11: The figure shows the results of the relative porosity simulation for the Santa Barbara sample. Line with squares represents the model results; black circles represent the experimental data. The model parameters were adjusted to reflect a match in the magnitude of the bulk modulus for the model and sample at 225 bars as well as a match in the porosity at 25 bars.

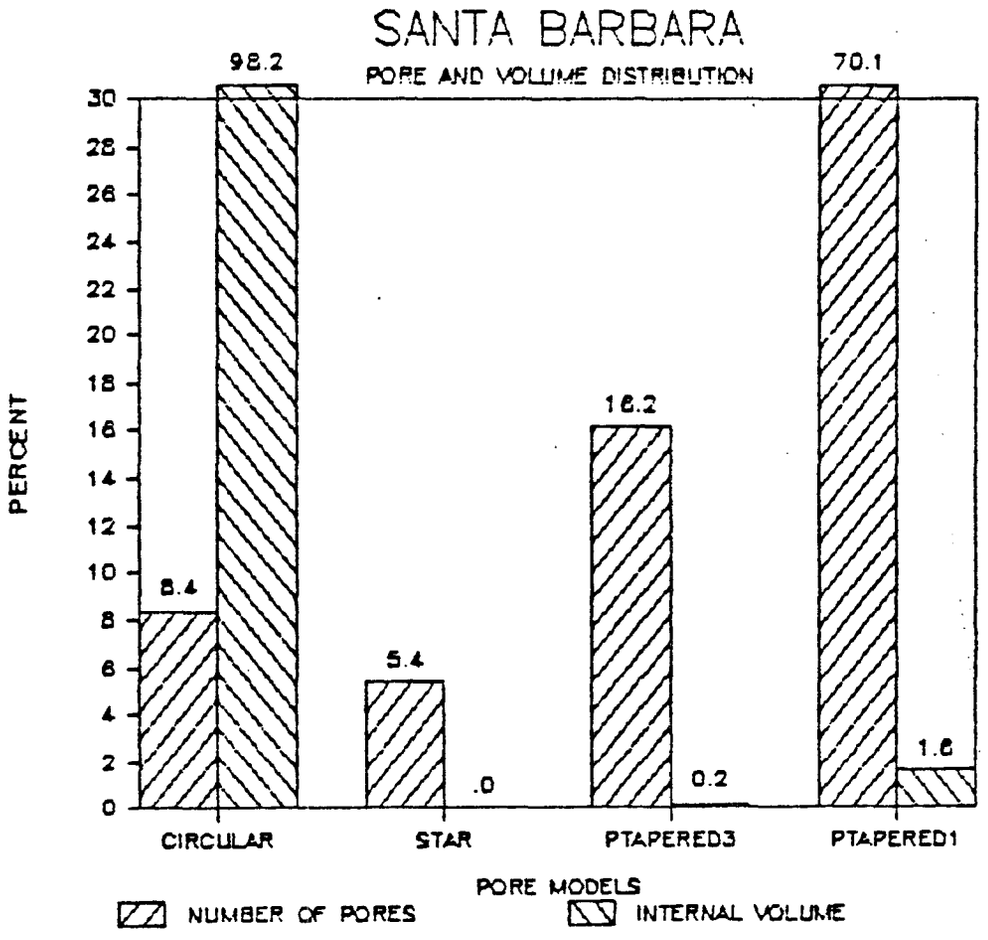

Figure 5-12: The figure shows a histogram representing the percent number of pores used per geometry and the percent volume occupied by all the pores of a given shape to model the Santa Barbara sample.

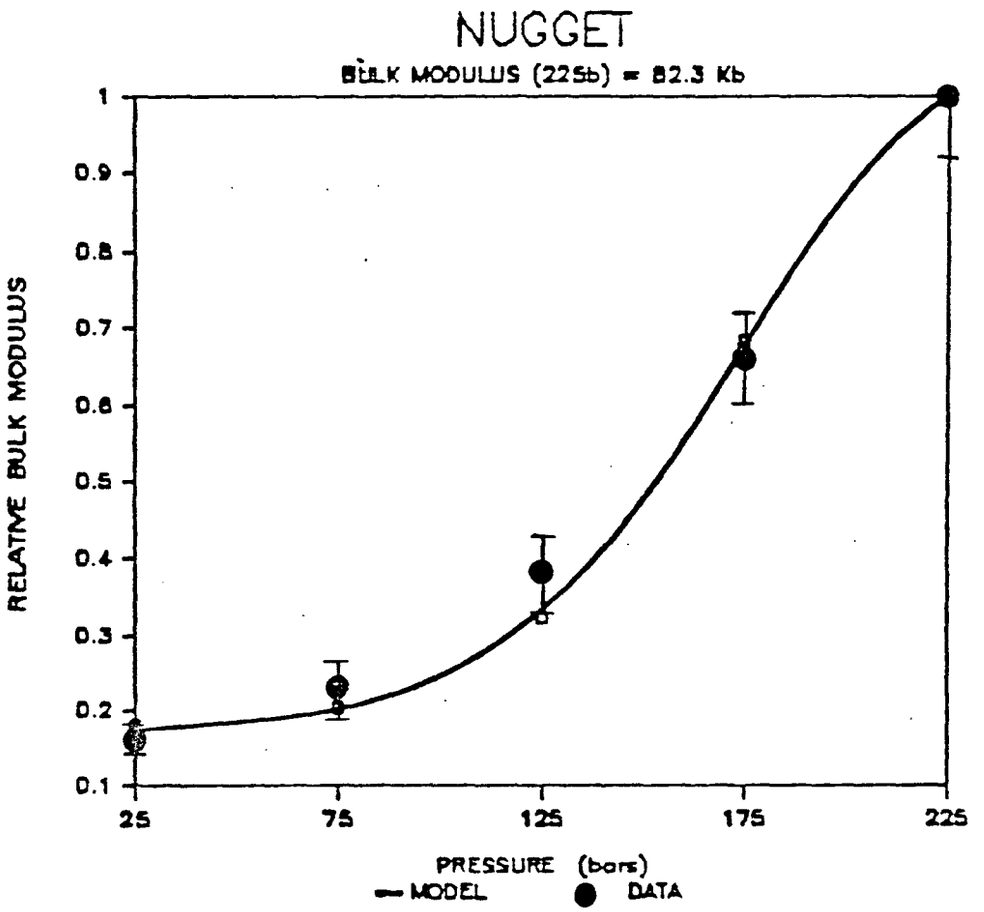

Figure 5-13: The figure shows the results of the relative bulk modulus simulation for the Nugget sample. Line with squares represents the model results; black circles represent the experimental data. The model parameters were adjusted to reflect a match in the magnitude of the bulk modulus for the model and sample at 225 bars as well as a match in the porosity at 25 bars.

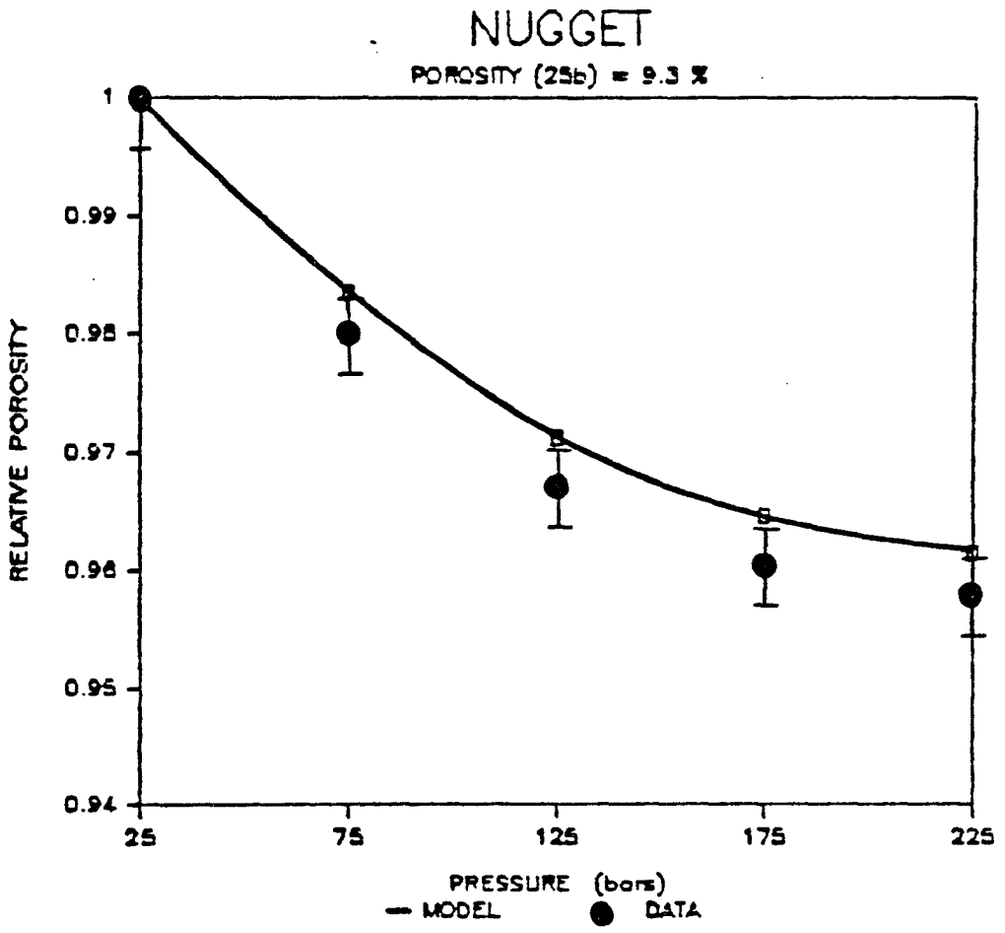

Figure 5-14: The figure shows the results of the relative porosity simulation for the Nugget sample. Line with squares represents the model results; black circles represent the experimental data. The model parameters were adjusted to reflect a match in the magnitude of the bulk modulus for the model and sample at 225 bars as well as a match in the porosity at 25 bars.

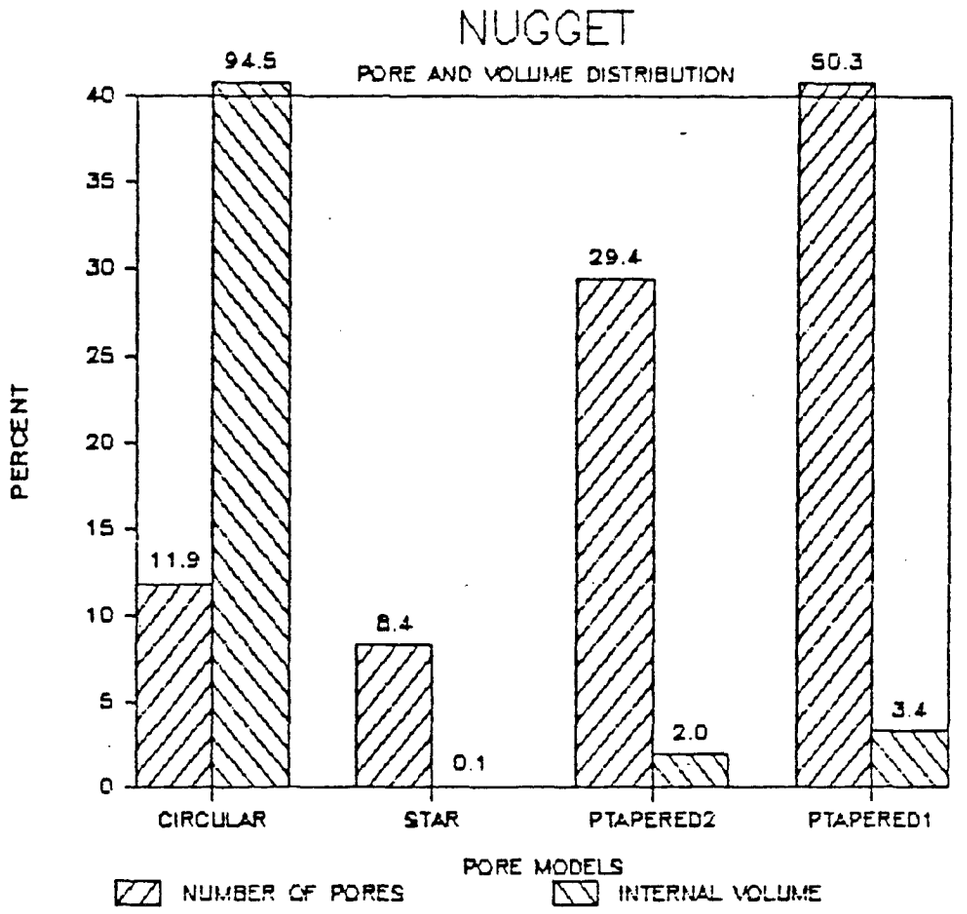

Figure 5-15: The figure shows a histogram representing the percent number of pores used per geometry and the percent volume occupied by all the pores of a given shape to model the Nugget sample.

it is simulated by a simple model.

The last modeled rock was the Tory sample. This rock is a little peculiar with respect to the rest of the samples because the change in bulk modulus between 25 and 225 bars is less than that of the other samples (65% against 74% or more). Because of this smaller change, we need to use a pair of interactive tapered pores with an aspect ratio of 0.002 and a separation between the tapered edges of $0.04c$ (c is the half length of the pore). Figures 5-16 to 5-18 show the results of the simulation.

6. UNIQUENESS OF THE SOLUTION

Once the theoretical models have been presented, it is important to discuss the scope and limitations of the simulation.

To start, we will say that the models presented in this study are terribly nonunique because the average values for the bulk modulus and porosity —which is what we measure— are independent of the geometrical disposition of the pores within the rock. In other words, we can locate all the pores in the model within one corner of the solid or we can randomly distribute the pores within the whole body and get the same result in both cases. The explanation of this fact is not difficult to understand. First, porosity refers only to the total volume occupied by the pores regardless of how such volume is distributed. Second, as was discussed in the last chapter, bulk modulus is measured (and also modeled) by subjecting the solid to hydrostatic stresses. Then, the pore spaces will deform at the same rate no matter how we orient them. We can refuse this argument by saying that the pores must be separated by some distance so that they do not interact but, with more than 80% of the solid occupied by the elastic matrix, there is enough room inside to safely distribute the pore spaces. Even though we may consider some interactive pores,

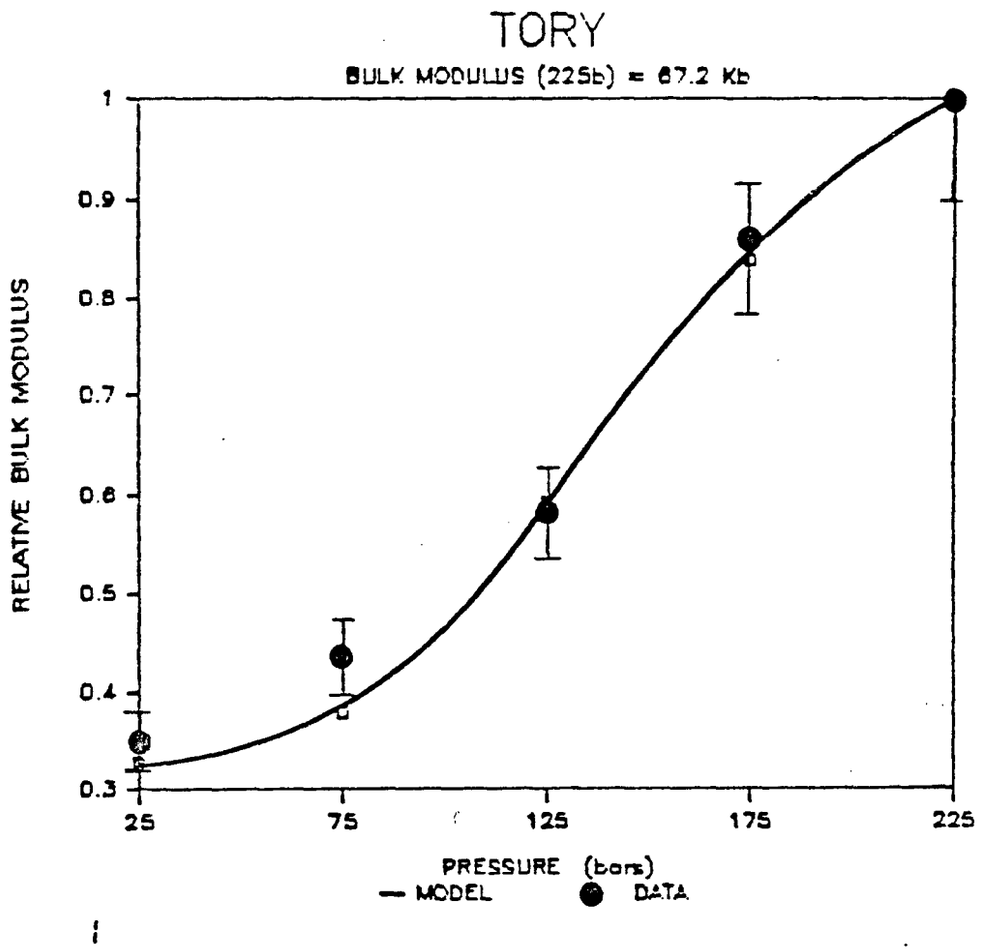

Figure 5-16: The figure shows the results of the relative bulk modulus simulation for the Tory sample. Line with squares represents the model results; black circles represent the experimental data. The model parameters were adjusted to reflect a match in the magnitude of the bulk modulus for the model and sample at 225 bars as well as a match in the porosity at 25 bars

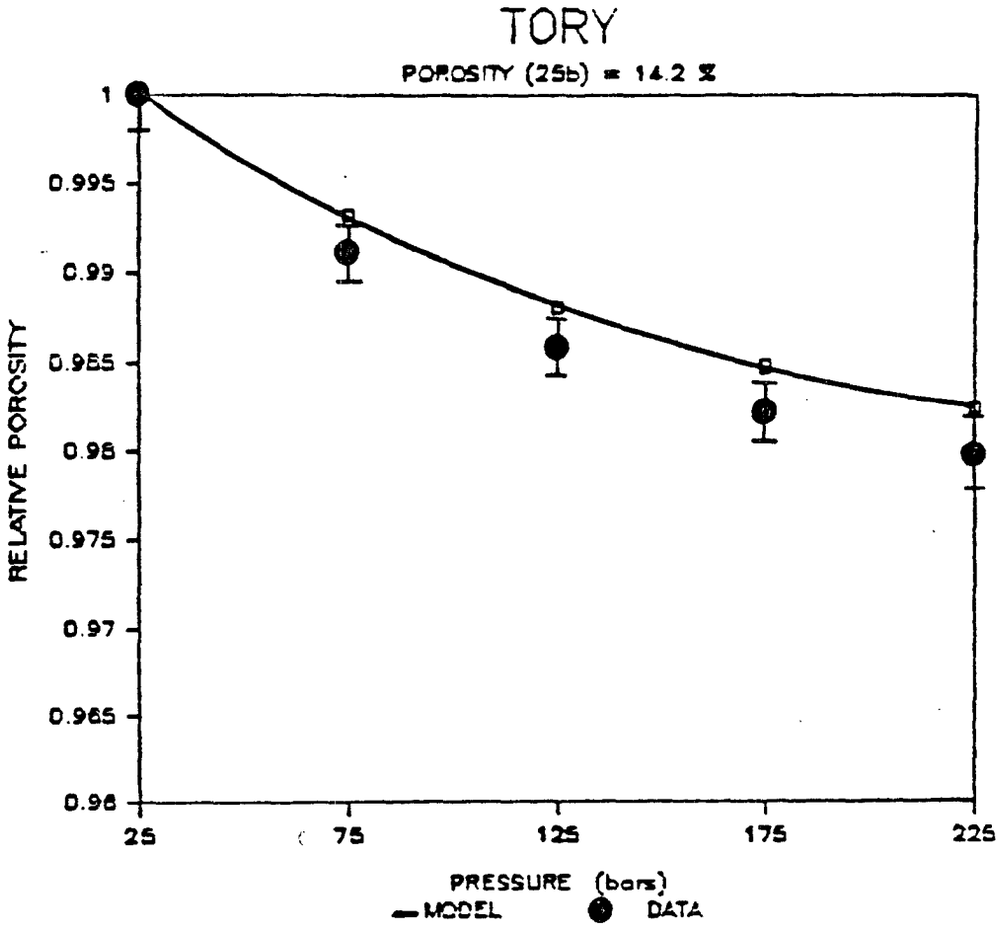

Figure 5-17: The figure shows the results of the relative porosity simulation for the Tory sample. Line with squares represents the model results; black circles represent the experimental data. The model parameters were adjusted to reflect a match in the magnitude of the bulk modulus for the model and sample at 225 bars as well as a match in the porosity at 25 bars.

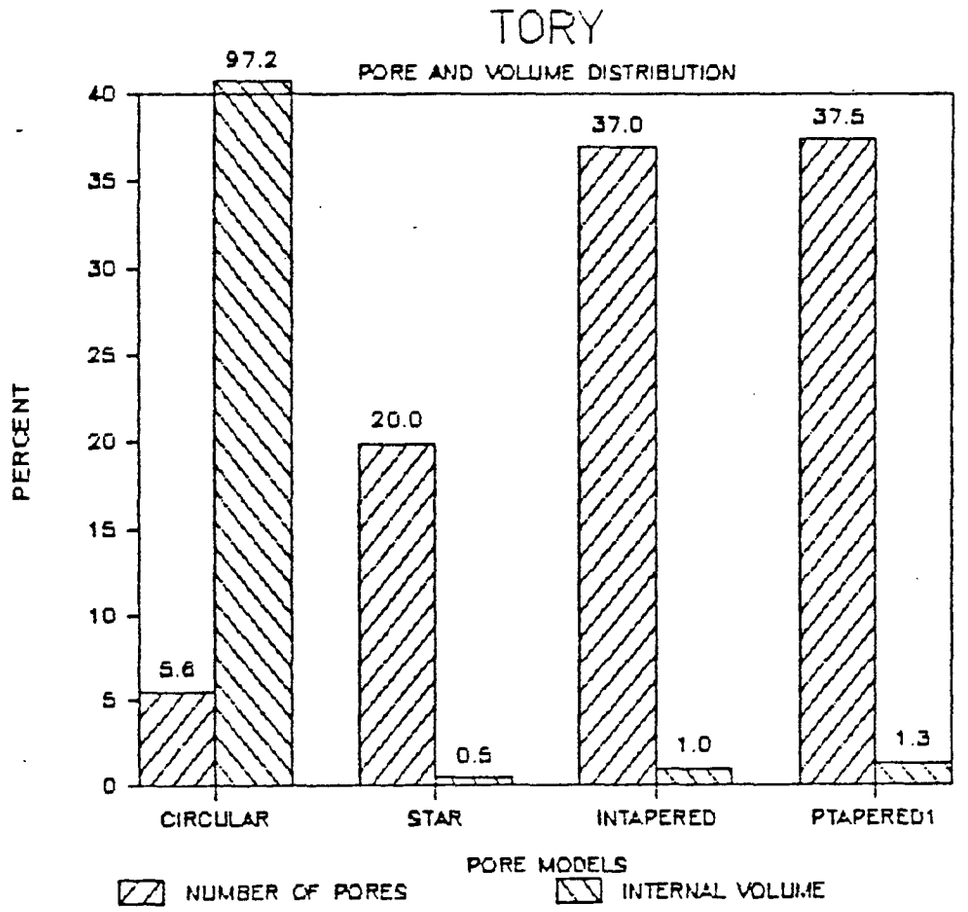

Figure 5-18: The figure Figure 2-1: The figure shows a typical plot of the relative porosity as a function of pressure for the Fontainebleau A sample. The magnitude of the porosity at 25 bars is 15.7%.

as in the case of the STAR1 pores, the space occupied by the matrix is enormous.

To constrain the pore distribution inside the solid, it is necessary to take into account other parameters which are more dependent on the spatial disposition than the two parameters we have considered in this study. Among the parameters that are spatially dependent we can cite: the Young's modulus or electrical and hydraulic properties *(Owen, 1952; Kirkpatrick, 1973; Seeburger, 1984)*. Future work will involve the use of these kind of parameters.

There are other factors which can also reduce the uniqueness of the simulation. For instance, the scaling property exhibited by the pore geometries can generate several models with the same ψ factor but with different magnification which produce exactly the same results. Again, we need to introduce a physical property which depends not only on the ψ factor but also on the magnification of the pore. The surface-to-volume ratio discussed in section 4 could be used to partially remove that ambiguity since such a ratio measures the proportion of internal area and perimeter of the pore which varies for two identical pores with different magnification.

From the above discussion, we can conclude that the porosity and bulk modulus are not the most convenient parameters to establish a unique model that represents the elastic properties in rocks. However, because the porosity and bulk modulus do not depend on the spatial distribution of pores in the rock, they are easier to modeled. Therefore, they represent a convenient way to develop and test theoretical models which incorporate new pore shapes. If a particular geometry is not suitable to match the observed bulk modulus and porosity data, we do not expect that such geometry fits any other elastic moduli. Therefore, a theoretical model as described in this study, can be used as a starting point to construct more complex and then realistic models of the elastic behavior of porous materials.

7. DISCUSSION

In the last section we discussed the main reasons why the numerical simulations considered in this study do not lead to a unique solution. In this section, other aspects of the simulation will be considered.

The main point to consider has to do with the kind of theoretical model used to describe the rocks. As was mentioned before, the solid is represented by an elastic solid matrix which has been filled with cavities. The stress and strain fields inside the matrix obey Hook's law, i.e. strains inside the solid are proportional to the applied stress field. In principle, this is a simplistic representation of a sedimentary rock, which in real life is more heterogeneous and complex than that. However, the good agreement observed between the experimental data and the simulation results indicate that in principle, a linear elastic model is a good approximation to the real behavior of the sandstones, at least for the samples considered in this study. We attribute most of the discrepancies observed between model and data mainly to the small number of pore geometries considered and, on a minor scale, to the simple representation of the solid matrix which does not take into account local phenomena like cementation, clay content, small changes in elastic properties (heterogeneities), and others. We have been careful to chose samples which are relatively clean so that the effect of clays is small. *(Tosaya and Nur, 1982; Han and Nur, 1986.)* However, *Han and Nur (1986)* have pointed out that in order to model elastic constants in solids with moderated to high clay contents, it is important to include some terms that account for the presence and effect of clays on the behavior of the elastic moduli and seismic velocities. Unfortunately, theoretical models that take into account the mechanical effect of the clays within the pores and matrix are scarce and more research must be done in that area.

8. CONCLUSIONS

The numerical models discussed in this study give us a global information about some elastic properties of the solid as well as the possible internal structure of the pore spaces, regardless of the geometrical disposition of the cavities within the body.

The use of the boundary elements method as a numerical technique to study the elastic response of solids opens a great number of possibilities because it allows exploration of more complex and real geometries than the analytical methods permit. Yet there are problems which can be solved by including more powerful and sophisticated algorithms, under the context of the boundary elements technique.

To remove some nonuniqueness, it is necessary to consider other properties, for example: Young's modulus and hydraulic properties.

An inversion technique is mandatory to produce a more concise model of the pore spaces.

REFERENCES

Biot, M. A., 1956, Theory of propagation of elastic Waves in a fluid-saturated porous solid. I. Low-frequency range, II. Higher frequency range. *J.A.S.A. vol 28 No. 2.*

Han, D., and A. Nur, 1986, Effects of porosity and clay content on velocities of sandstones. *Geophysics, in print.*

Kirkpatrick, S., 1973, Percolation and conduction. *Rev. Mod. Phys., vol 45.*

Kutter, H. K., 1970, Stress analysis of a pressurized circular hole with radila cracks in an infinity elastic plate. *Int. J. Frac. Mech., vol 6, No. 3.*

Mavko, G., and A. Nur, 1978, The effect of nonelliptical cracks on the compressibility of rocks. *J. Geophys. Res., vol 83.*

Mendoza, J., and D. Morgan, 1985, BASIC-HYPO: A basic language hypocenter location program. User's guide. *Stanford University publications in geological sciences, vol XIX, No. 1.*

O'Connel, R. J. and B. Budiansky, 1974, Seismic velocities in dry and saturated cracked solids. *J. Geophys. Res., vol 79.*

Owen, J. E., 1952, The resistivity of a fluid-filled porous body. *Trans, AIME, vol 195.*

Rooke, D. E., and I. Sneddon, 1969, The crack energy and the stress intensity factor for a cruciform crack deformed by internal pressure. *Int. J. Engng. Sci., vol 7.*

Seeburger, D., 1984, A pore space model for rock permeability and bulk modulus. *J. Geophys. Res., vol 89.*

Simmons, G., and W. F. Brace, 1965, Comparison of static and dynamic measurements of compressibility of rocks. *J. Geophys. Res., vol 70, No. 22.*

SRP, 1986, The Stanford Rock Physics catalog. *Stanford Rock Physics project, vol 3, Stanford University, Stanford, CA 94305.*

Toksöz, M. N., and C. A. Cheng, and A. Timur, 1976, Velocities of seismic waves in porous rocks. *Geophysics, vol 41, No. 4.*

Tosaya, C., and A. Nur., 1982, Effect of diagenesis and clay on compressional velocities in rocks. *Geo. Res. Let., vol 9, No. 1.*

Williams, W. E., 1971, A star-shaped crack deformed by an arbitrary internal pressure. *Int. J. Engng. Sci., vol 9.*

Winkler, K. W., 1983, Frequency dependent ultrasonic properties of high-porosity sandstones. *J. Geophys. Res., vol 88, No. B11.*

CHAPTER IV
COMPUTER LIST OF THE PROGRAM BEM_5

```
/* PROGRAM BEM_5 (c) STANFORD UNIVERSITY 1986
   JORGE MENDOZA
   ROCK PHYSICS PROJECT
   DEPARTMENT OF GEOPHYSICS
   STANFORD UNIVERSITY
   STANFORD, CA 94305

   This is version 5.30 (07/09/1986)  IBM PC/XT/AT.
*/

/* ********************************************************************** *
*  BEM_5 is a program that uses the Displacement Discontinuity Method    *
*  (A boundary elements algorithm) to compute the deformation of a       *
*  pore subjected to external stresses. This program has its roots in    *
*  the program TWODD described by Crouch and Starfield (1983) Bounda-    *
*  ry Element Methods in Solids Mechanics (George Allen & Unwin Ltd).    *
*  The program is totally written in C language and it has been run      *
*  sucessfully in an IBM PC personal computer using Microsoft C ver-     *
*  sions 3.x and 4.x as well as in a VAX 750 running under UNIX ope-     *
*  rating system. The program reads an input file containing the data    *
*  from the command line argument. The syntax is:                        *
*                        bem_5 <input>                                   *
*  No extra options are available.                                       *
*  The input file must contain the following format:                     *
*  (All items within the same line are separated by at least a blank,    *
*  no special location within the line is necessary for the items).      *
*  Line 1:                                                               *
*  program name : Name of the output files (up to 8 characters). This    *
*                 name will be used to build the output names by         *
*                 adding the corresponding extensions. For example:      *
*                 for a program name = test, the program will gene-      *
*                 rate the following output files:                       *
*                 test.def : contains deformations.                      *
*                 test.prn : contains areas and energy factors           *
*                 test.ext : contains external stresses                  *
*  Line 2:                                                               *
*  NUMBS NUMOS KSYM                                                      *
*  NUMBS        : number of straight line boundary segments used to      *
*                 define boundary contours (Up to 30 lines)              *
*  NUMOS        : number of other line segments (not on a boundary)      *
*                 along which displacements and stresses are to be       *
*                 computed. Do not use it for multiple pressures         *
*  KSYM         : 3  y=0 is a line of symmetry (see fig.  1)             *
*                 4  x=0 and y=0 are lines of symmetry                   *
*                 5  y=0 is a line of symmetry and pore has conjugate    *
*  Line 3:                                                               *
*  PR E 0 0                                                              *
*  PR           : Poisson's ratio                                        *
*  E            : Young's modulus                                        *
*  0 0          : Zero Zero. Not used in this version (but required)     *
*  Line 4:                                                               *
*  NUPRES                                                                *
*  NUPRES       : Number of stresses or pressures to compute.            *
```

```
*  Line 5 to 5+NUPRES-1:                                                  *
*  PXX PYY PXY                                                            *
*  PXX          : Stress along x axis (negative means compression)        *
*  PYY          : Stress along y axis                                     *
*  PXY          : shear stress in plane x-y                               *
*  Note: stresses must br given in the same units as Young's modulus      *
*  Line 5+NUPRES to 5+NUPRES+NUMBS-1:                                     *
*  1 XBEG YBEG XEND YEND 1 0 0                                            *
*  1            : One. No used in this version (but required)             *
*  XBEG         : x coordinate of begining of line segment                *
*  YBEG         : y coordinate of begining of line segment                *
*  XEND         : x coordinate of end of line segment                     *
*  YEND         : y coordinate of end of line segment                     *
*  1 0 0        : One Zero Zero. Not used (but required)                  *
*  Note: the information for each segment uses one line                   *
*  Line 5+NUPRES+NUMBS:                                                   *
*  XBEG YBEG XEND YEND NUMPB                                              *
*  Note: These coordinates define the segments external to the boun-      *
*        daries of the pore where displacements and stresses are to       *
*        be computed.                                                     *
*  XBEG         : x coordinate of first point on line                     *
*  YBEG         : y coordinate of first point on line                     *
*  XEND         : x coordinate of last point on line                      *
*  YEND         : x coordinate of last point on line                      *
*  NUMPB        : number of equally spaced points between the spe-        *
*                 cified first and last points                           *
*                                                                        *
*  See examples at the end of the program                                 *
*  ********************************************************************** */



#include<stdio.h>
#include<math.h>

#define size1 50          /* Defining vector size */
#define size2 100         /* Defining matrix size */
#define pressu 20         /* Defining # of pressures */
float pi,pr,pr1,pr2,con,cons,xtemp,ytemp,yitemp;
float sxxs,sxxn,syys,syyn,sxys,sxyn,uxs,uxn,uys,uyn;
static float c[size2][size2],xnew[size1],ynew[size1],bbuff[size2];
main(argc, argv)
int argc;
char *argv[];
{                              /* start main */

  FILE *fp1,*fp2,*fp3,*fp4,*fopen(),*fclose();
  int j,numbs,numos,ksym,n,numbe,num,kode,ne,m,mn,ms,nn,ns,i,
      in,is,jn,js,npoint,nump,numpb,ni,jjj,nupres,jpre,sectiag=0,QQ=0;

  static int kod[size1];

  float e,xsym,ysym,pxx,pyy,pxy,sw,xend,xbeg,yend,ybeg,bvs,bvn,
```

```
        size,angle,cosb,sinb,delx,dely,temp1,temp2,area;

  static float xm[size1],ym[size1],a[size1],sinbet[size1],cosbet[size1],
               b[size2],d[size2],area2[pressu],epre[pressu];

  static float ppxx[pressu],ppyy[pressu],ppxy[pressu],ene-gy[pressu];

  char title[80],name[70],*aname[3],name2[70];

/* fp1 & argv[1] contain input file   */
/* fp2  contains output deformation file  */
/* fp3  contains output external field file */
  cls();
  printf("               BEM  version 5.3 (07/09/96) IBM PC.\n");
  printf("                      Stanford Rock Physics\n");
  printf("                     (c) Stanford University\n\n");


if (argv[1] == NULL)              /* check data file */
{ printf("Usage:  bem_5 input_data.pre \n");
   exit(0);  }

/* read input data */

fp1 = fopen(argv[1],"r");          /* check if file exist */
if (fp1 == NULL)
  {  perror("Couldn't open data file");
     abort();  }
printf("Reading file %s\n",argv[1]);
 j = fscanf(fp1,"%s",title);       /* read title */
 if (j != 1)  {rerror(1);}            /* check number of arguments */
 printf(".");
 j = fscanf(fp1,"%d %d %d",&numbs,&numos,&ksym);
 if ( j != 3) {rerror(2);}
 printf("...");
 if (numbs > (size1 - 1))   /* check max size of array */
  { printf("Maximum number of points at boundary exceeded\n"); abort(); }
 if (ksym < 3 || ksym > 5)
  { printf("Symmetry (ksym = %d) not allowed\n",ksym); abort(); }
 if (ksym == 3 || ksym == 5)
   sectiag = 1;
 if (ksym == 5)
    ksym = 4;

 j = fscanf(fp1,"%f %f %f %f",&pr,&e,&xsym,&ysym);
 if ( j !=4)  {rerror(3);}
 printf("....");
 j = fscanf(fp1,"%d",&nupres);             /* Read # of pressures */
 if ( j !=1)  {rerror(7);}
 printf(".\n");
 for (i=0;i< nupres;i++)
  {
   j = fscanf(fp1,"%f %f %f",&pxx,&pyy,&pxy);  /* Read pressures */
```

```
   if ( j !=3)  {rerror(4);}
   ppxx[i] = pxx;
   ppyy[i] = pyy;
   ppxy[i] = pxy;
   printf("...");
  }
 printf("\n");
   strcpy(name2,title);
   strcat(name2,".def");
 fp2 = fopen(name2, "w");
 if (fp2 == NULL)
   {   perror("Couldn't open output file");
       abort(); }
  fprintf(fp2,"%d \n",nupres);      /* Number of pressures */

/* Writes the symmetry conditions */

 switch (ksym) {
/* case 1: printf("No symmetry conditions imposed.\n");
           break;
   case 2: printf("The line x = %f is a line of symmetry\n",xsym);
           break; */
   case 3: printf("The line y = %f is a line of symmetry\n",ysym);
           break;
   case 4: printf("The lines x = %f and y = %f are lines of symmetry\n"
           ,xsym,ysym);
           break;
   default: perror("Symmetry condition are not well defined");
            abort();
               }            /* end switch */


 if (numos > 0)    /* Open output file for external field */
  {                                              /* Start If 1001 */
      strcpy(name,title);
      strcat(name,".ext");
      fp3 = fopen(name,"w");
       if ( fp3 == NULL)
        {  perror("Couldn't open external field file");
           exit(9);    }
  }                                             /* End If 1003 */

 /* Initializes common variables */

 invariable(e);

/*     define locations, sizes, orientations and boundary conditions of */
/*     boundary elements.                */

 bouncond(&numbe,&numbs,&num,kod,&kode,&xbeg,&xend,&yend,&ybeg,&bvs,&bvn,
         &sw,xm,ym,a,sinbet,cosbet,b,fp1);
```

```
  for (m=1;m<=numbe;m++)
   {
    size =2.*a[m];
    angle = 180.*atan2(sinbet[m],cosbet[m])/pi;

   }

printf("\nPressure loop\n");
/* Pressure loop start here */
   for (jpre=0;jpre<nupres;jpre++)
    {                                /* Start pressure loop P001 */
      pxx =_ppxx[jpre];
      pyy = ppyy[jpre];
      pxy = ppxy[jpre];

         if ( jpre > 0)
           initbuff(b);

/* Adjust stress boundary values for initial stresses. */

   instress(numbe,kod,pxx,pyy,pxy,cosbet,sinbet,b);

/* In this block, the program will compute the influence coefficients
   and set up the system of algebraic equations.                    */

   influcoeff(numbe,&kode,kod,ksym,xm,ym,cosbet,sinbet,a,xsym,ysym);


/*  Solve system of algebraic equations. */
    n = 2*numbe;
    solve(b,d,n);

/*  compute boundary displacements and stresses */

    printf("P = %d ",jpre+1);
compbound(numbe,ksym,pxx,pyy,pxy,xsym,ysym,xm,ym,cosbet,sinbet,a,d,fp2,jpre);

/*  Compute displacements and stresses at specified points in the body */

 if (numos > 0)
  {                                          /* Start If 1003 */

       extfield(numos,numbe,ksym,pxx,pyy,pxy,xsym,ysym,xm,ym,a,d,
              cosbet,sinbet,fp1,fp3,jpre);
  }                                          /* End If 1003 */

/* Compute the new position of the boundary regarness of the symmetry */

    newbound(numbe,fp2,&area,secflag);
    area2[jpre] = -area;
   }                 /* End pressure loop P001 */

      strcpy(name,title);
```

```
      strcat(name,".prn");
      fp4 = fopen(name,"w");
       if ( fp4 == NULL)
        {  perror("Couldn't open energy/area file");
           exit(10);    }
      fprintf(fp4,"1\n");
      fprintf(fp4,"%d\n",nupres);
      fprintf(fp4,"xs\n");
 fprintf(fp2,"%s\n",title);
 fprintf(fp2,"Poisson's Ratio , Young's modulus\n");
 fprintf(fp2,"%6.2f   %10.6E\n",pr,e);
 fprintf(fp2,"External stresses xx, yy, zz, Area\n");
for (jpre=0;jpre<nupres;jpre++)
{
 area2[jpre] *= 2.;   /* Compute the whole area */
 if (sectlag == 0)
  area2[jpre] *= 2.;  /* Compute area for 1/4 of symmetry */

fprintf(fp2,"%g  %g  %g  %g\n",ppxx[jpre],ppyy[jpre],ppxy[jpre],area2[jpre]);
 fprintf(fp4,"%g %g\n",fabs(ppyy[jpre]),area2[jpre]);
}
  fprintf(fp4,"%d\n",nupres-1);
   fprintf(fp4,"cd\n");
/* Computing strain energy factor:
   This routine only works for uniaxial and hydrostatic pressures.
   The uniaxial stress must be applied to the Y axis

        d /dp [ integral ( U(x,p) ) ] from c to -c  */

  if (nupres > 1)
  fprintf(fp2,"External stress yy , Energy Factor\n");
  for (jpre=0;jpre<(nupres-1);jpre++)
  {   /* computing the derivative at epre[] pressure */
   energy[jpre] = (area2[jpre] - area2[jpre+1])/(ppyy[jpre] - ppyy[jpre+1]);
   epre[jpre]   = (ppyy[jpre] + ppyy[jpre+1])/2;
   fprintf(fp2,"%g  %g\n",epre[jpre],energy[jpre]);
    fprintf(fp4,"%g  %g\n",fabs(epre[jpre]),energy[jpre]);
  }
     fprintf(fp4,"%s\n",title);
      fprintf(fp4,"Internal area\n");
      fprintf(fp4,"Energy factor\n");
}                                       /* End main */

/*                  (((((((((( 0 ))))))))))                 */

initl()
{                                       /* Start initl */
      sxxs=sxxn=syys=syyn=sxys=sxyn=uxs=uxn=uys=uyn=0.;
}                                       /* End intil */

solve(b,x,n)      /* Solve the system of linear equations */
int n;
float *b,*x;
```

```
{                              /* Start solve */
  int nb,l,j,jj,i;
  float sum,xm;

 nb = n-1;
 for(j=1;j(=nb;j++)
 {                           /* Start loop solve 0001 */
  l = j+1;
  for(jj=l;jj(=n;jj++)
   {                         /* Start loop solve 0002 */
     xm = (c[jj][j])/(c[j][j]);
      for (i=j;i(=n;i++)
       (c[jj][i]) = (c[jj][i]) - (c[j][i])*xm;
     *(b+jj) = (*(b+jj)) - (*(b+j))*xm;
   }                         /* End loop solve 0002 */
 }                          /* End loop solve 0001 */

 *(x+n) = (*(b+n))/(c[n][n]);
  for (j=1;j(=nb;j++)
  {                            /* Start loop solve 0003 */
    jj = n-j;
    l = jj+1;
    sum =0.;
     for (i=l;i(=n;i++)
      sum = sum + (c[jj][i]) * (*(x+i));
    *(x+jj) = ( (*(b+jj)) -sum)/( c[jj][jj] );
  }                            /* End loop solve 0004 */
}                                /* End solve */

coeff(x,y,cx,cy,a,cosb,sinb,msym)
int msym;
float x,y,cx,cy,a,cosb,sinb;
{                                  /* Start coeff */
  float sin2b,cos2b,xb,yb,r1s,r2s,f11,f12,fb2,fb3,fb4,fb5,fb6,fb7,
        uxds,uxdn,uyds,uydn,sxxds,sxxdn,syyds,syydn,sxyds,sxydn,
        cosb2,sinb2;

      cos2b=cosb*cosb-sinb*sinb;
      sin2b=2.*sinb*cosb;
      cosb2=cosb*cosb;
      sinb2=sinb*sinb;

      xb=(x-cx)*cosb+(y-cy)*sinb;
      yb= -(x-cx)*sinb+(y-cy)*cosb;

      r1s=(xb-a)*(xb-a)+yb*yb;
      r2s=(xb+a)*(xb+a)+yb*yb;
      f11=.5*log(r1s);
      f12=.5*log(r2s);
      fb2=con*(f11-f12);

      if (yb != 0.)
       fb3= -con*(atan((xb+a)/yb)-atan((xb-a)/yb));
```

```
      else
       {
         fb3=3.;
         if (fabs(xb) < a)
          fb3=con*pi;
       }

      fb4=con*(yb/r1s-yb/r2s);
      fb5=con*((xb-a)/r1s-(xb+a)/r2s);
fb6=con*(((xb-a)*(xb-a)-yb*yb)/(r1s*r1s)-((xb+a)*(xb+a)-yb*yb)/(r2s*r2s));

      fb7=2.*con*yb*((xb-a)/(r1s*r1s)-(xb+a)/(r2s*r2s));

      uxds= -pr1*sinb*fb2+pr2*cosb*fb3+yb*(sinb*fb4-cosb*fb5);
      uxdn= -pr1*cosb*fb2-pr2*sinb*fb3-yb*(cosb*fb4+sinb*fb5);
      uyds=pr1*cosb*fb2+pr2*sinb*fb3-yb*(cosb*fb4+sinb*fb5);
      uydn= -pr1*sinb*fb2+pr2*cosb*fb3-yb*(sinb*fb4-cosb*fb5);

      sxxds=cons*(2.*cosb2*fb4+sin2b*fb5+yb*(cos2b*fb6-sin2b*fb7));
      sxxdn=cons*(-fb5+yb*(sin2b*fb6+cos2b*fb7));
      syyds=cons*(2.*sinb2*fb4-sin2b*fb5-yb*(cos2b*fb6-sin2b*fb7));
      syydn=cons*(-fb5-yb*(sin2b*fb6+cos2b*fb7));
      sxyds=cons*(sin2b*fb4-cos2b*fb5+yb*(sin2b*fb6+cos2b*fb7));
      sxydn=cons*(-yb*(cos2b*fb6-sin2b*fb7));

      uxs=uxs+msym*uxds;
      uxn=uxn+uxdn;
      uys=uys+msym*uyds;
      uyn=uyn+uydn;

      sxxs=sxxs+msym*sxxds;
      sxxn=sxxn+sxxdn;
      syys=syys+msym*syyds;
      syyn=syyn+syydn;
      sxys=sxys+msym*sxyds;
      sxyn=sxyn+sxydn;
}                                     /* End coeff */

/* This routine warns that an error has occurred
when the program read the data file */
rerror(i)
 int i;
{
 printf("Fscanf # = %d",i);
 perror(" Argument mismatch in data file");
 abort();
}

/* This routine compute displacements and stresses at specified points
   in the body */

extfield(numos,numbe,ksym,pxx,pyy,pxy,xsym,ysym,xm,ym,a,d,cosbet,sinbet,fp1,
        fp3,jpre)
```

```
int numcs,numbe,ksym,jpre;
float pxx,pyy,pxy,xsym,ysym;
float *xm,*ym,*a,*d,*cosbet,*sinbet;
FILE *fp1,*fp3;
{                                          /* Start extfield */
  int npoint,nump,numpb,ni,j,jn,js,jjj,ni
  float xbeg,ybeg,xend,yend,delx,dely,xp,yp,ux,uy,sigxx,sigyy,sigxy,
        xj,yj,aj,cosbj,sinbj;

   fprintf(fp3,"Pressure # = %d\n",jpre+1);
   fprintf(fp3,"Displacements and stresses at specified points in the body.\n");
   fprintf(fp3,"X CO-ORD  Y CO-ORD     UX            UY          ");
   fprintf(fp3,"  SXX        SYY       SXY\n");
   fflush(fp3);
    npoint = 0;
    printf("\n");
    for (n=1;n<=numcs;n++)
     {                                     /* Start loop 0009 */
      jjj =fscanf(fp1,"%f %f %f %f %d",&xbeg,&ybeg,&xend,&yend,&numpb);
      if ( jjj != 5 ) { rerror(6); }
      printf("6");

      nump = numpb+1;
      delx = (xend-xbeg)/nump;
      dely = (yend-ybeg)/nump;
      if (numpb > 0)
         nump++;
      if (delx*delx + dely*dely == 0.)
         nump =1;

      for (ni=1;ni<=numpin;ni++)
       {                                   /* Start loop 0010 */
        xp=xbeg+(ni-1)*delx;
        yp=ybeg+(ni-1)*dely;

        ux=0.;
        uy=0.;
        sigxx=pxx;
        sigyy=pyy;
        sigxy=pxy;

        for (j=1;j<=numbe;j++)
         {                                    /* Start loop 0011 */
          jn=2*j;
          js=jn-1;
          init1();
          xj= *(xm+j);
          yj= *(ym+j);
          aj= *(a+j);

          if (sqrt((xp-xj)*(xp-xj) + (yp-yj)*(yp-yj)) < 2.*aj)
          goto error;
```

```
        cosbj = *(cosbet+j);
        sinbj = *(sinbet+j);
        coeff(xp,yp,xj,yj,aj,cosbj,sinbj,1);

        switch (ksym) {       /* Start switch */
         case 1: break;
         case 2: xj = 2.*xsym-(*(xm+j));
                 coeff(xp,yp,xj,yj,aj,cosbj,-sinbj,-1);
                 break;
         case 3: yj = 2.*ysym-(*(ym+j));
                 coeff(xp,yp,xj,yj,aj,-cosbj,sinbj,-1);
                 break;
         case 4: xj = 2.*xsym-(*(xm+j));
                 coeff(xp,yp,xj,yj,aj,cosbj,-sinbj,-1);
                 xj = *(xm+j);
                 yj = 2.*ysym-(*(ym+j));
                 coeff(xp,yp,xj,yj,aj,-cosbj,sinbj,-1);
                 xj = 2.*xsym-(*(xm+j));
                 coeff(xp,yp,xj,yj,aj,-cosbj,-sinbj,1);
                 break;
         default: break;
         }                    /* End switch */

           ux=ux+uxs*(*(d+js))+uxn*(*(d+jn));
           uy=uy+uys*(*(d+js))+uyn*(*(d+jn));
           sigxx=sigxx+sxxs*(*(d+js))+sxxn*(*(d+jn));
           sigyy=sigyy+syys*(*(d+js))+syyn*(*(d+jn));
           sigxy=sigxy+sxys*(*(d+js))+sxyn*(*(d+jn));
        }                                    /* End loop 0011 */

      npoint++;
      fprintf(fp3,"%8.6f  %8.6f  %8.6e  %8.6e  %8.2f  %8.2f  %8.3f\n",
             xp,yp,ux,uy,sigxx,sigyy,sigxy);
      fflush(fp3);
       error:
       jjj = jjj;

       }                                     /* End loop 0010 */
     }                                       /* End loop 0009 */
    printf("\n");
}                                    /* End extfield */

/* This routine adjust stress boundary values for initial stresses */
instress(numbe,kod,pxx,pyy,pxy,cosbet,sinbet,b)
int numbe,*kod;
float pxx,pyy,pxy;
float *cosbet,*sinbet,*b;
{                              /* Start instress */
  int n,nn,ns;
  float cosb,sinb,sigs,sign;

  for (n=1;n<=numbe;n++)
  {                           /* Start loop 0003 */
```

```
      nn=2*n;
      ns=nn-1;
      cosb= *(cosbet+n);
      sinb= *(sinbet+n);
      sigs=(pyy-pxx)*sinb*cosb+pxy*(cosb*cosb-sinb*sinb);
      sign=pxx*sinb*sinb-2.*pxy*sinb*cosb+pyy*cosb*cosb;

      switch (*(kod+n)) {                /* Start switch */
        case 1: *(b+ns) = *(b+ns) - sigs;
                *(b+nn) = *(b+nn) - sign;
                break;
        case 2: break;
        case 3: *(b+nn) = *(b+nn) - sign;
                break;
        case 4: *(b+ns) = *(b+ns) - sigs;
                break;
        default: break;
        }                                  /* End switch  */
  }                                /* End loop 0003 */
}                                  /* End instress */

/* This routine initializes common variables */
invariable(e)
float e;
{                                  /* Start invariable */
  pi=4.*atan(1.);
   con = 1./(4.*pi*(1.-pr));
    cons = e/(1.+pr);
     pr1 = 1.-2.*pr;
      pr2 = 2.*(1.-pr);
}                                  /* End invariable */

/* This routine define location, size, etc of boundary elements */
bouncond(numbe,numbs,num,kod,kode,xbeg,xend,yend,ybeg,bvs,bvn,sw,xm,ym,
        a,sinbet,cosbet,b,fp1)
int *numbe,*numbs,*num,*kod,*kode;
float *xbeg,*xend,*yend,*ybeg,*bvs,*bvn,*sw,*xm,*ym,*a,*sinbet,*cosbet,
     *b;
FILE *fp1;

{                                        /* Start bouncond */
 int j,ne,m,mn,ms,jjj;
 float xd,yd;

 *numbe = 0;

  for (j=1;j<=(*numbs);j++)
  {                            /* Start loop  0001 */
    jjj=fscanf(fp1,"%d %f %f %f %f %d %f %f",num,
                xbeg,ybeg,xend,yend,kode,bvs,bvn);
    if (jjj != 8) { rerror(5); }
    printf("+");
    if ( j == 1)
```

```
    {
      xtemp = *xbeg;
      ytemp = *ybeg;
    }
   xd = (*xend - *xbeg)/(*num);
    yd = (*yend - *ybeg)/(*num);
     *sw = sqrt(xd*xd + yd*yd);

     for (ne=1;ne<=(*num);ne++)
     {                          /* Start loop 0002 */
       (*numbe)++;
        m=(*numbe);
         *(xm+m)=(*xbeg)+.5*(2.*ne-1.)*xd;
          *(ym+m)=(*ybeg)+.5*(2.*ne-1.)*yd;
           *(a+m)=.5*(*sw);
            *(sinbet+m)=yd/(*sw);
           *(cosbet+m)=xd/(*sw);
           *(kod+m)= *kode;
         mn=2*m;
        ms=mn-1;
       *(b+ms)= *bvs;
        *(b+mn)= *bvn;
         bbuff[ms] = *bvs;
         bbuff[mn] = *bvn;
     }                          /* End loop 0002 */
  }                             /* End loop 0001 */
  printf("\n");
  jjj = *numbe;
  xnew[jjj+1] = *xend;
  ytemp = *yend;
}                               /* End bouncond */

/* This routine computes the influence coefficients and set up the system
   of algebraic equations.                                                */
influcoeff(numbe,kode,kod,ksym,xm,ym,cosbet,sinbet,a,xsym,ysym)
int numbe, *kode, ksym, *kod;
float xsym,ysym;
float *xm,*ym,*cosbet,*sinbet,*a;
{                                   /* Start influcoeff */
 int in,is,jn,js;
 register j,i;
 float xi,yi,cosbi,sinbi,xj,yj,cosbj,sinbj,aj;

 for(i=1;i<=numbe;i++)
 {                              /* Start loop 0004 */
      in=2*i;
      is=in-1;
      xi= *(xm+i);
      yi= *(ym+i);
      cosbi= *(cosbet+i);
      sinbi= *(sinbet+i);
      *kode= *(kod+i);
```

```
for(j=1;j(=numbe;j++)
 {                              /* Start loop 0005 */
  jn=2*j;
  js=jn-1;
  init1();
  xj= *(xm+j);
  yj= *(ym+j);
  cosbj= *(cosbet+j);
  sinbj= *(sinbet+j);
  aj= *(a+j);

  coeff(xi,yi,xj,yj,aj,cosbj,sinbj,1);

  switch (ksym) {                  /* Start switch */
    case 1: break;
    case 2: xj = 2.*xsym- *(xm+j);
            coeff(xi,yi,xj,yj,aj,cosbj,-sinbj,-1);
            break;
    case 3: yj = 2.*ysym- *(ym+j);
            coeff(xi,yi,xj,yj,aj,-cosbj,sinbj,-1);
            break;
    case 4: xj = 2.*xsym- *(xm+j);
            coeff(xi,yi,xj,yj,aj,cosbj,-sinbj,-1);
            xj =  *(xm+j);
            yj = 2.*ysym- *(ym+j);
            coeff(xi,yi,xj,yj,aj,-cosbj,sinbj,-1);
            xj = 2.*xsym- *(xm+j);
            coeff(xi,yi,xj,yj,aj,-cosbj,-sinbj,1);
            break;
     default: break;
     }                             /* End switch  */

  switch ( *(kode) ) {                 /* Start switch */
    case 1:
    (c[is][js])=(syys-sxxs)*sinbi*cosbi+sxys*(cosbi*cosbi-sinbi*sinbi);
    (c[is][jn])=(syyn-sxxn)*sinbi*cosbi+sxyn*(cosbi*cosbi-sinbi*sinbi);
    (c[in][js])=sxxs*sinbi*sinbi-2.*sxys*sinbi*cosbi+syys*cosbi*cosbi;
    (c[in][jn])=sxxn*sinbi*sinbi-2.*sxyn*sinbi*cosbi+syyn*cosbi*cosbi;
        break;
    case 2:
      (c[is][js])=uxs*cosbi+uys*sinbi;
      (c[is][jn])=uxn*cosbi+uyn*sinbi;
      (c[in][js])= -uxs*sinbi+uys*cosbi;
      (c[in][jn])= -uxn*sinbi+uyn*cosbi;
        break;
    case 3:
      (c[is][js])=uxs*cosbi+uys*sinbi;
      (c[is][jn])=uxn*cosbi+uyn*sinbi;
     (c[in][js])=sxxs*sinbi*sinbi-2.*sxys*sinbi*cosbi+syys*cosbi*cosbi;
     (c[in][jn])=sxxn*sinbi*sinbi-2.*sxyn*sinbi*cosbi+syyn*cosbi*cosbi;
        break;
    case 4:
    (c[is][js])=(syys-sxxs)*sinbi*cosbi+sxys*(cosbi*cosbi-sinbi*sinbi);
```

```
        (c[is][jn])=(syyn-sxxn)*sinbi*cosbi+sxyn*(cosbi*cosbi-sinbi*sinbi);
          (c[in][js])= -uxs*sinbi+uys*cosbi;
          (c[in][jn])= -uxn*sinbi+uyn*cosbi;
            break;
        default: break;
        }                                   /* End switch  */
      }                                     /* End loop 0005 */
 }                                          /* End loop 0004 */

}                                           /* End influcoeff */

/* This routine computes boundary displacements and stresses */
compbound(numbe,ksym,pxx,pyy,pxy,xsym,ysym,xm,ym,cosbet,sinbet,a,d,fp2,jpre)
int numbe,ksym,jpre;
float pxx,pyy,pxy,xsym,ysym;
float *xm,*ym,*cosbet,*sinbet,*a,*d;
FILE *fp2;
{                                           /* Start compbound */
  int in,is,jn,js;
  register j,i;
  float xi,yi,cosbi,sinbi,uxneg,uyneg,sigxx,sigyy,sigxy,xj,yj,aj,cosbj,
        sinbj,uspos,unpos,usneg,unneg,uxpos,uypos,sigs,signi

 for (i=1;i<=numbe;i++)
 {                                      /* Start loop 0006 */
  in = 2*i;
  is = in-1;
  xi =  *(xm+i);
  yi =  *(ym+i);
  cosbi =  *(cosbet+i);
  sinbi =  *(sinbet+i);

  uxneg = 0.;
  uyneg = 0.;
  sigxx = pxx;
  sigyy = pyy;
  sigxy = pxy;

  for (j=1;j<=numbe;j++)
   {                                    /* Start loop 0007 */
     jn = 2*j;
     js = jn-1;
     initl();
     xj =  *(xm+j);
     yj =  *(ym+j);
     aj =  *(a+j);
     cosbj =  *(cosbet+j);
     sinbj =  *(sinbet+j);
     coeff(xi,yi,xj,yj,aj,cosbj,sinbj,1);

     switch (ksym) {                    /* Start switch */
       case 1: break;
       case 2: xj = 2.*xsym- *(xm+j);
```

```
            coeff(xi,yi,xj,yj,aj,cosbj,-sinbj,-1);
            break;
      case 3: yj = 2.*ysym- *(ym+j);
            coeff(xi,yi,xj,yj,aj,-cosbj,sinbj,-1);
            break;
      case 4: xj = 2.*xsym- *(xm+j);
            coeff(xi,yi,xj,yj,aj,cosbj,-sinbj,-1);
            xj =  *(xm+j);
            yj = 2.*ysym- *(ym+j);
            coeff(xi,yi,xj,yj,aj,-cosbj,sinbj,-1);
            xj = 2.*xsym- *(xm+j);
            coeff(xi,yi,xj,yj,aj,-cosbj,-sinbj,1);
            break;
      default: break;
           }                          /* End switch */


     uxneg=uxneg+uxs* (*(d+js))+uxn* (*(d+jn));
     uyneg=uyneg+uys* (*(d+js))+uyn* (*(d+jn));
     sigxx=sigxx+sxxs* (*(d+js))+sxxn* (*(d+jn));
     sigyy=sigyy+syys* (*(d+js))+syyn* (*(d+jn));
     sigxy=sigxy+sxys* (*(d+js))+sxyn* (*(d+jn));

  }                                  /* End loop 0007 */

     usneg=uxneg*cosbi+uyneg*sinbi;
     unneg= -uxneg*sinbi+uyneg*cosbi;
     uspos=usneg- *(d+is);
     unpos=unneg- *(d+in);
     uxpos=uspos*cosbi-unpos*sinbi;
     uypos=uspos*sinbi+unpos*cosbi;
     sigs=(sigyy-sigxx)*sinbi*cosbi+sigxy*(cosbi*cosbi-sinbi*sinbi);
     sign=sigxx*sinbi*sinbi-2.*sigxy*sinbi*cosbi+sigyy*cosbi*cosbi;

     printf(".");

/* Compute the new position of the boundary regarless of the axes of
   symmetry. The new position is stored in xnew[] and ynew[]       */

   if (i == 1)
    {
       xnew[0] = xtemp + uxneg;
       ynew[0] = ytemp + uyneg;
    }
   xnew[i] = xm[i] + uxneg;
   ynew[i] = ym[i] + uyneg;

 }                                   /* End loop 0006 */
   if ( uxneg < 0 )
   xnew[numbe+1] += uxneg;
   ynew[numbe+1] = yltemp + uyneg;
   printf("\n");
}                                   /* End compbound */
```

```
/* This routine compute the new position of the boundary regarness of
   the symmetry                                                        */

newbound(numbe,fp2,area,sectiag)
int numbe,sectiag;
float *area;
FILE *fp2;
{                              /* Start newbound */
  int number=0,j=0,number2=0;
  float temp;
  float integral();
  register i,numba,numba2;

   numba = numbe;              /* number of elements of the array */

/*       ********** START Y right SECTION ***********  */
   if ( ynew[0] >= 0.)
   {
      number = 0;              /* index of the first element of the array */
      numbe++;
   }

   else
   {          /* Start else */
    for(i=1;i(=numbe;i++)
    {                          /* Start for */
      if ( ynew[i] == 0.)
       {
         number = i;
         numba  = numba - number +1;
         break;
        }

      else if ( ynew[i] > 0.)
       {
         number = i-1;
         numba = numba - number +1;
         temp = (xnew[i] - xnew[i-1])/(ynew[i] - ynew[i-1]);
         xnew[number] = xnew[i-1] - temp * ynew[i-1];
         ynew[number] = 0.;
         break;
       }
     }                         /* End for */
   }          /* End else */

   if ( i == numbe+1)
    [
      printf("Pore colapses\n");
      exit(1);
    ]
   /* ************  END Y SECTION *************  */
```

```
   /* ***********  X left SECTION  *********  */
   if ( secflag == 0 )
   {                        /* Start if X section */
   numba2 = numba-1;           /* number of elements of the array */

   if ( xnew[numbe+1] >= 0.)
   {
      number2 = numbe+1;    /* index of the last element of the array */
      numba2++;
   }

   else
   {         /* Start else */
    for (i=numbe;i>number;i--)
    {                        /* Start for */
      if ( xnew[i] == 0.)
       {
         number2 = i;
         numba2  = numba2 - (numbe -number2);
         break;
       }

      else if ( xnew[i] > 0.)
       {
         number2 = i+1;
         numba2 = numba2 - (numbe-number2);
         temp = (ynew[i] - ynew[i+1])/(xnew[i] - xnew[i+1]);
         ynew[number2] = ynew[i+1] - temp * xnew[i+1];
         xnew[number2] = 0.;
         break;
       }
     }        /*  End for          */
   }         /*  End else         */
   }        /*  End if X section */
/*       *************  END X left SECTION ************** */

   /*   ***********    Y left SECTION    ************  */
 if (secflag == 1)
 {                      /* Start "if" Y, left section */

   numba2 = numba-1;           /* number of elements of the array */

   if ( ynew[numbe+1] >= 0.)
   {
      number2 = numbe+1;    /* index of the last element of the array */
      numba2++;
   }

   else
   {         /* Start else */
    for (i=numbe;i>number;i--)
    {                        /* Start for */
```

```
      if ( ynew[i] == 0.)
       {
         number2 = i;
         numba2  = numba2 - (numbe -number2);
         break;
        }

      else if ( ynew[i] > 0.)
       {
         number2 = i+1;
         numba2 = numba2 - (numbe-number2);
         temp = (xnew[i] - xnew[i+1])/(ynew[i] - ynew[i+1]);
         xnew[number2] = xnew[i+1] - temp * ynew[i+1];
         ynew[number2] = 0.;
         break;
       }
     }                    /*  End for              */
   }                      /*  End else             */
 }                        /*  End if Y left section */
/*      ************  End Y left Section ************** */

  fprintf(fp2,"%d \n",numba2+1);
  fprintf(fp2,"ns \n");            /* Type of graphic */
  for ( i=number;i<=number2;i++)
  fprintf(fp2,"%12.8f     %12.8f\n",xnew[i],ynew[i]);
  fflush(fp2);
/* Compute 1/4 of the area of the pore */
  *area = integral(&xnew[number],&ynew[number],numba2+1);
}                                                  /* End newbound */

/* This routine re-initializes the array b[]  */
initbuff(b)
float *b;
{
  int i;
  for(i=0;i<size2;i++)
    *(b+i) = bbuff[i];
}

float integral(xin,yin,ndata)

/* This routine computes the integral of a function defined by a
   set of points xin,yin                                          */

float xin[],yin[];
int ndata;
{
  int i,ni;
  float xout,initial,final,interval,temp1,temp2;
  float fout[size2];

/* ndata = number of points of the function to integrate
   xin[] = array of X axis of function to integrate
```

```
   yin[] = array of Y axis of function to integrate
   function return the value of integral
   n  = number of interpolated points ( Approx 2*ndata )       */

  n = 2*ndata;
  initial  = xin[0];
  final    = xin[ndata-1];
  interval = ( final - initial ) /n;
  n++;
  for (i=0;i<n;i++)
  {
     if ( i == n-1 )
      xout = final;
     else
      xout = initial + (i*interval);
     lineint(ndata,xin,yin,xout,&temp1);
     fout[i] = temp1;
   }
  /* Compute the integral */
  tpzod(n,initial,final,fout,&temp2);
  return(temp2);
}

lineint(n,x,f,xx,fx)

 /* This routine approximates a function whose value is given
    at n points on a n interval of the x axis. The interpolation
    uses a straigh line between two adyacents points.

    The arguments are:
    n    input    Number of points used to approximate the function
    x    input    Array of X axis values of N given points
    f    input    Array of function values of N given points
    xx   input    Value at which approximation is to be made
    fx   output   Function approximation at xx
    x[0] is the maximum x value and x[n-1] is the minimum x value. */

int n;
float x[],f[],xx,*fx;
{                       /*  start lineint  */

  int i,j;
  float temp;

  if ( xx > x[0] || xx < x[n-1] )
   {  printf("Number out of range xx = %f \n",xx);
      exit(1);     }

  for ( i=0;i<n;i++ )
  {                             /* Start For */
     if ( xx == x[i] )
      {
        *fx = f[i];
```

```
        break;
      }

     else if ( xx < x[i] && xx > x[i+1] )
      {
        temp = (f[i+1] - f[i])/(x[i+1] - x[i]);
        *fx = f[i] + temp * (xx - x[i]);
        break;
      }
  }                              /* End For */
}                                /* End lineint */

/* This routine computes the definide integral of a function
   or a set of points by the trapezoidal rule                  */

tpzod(m,xo,xh,y,tpa)
int m;
float xo,xh,y[],*tpa;

/* Arguments are:
   m   = Number of function values (input).
   xo  = Lower limit of integration (input).
   xh  = Upper limit of integration (input).
   y   = One-dimensional array of function
         values given at m equally spaced
         points between xo and xh (input).
   tpa = Value of integral (output).
*/
{
  int i,tm;
  float di,ar;

   tm = m-1;
   di = (xh - xo)/(tm*2.);
   *tpa = 0.;

   for (i=0;i<=m-2;i++)
    {
     ar = di * (y[i] + y[i+1]);
     *tpa = *tpa + ar;
    }
}
/* ***************************************************************************
 * The following is an example of an input file for a 18 elements
   tapared pore as shown in figure  2:
   digitation is always counterclockwise

testing                                  (program name)
18 0 4                                   (NUMBS NUMOS KSYM)
0.230000 4.000000e+005 0 0               (PR E 00)     (Bars)
2                                        (NUPRES)
0 0 0                                    (PXX PYY PXY) (Bars)
-50 -50 0                                (PXX PYY PXY)
```

```
1 1.000000 0.000030 0.978610 0.000030 1 0 0  (1 XBEG YBEG XEND YEND 1 0 0)
1 0.978610 0.000030 0.942959 0.000107 1 0 0
1 0.942959 0.000107 0.905526 0.000198 1 0 0
1 0.905526 0.000198 0.855615 0.000320 1 0 0
1 0.855615 0.000320 0.800357 0.000442 1 0 0
1 0.800357 0.000442 0.711230 0.000701 1 0 0
1 0.711230 0.000701 0.629234 0.000960 1 0 0
1 0.629234 0.000960 0.556150 0.001189 1 0 0
1 0.556150 0.001189 0.495544 0.001326 1 0 0
1 0.495544 0.001326 0.438503 0.001463 1 0 0
1 0.438503 0.001463 0.392157 0.001570 1 0 0
1 0.392157 0.001570 0.338681 0.001692 1 0 0
1 0.338681 0.001692 0.278075 0.001814 1 0 0
1 0.278075 0.001814 0.213904 0.001875 1 0 0
1 0.213904 0.001875 0.140820 0.001951 1 0 0
1 0.140820 0.001951 0.058824 0.002012 1 0 0
1 0.058824 0.002012 0.008913 0.002027 1 0 0
1 0.008913 0.002027 0.000000 0.002027 1 0 0
```

**** end example ***

In case NUMOS = 1 and NUPRES = 1 (PXX = -50 PYY = -50 PXY = 0)
the last input of above example is follows by:

```
0 0.00203 0 3 10                              (XBEG YBEG XEND YEND NUMPS)
```

The output files are:
(1) deformation file = testing.def

```
2                             (NUPRES)
20                            (Number of midpoints)
ns                            (ignore this line, plotting information)
  1.00000000      0.00000000  (coordinates x,y of right most point of pore)
  0.98930502      0.00001500
  0.96078449      0.00006850
  0.92424250      0.00015250  (new positions of midpoints of pore boundary
  0.88057653      0.00025900  after PXX and PYY number 1 have been
  0.82798600      0.00038100  applied.      .
  0.75579345      0.00057150                .
  0.67023200      0.00083050                .
  0.59269202      0.00107450                .
  0.52584702      0.00125750                .
  0.46702349      0.00139450              x,y
  0.41532999      0.00151650                .
  0.36541900      0.00163100                .
  0.30837801      0.00175300                .
  0.24598950      0.00184450                .
  0.17736199      0.00191300                .
  0.09982200      0.00198150                .
  0.03386850      0.00201950                .
  0.00445650      0.00202700                .)
  0.00000000      0.00202700  coordinates x,y of left most point of pore)
19
ns
  0.96137321      0.00000000
  0.96081918      0.00000056  (same as above but for second set
```

```
  0.92427397       0.00006633    of PXX, PYY, PXY)
  0.88059747       0.00016372
  0.82800841       0.00028170
  0.75581032       0.00047593
  0.67024362       0.00074330
  0.59270000       0.00100174
  0.52585262       0.00120288
  0.46702769       0.00135620
  0.41533276       0.00149183
  0.36542085       0.00160577
  0.30837980       0.00172195
  0.24599132       0.00180699
  0.17736353       0.00186923
  0.09962377       0.00193594
  0.03387117       0.00198279
  0.00446140       0.00199886
  0.00000000       0.00199886
testing
Poisson's Ratio , Young's modulus
  0.23   4.000000E+005
External stresses xx, yy, zz, Area (Area is the new internal area of the
0  0  0  0.004793                  pore for the given stresses)
-50  -50  0  0.004561
External stress yy , Energy Factor
-25  4.631625e-006                (Energy factor is the w factor defined
                                   in chapter 3)

(2) stress -energy file = testing.prn
Ignore this file. It is only used to export the internal area and
energy factor data to LOTUS 123 spreadsheet program.

(3) External field = testing.ext
Pressure # = 1
Displacements and stresses at specified points in the body.
X CO-ORD  Y CO-ORD     UX            UY             SXX       SYY       SXY
0.000000  0.274573  0.000000e+000  -3.998727e-005   -44.40    -48.94    0.000
0.000000  0.547115  0.000000e+000  -4.037236e-005   -44.22    -48.05    0.000
0.000000  0.819658  0.000000e+000  -3.923013e-005   -46.70    -45.81    0.000
0.000000  1.092201  0.000000e+000  -3.657742e-005   -48.74    -44.88    0.000
0.000000  1.364744  0.000000e+000  -3.339220e-005   -49.85    -44.97    0.000
0.000000  1.637286  0.000000e+000  -3.027000e-005   -50.36    -45.47    0.000
0.000000  1.909829  0.000000e+000  -2.744451e-005   -50.57    -46.06    0.000
0.000000  2.182372  0.000000e+000  -2.496910e-005   -50.63    -46.62    0.000
0.000000  2.454914  0.000000e+000  -2.282616e-005   -50.62    -47.10    0.000
0.000000  2.727457  0.000000e+000  -2.097455e-005   -50.58    -47.51    0.000
0.000000  3.000000  0.000000e+000  -1.937060e-005   -50.53    -47.84    0.000

UX  : Displacement along x axis
UY  : Displacement along y axis
SXX : Normal stress along x axis
SYY : Normal stress along y axis
SXY : Shear stress along plane x-y
```

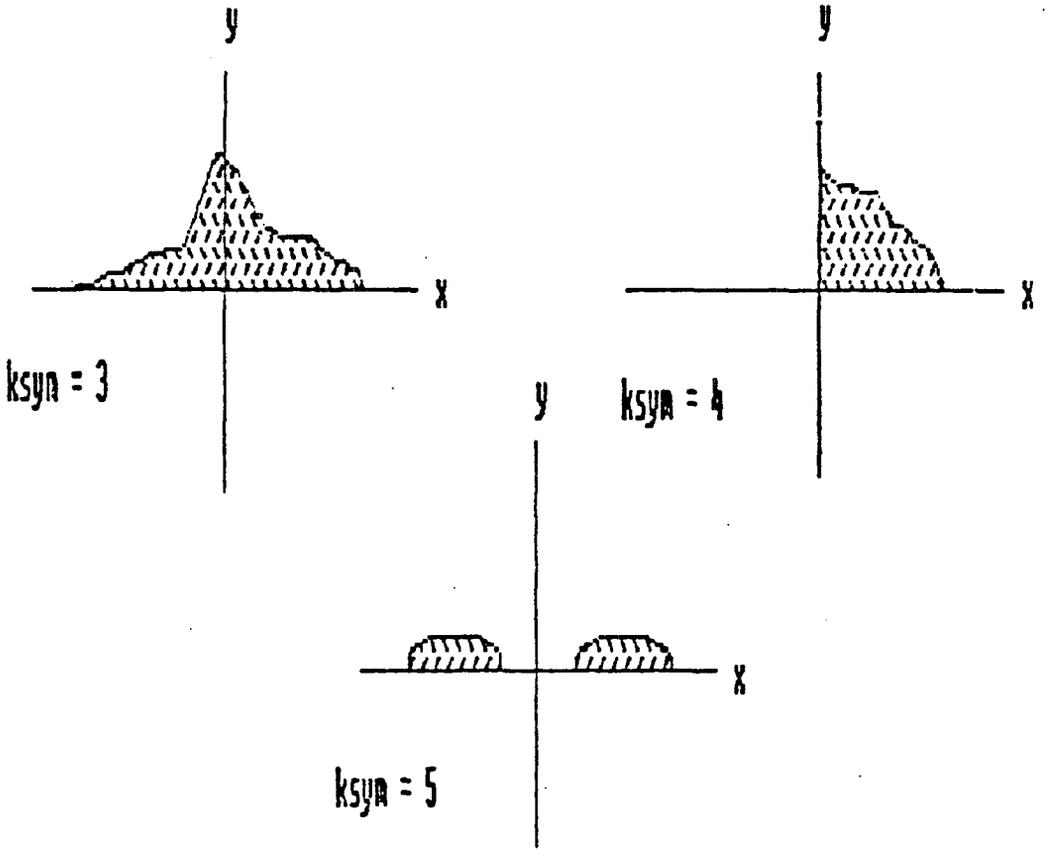

Figure 1: Symmetries supported by the program BEM-5.

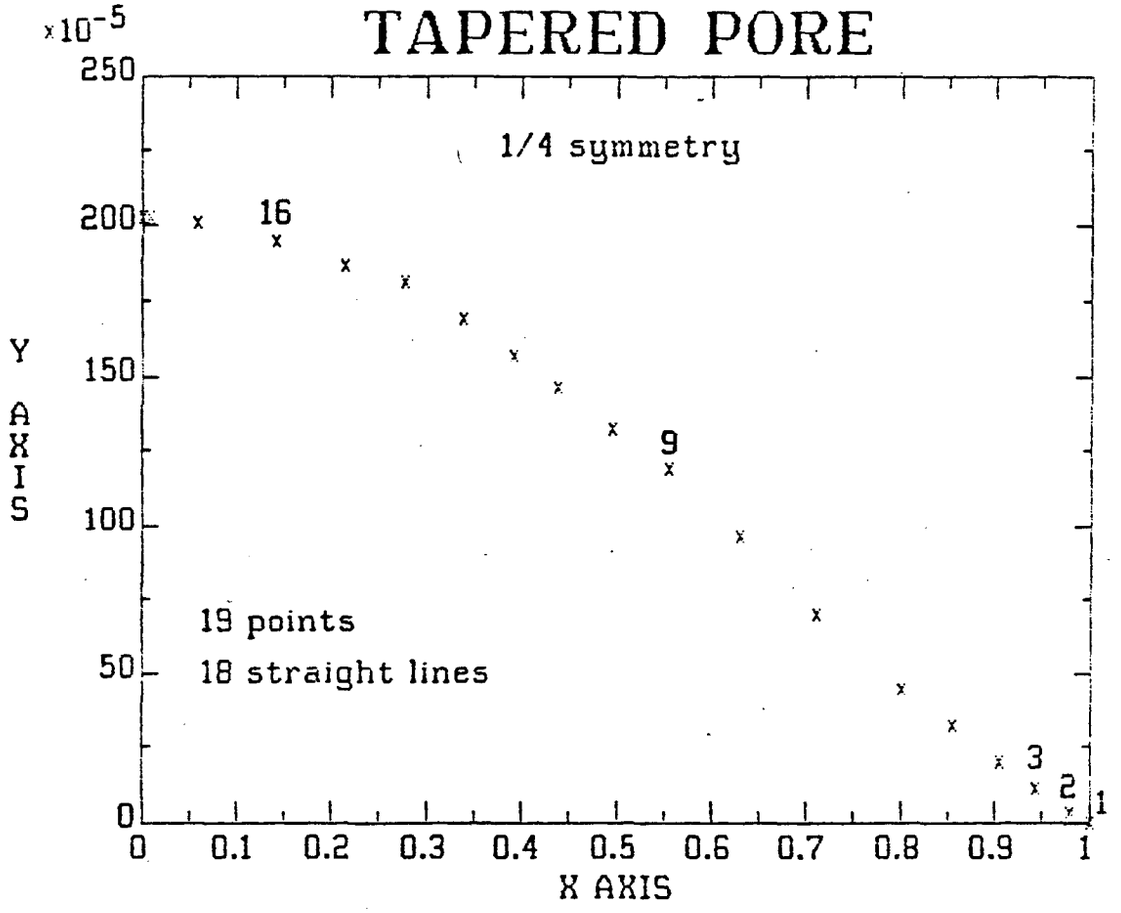

Figure 2: Digitation of a 18 elements tapered pore. Notice the digitation process goes from right to left. Due to 1/4 symmetry, we have used $ksym = 4$.